THESIS FOR THE DEGREE OF MASTER OF SCIENCE

CONDOR – CITVAP CALCULATION LINE VALIDATION USING RA-6 EXPERIMENTAL DATA

Eng. Yousef I. AlZaben
Author

Dr. Eduardo A. Villarino
Director

Eng. Carlos A. Lecot
Co-Director

November 2013

Instituto Balseiro
Universidad Nacional de Cuyo
Comisión Nacional de Energía Atómica
Argentina

To all those who believed in me to achieve this goal particularly my family

ACKNOWLEDGEMENT

First of all, I am indebted to Almighty Allah for giving me the opportunity and ability to conduct this research for my Master thesis.

It is with immense gratitude that I acknowledge Dr. Eduardo Villarino, director, and Eng. Carlos Lecot, co-director, for their guidance to achieve this work.

I cannot find words to express my gratitude to my parents who encouraged me and prayed for me throughout my study journey. May God bless them both for believing in me.

I am thankful to King Abdulaziz City for Science and Technology (KACST) for their financial support during my study period.

I am also grateful to Eng. Herman Blaumann for his authorization to obtain the experimental data of the RA-6 commissioning. I am thankful as well to all the staff at RA-6 reactor whom made the experimental measurement during the commissioning.

ABSTRACT

The deterministic calculation line CONDOR-CITVAP has been extensively verified and validated. In this research, CONDOR-CITVAP is verified against IAEA numerical benchmarks: IAEA-Benchmark-233 and IAEA-Benchmark-643. These benchmarks were about a feasibility study and guidelines for a safe core conversion from the use of Highly Enriched Uranium (HEU) fuel to the use of Low Enriched Uranium (LEU) fuel. Benchmark calculations were performed to compare the computational methods of various organizations. In these two benchmarks, there were 10 organizations participating from all the world to calculate certain parameters of common of interest. These parameters are: (a) K_∞ as a function of burnup, (b) Pu^{239} content at 50% burnup, (c) K_{eff} in three core states: Fresh (without Xe), Beginning of Life (BOL) and End of Life (EOL), (d) thermal and fast flux ratio in BOL state along the X-axis, (e) Control Element Worth (CEW), and (f) feedback coefficients. Results of the calculation line CONDOR-CITVAP for all these parameters were obtained and compared with other participants' results. The results' obtained using CONDOR-CITVAP were within other participants' results and close to the average values of participants' results.

The deterministic calculation line CONDOR-CITVAP is, then, validated against the experimental data of RA-6. RA-6 (Spanish acronym for Argentinean Reactor – Number 6) is a Material Testing Reactor (MTR) located in Centro Atómico, Bariloche, Argentina, to support training and research activities of Balseiro Institute. In the framework of Reduced Enrichment Research and Test Reactors (RERTR) program, RA-6 core was converted in 2008 from High Enriched Uranium (HEU) to Low Enriched Uranium (LEU) fuel. During the commissioning of the new core, a series of measurements took place. This research is focused on the following measurement: (a) approach to criticality by control elements, (b) control elements calibration, measurement of (c) excess reactivity, (d) total Shutdown Margin (SDM), (e) SDM with a single failure of a control element, (f) isothermal feedback coefficient, (g) void feedback coefficient, (h) power feedback coefficient and (i) α-kinetic parameter. All the previous measurements were simulated per the experimental procedures by using the deterministic calculation line CONDOR-CITVAP and validated against the measured data. A good agreement between the measured data and the calculated values were found.

Contents

List of Abbreviations

MTR: Material Test Reactor.

RA-6: Spanish acronym for Argentinean Reactor – Number 6.

IAEA: International Atomic Energy Agency.

HEU: High Enriched Uranium.

LEU: Low Enriched Uranium.

BOL: Beginning of Life.

EOL: End of Life.

CEW: Control Element Worth.

SFA: Standard Fuel Assembly.

CFA: Control Fuel Assembly.

MC: Meat Conservation.

PC: Pitch Conservation.

CE: Control Element.

SDM: Shutdown Margin.

CIC: Compensated Ionization Chamber.

CP: Critical Position.

List of Figures

List of Tables

CHAPTER 1: INTRODUCTION

1.1. Motivation and Objective.

The deterministic calculation line CONDOR-CITVAP, [1], has been validated extensively. In this thesis, the calculation line is validated against a MTR numerical benchmark and RA-6 experimental data. The IAEA benchmark, [8] and [9], was utilized as a numerical benchmark. The RA-6 experimental data was measured during the commissioning of the converted core to LEU fuel.

This work was done to fulfill the following objectives:

- Learn the calculation line through the use of a well-defined benchmark (IAEA numerical benchmark).
- Expand the experimental base line validation of the calculation line through the use of RA-6 experimental benchmark.
- Develop a predictable model for the RA-6 reactor using the calculation line. Then, validating this model against the measured data during the RA-6 commissioning.
- Seeking to improve the calculation – experiment comparison in order to examine the experimental details that is not measured so far.
- Using Monte Carlo calculation tool, if possible, in case of a discrepancy between the calculation line and the experimental data.

1.2. Calculation Line Description.

The deterministic calculation line CONDOR-CITVAP is used to accomplish the objective of this thesis. CONDOR, [2], is a cell calculation code developed by INVAP's Nuclear Engineering Department. The method applied to obtain the neutronic flux (in a multi – group scheme) can be:

- Collision probability in general two-dimensional cylindrical geometry.
- Collision probability in one-dimensional slab geometry.
- Heterogeneous Response Method (HRM) in 2D general geometry.

The HRM, is also known as the Current-Coupling Collision Probability method (CCCP), [3], uses an angular dependent coupling currents to calculate the flux distribution along fuel assembly's components. In research reactors, fuel assembly optimization is still a challenge and this method provides a fast and accurate alternative to the most common collision probability method for a large complex fuel assembly. Using the HRM, the final model can be constructed

repeating or combining several different cellblocks. These blocks are then individually calculated using the collision probability method and coupled by the inward and outward angular dependent currents (white current coupling) of the connecting boundaries of each cellblock. This methodology is suitable for most calculations and provides a more compact geometric definition of a problem and a shorter calculation time, [1].

The microscopic cross section data library was provided to CONDOR as 69 energy - group structure. This library is called ESIN 2001. The ESIN 2001 library originally comes from ENDF/B-IV. The information of this library is presented in table 1.1.

Table 1.1: Information of the ESIN 2001 microscopic cross section library.

Number of energy groups	69
Number of thermal groups	42
Number of epithermal groups	13
Number of fast groups	14
Groups with fission spectra	17
Number of elements	99
Number of resonant elements	5
Number of fissile elements	7
Number of fission product	35
Number of P1 elements	4

For the core calculation, a condensation was applied from 69 energy-group to 3 energy-group. In this work, CONDOR version 2.62 was used.

A graphical postprocessor program was used to enhance the user interaction with CONDOR code which is called POSCON, [1]. POSCON version 3.0 was used in this work. This program allow the user to examine the geometrical input, the infinite multiplication factor verses burnup, flux shape in 2D or 1D of the geometrical input, etc.

An auxiliary program was used to extract the macroscopic cross sections, which were generated by CONDOR. This program is called HXS (Handle Cross Sections), [1]. This program has the ability to merge all the generated macroscopic cross sections in a single library. In addition, this program has a various modifying options on the obtained library, one of these options: mix different macroscopic cross sections and store them as a new macroscopic cross section. In this work, HXS version 5.0b was used.

An auxiliary program was used to treat the output microscopic cross sections from CONDOR to be reused in CITVAP code to calculate kinetic parameters. This program is called POS_LIB, [4]. The input file of POS_LIB program requires: (a) CONDOR's output file of microscopic cross sections in CITATION format and (b) CITVAP's database output file. The output files of POS_LIB program are: section 000, section 012 and section 020. These sections would be used later in CITVAP's input file. POS_LIB version 2.0 was used in this work.

CITVAP, [5], is a new version of the core calculation code CITATION II, [6]. CITVAP was developed by INVAP's Nuclear Engineering Department. It uses the finite difference representation to solve neutron diffusion equation. It can be used to solve 1D, 2D and 3D multigroup diffusion equation in a rectangular, cylindrical, triangular and hexagonal geometry. In CITVAP, nuclear data are provided as microscopic or macroscopic cross section libraries. CITVAP performs flux and adjoint flux calculations in order to calculate the prompt neutron lifetime and delayed neutron fraction. CITVAP is able to conduct thermal-hydraulics calculations either forced or natural convection calculation in a steady state condition. The internally coupled code for forced convection calculation is called TERMIC while the code that preform natural convection calculation is called CONVEC. CITVAP version 3.8 was used to conduct this work. Fig. 1.1 shows a chart of interaction of the calculation line CONDOR-CITVAP within each other.

A graphical postprocessor program was used to enhance the user interaction with the core calculation code CITVAP. This program is called FLUX program, [7]. FLUX version 2.8 has been used for this work. FLUX program enable the user to view, export information and graphics for the core geometry and the calculated variables from the database of CITVAP code.

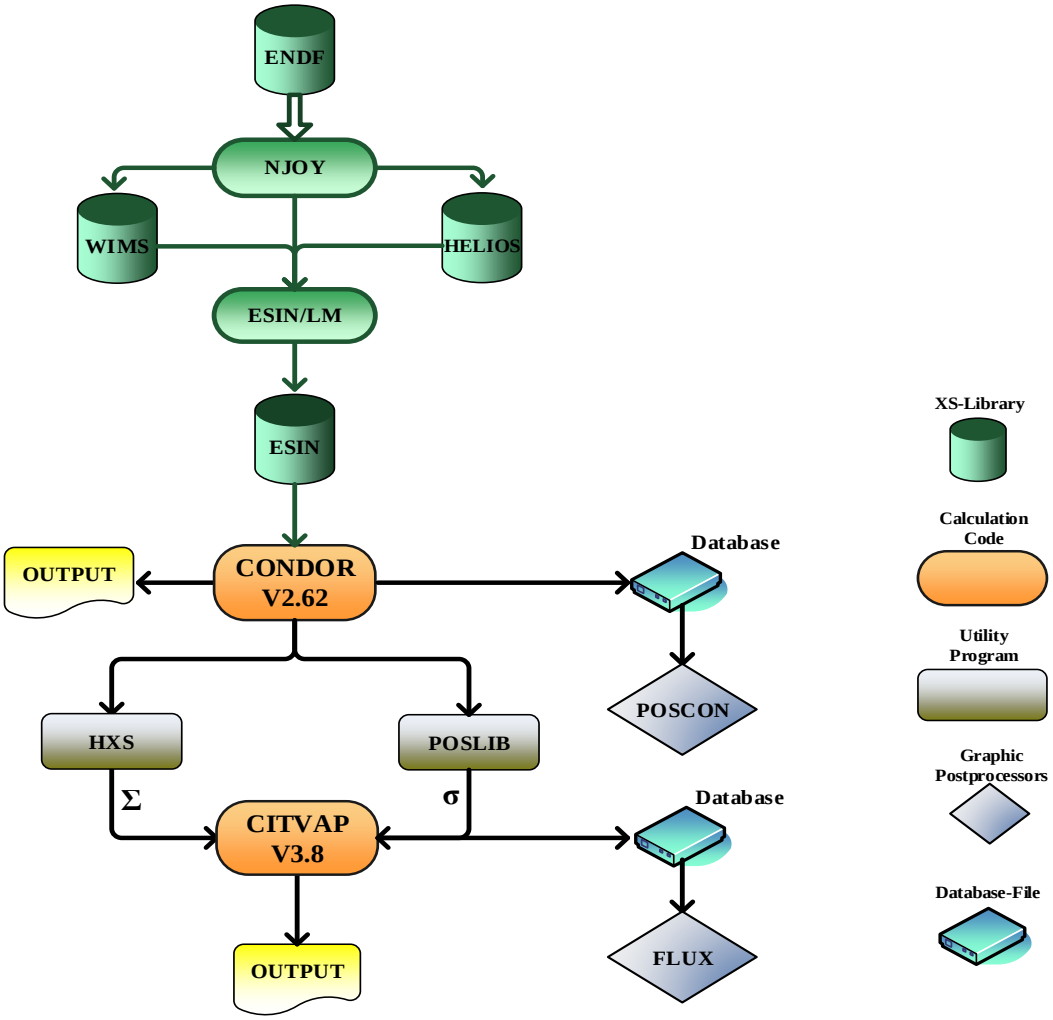

Fig. 1.1: Schematic of the deterministic calculation line CONDOR-CITVAP.

1.3. Publication.

A paper out of this Master thesis was published and presented in the 6th International Symposium on Material Testing Reactors (ISMTR-6). The title of the paper is "SAFETY PARAMETERS VALIDATION AFTER THE COMMISSIONING OF RA6 CORE CONVERSION TO LEU FUEL", [8].

1.4. Work Structure.

This Master thesis is organized as following:

- In **Chapter 1**, objective and motivation of the Mater thesis are firstly presented. Secondly, the calculation line that is used to accomplish this research is described.
- In **Chapter 2**, preliminary verification against the IAEA numerical benchmark is presented. The main goal of this chapter is to learn the calculation line with a well-defined benchmark and compare the obtained results with 10 international participants' organizations. The verification was achieved on two stages: cell calculations verification and core calculations verification. Two parameters were utilized for the cell calculations verification: K_∞ as a function of burnup and Pu^{239} content at 50% burnup. Four parameters, on the other hand, were utilized for the core calculations verification: K_{eff} in three core states: Fresh (without Xe), BOL and EOL, thermal and fast flux ratio in BOL state along the x-axis, control element worth, and feedback coefficients.
- In **Chapter 3**, the core of the Master thesis is presented in this chapter. The main objective of this chapter is to demonstrate the validation of the calculation line against experimental data of the RA-6 reactor. The validation took place for the following experiments: approach to criticality by control elements, control elements calibration, measurement of excess reactivity, total Shutdown Margin (SDM), SDM with a single failure of a control element, isothermal feedback coefficient, void feedback coefficient, power feedback coefficient and α-kinetic parameter.
- In **Chapter 4**, a summary of the IAEA numerical benchmarks and RA-6 experimental benchmark differences is presented. Following this summary, a recommendation of future works is shown.

CHAPTER 2: IAEA NUMERICAL BENCHMARK

2.1. Introduction.

In this chapter, there are two IAEA numerical benchmarks utilized in the learning process to produce appropriate modeling for the cell and core calculations codes. These two benchmarks are: benchmark 233, [8] and benchmark 643, [9]. The IAEA-benchmark-233 is about a feasibility study to convert research reactor core from the use of Highly Enriched Uranium (HEU) to the use of Low Enriched Uranium (LEU) fuels. The benchmark problem has an idealized core of 6 x 5 fuel elements, plate-type with a power of 10 MW_{th} reflected by a single graphite rows on two sides and surrounded by a light water.

The IAEA-benchmark-643 is a continuation study of the benchmark-233. It is about safety core conversion from the use of HEU to the use of LEU fuels. The reactor and fuel loading specifications are identical to the benchmark-233 except for the central flux trap.

These two benchmarks have been done by 10 participants, table 2.1.

Table 2.1: List of benchmark participants.

Organization Name	Abbreviation	Country
Argonne National Laboratory	ANL	United State
Australian Atomic Energy Commission	AAEC	Australia
Comisión Nacional de Energia Atómica	CNEA	Argentina
Commissariat a 1' Energie Atomique	CEA	France
Eldg. Institut fur Reaktorforshung	EIR	Switzerland
Internationale Atomreaktorbau GmbH	INTERATOM	Germany
Japan Atomic Energy Research Institute	JAERI	Japan
Junta de Energia Nuclear	JEN	Spain
Kyoto University Research Reactor Ins.	KURRI	Japan
Riso National Laboratory	RISO	Denmark

The benchmarks specifications, requirements and calculation models are listed in Appendix-A. Author's results are shown in the subsequent section.

2.2. Results and Comparisons.

In this section, the results of the two benchmarks are demonstrated: Benchmark-233 and Benchmark-643. First, cell calculation results are shown. Second, core calculation results are presented. In each stage, Author's results are compared with other participants' results.

2.2.1. Cell Calculation Results.

2.2.1.1. K_∞ as a function of burnup (Lost of U^{235} %) for both HEU and LEU.

The infinite multiplication factor (K_∞) of the SFA was compared against one of the participants who used WIMS-D1[1] code as a cell code. Both results (CONDOR & WIMS) were summarized in table 2.2. The following two figures show the K_∞ as a function of burnup for the 1D SFA model (MC and PC) of both codes.

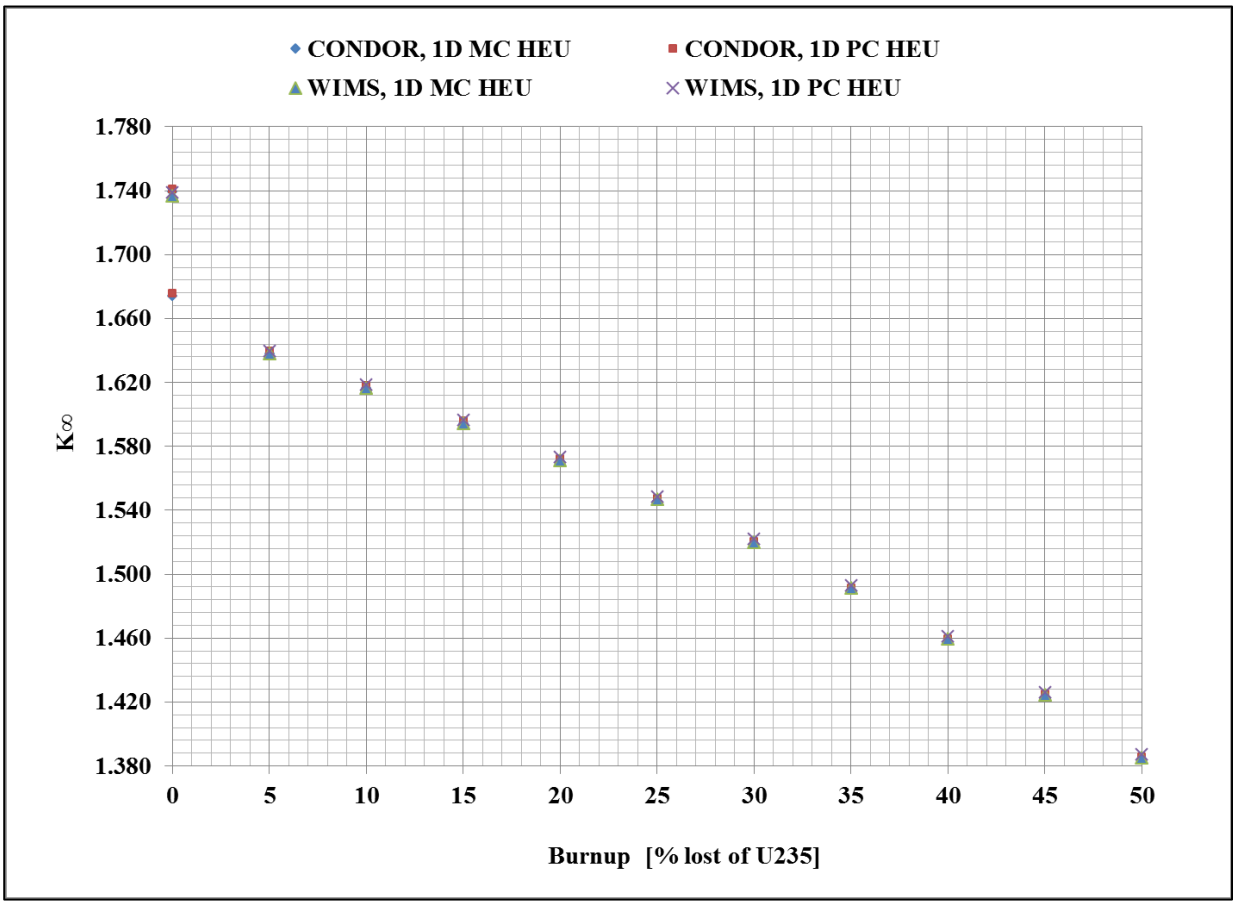

Fig. 2.1: K_∞ as a function of burnup [%] for HEU.

[1] Done by EIR, Switzerland.

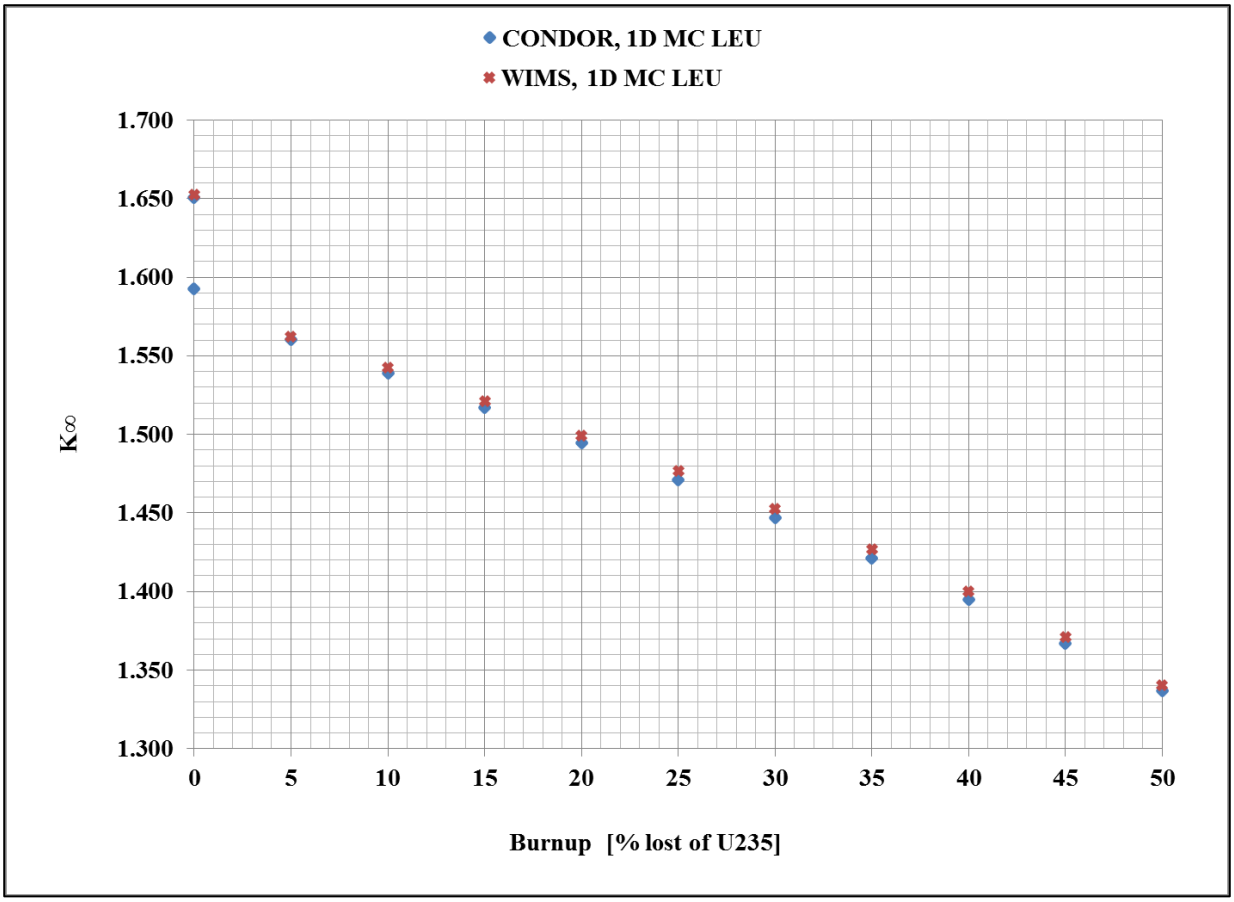

Fig. 2.2: K_∞ as a function of burnup [%] for LEU.

Fig. 2.2 presents only the 1D MC SFA results, because the 1D PC SFA results were not informed by the participant who used WIMS code.

It can be observed from (Fig. 2.1 & Fig. 2.2) an insignificant difference between the results of CONDOR's SFA model and WIMS's SFA model.

Table 2.2 shows the Author 2D SFA results using CONDOR for both HEU and LEU fuel. Also, it shows the reactivity difference between CONDOR and WIMS in HEU-MC. As well as, in case of HEU-PC and LEU-MC. In addition, table 2.2 presents the reactivity difference between 2D and 1D-MC Author's model of the SFA. All the differences in reactivity were within the acceptable limit.

Table 2.2: K_∞ as a function of burnup [%] For HEU and LEU.

IAEA Benchmark Cell Calculation Results For 1D SFA K_∞				**Author Results for 1D SFA K_∞, Δρ (pcm) between WIMS and CONDOR are (*shown in parentheses*).**				**Author Results for 2D SFA K_∞, Δρ (pcm) between CONDOR 1D-MC and 2D are (*shown in parentheses*).**	
Burnup, [%]	**HEU [MC] WIMS**	**HEU [PC] WIMS**	**LEU [MC] WIMS**	**HEU [MC] CONDOR**	**HEU [PC] CONDOR**	**LEU [MC] CONDOR**	**LEU [PC] CONDOR**	**HEU 2D CONDOR**	**LEU 2D CONDOR**
0 (No Xe)	1.736777	1.738854	1.652470	1.739356 **(85)**	1.740981 **(70)**	1.650466 **(73)**	1.648580	1.734121 **(174)**	1.648296 **(80)**
0 (With Xe)	This data was not informed			1.674355 **-**	1.675917 **-**	1.592366 **-**	1.590550	1.669254 **(183)**	1.590230 **(84)**
5	1.637918	1.639875	1.562400	1.638242 **(12)**	1.639792 **(3)**	1.560184 **(91)**	1.558393	1.633235 **(187)**	1.558025 **(89)**
10	1.616634	1.618590	1.542274	1.616528 **(4)**	1.618076 **(20)**	1.538862 **(144)**	1.537100	1.611573 **(190)**	1.536725 **(90)**
15	1.594637	1.596586	1.521404	1.594227 **(16)**	1.595774 **(32)**	1.517080 **(187)**	1.515352	1.589361 **(192)**	1.515001 **(90)**
20	1.571440	1.573389	1.499518	1.570801 **(26)**	1.572345 **(42)**	1.494546 **(222)**	1.492849	1.566020 **(194)**	1.492492 **(92)**
25	1.546763	1.548677	1.476540	1.545869 **(37)**	1.547408 **(53)**	1.471166 **(247)**	1.469506	1.541191 **(196)**	1.469138 **(94)**
30	1.520066	1.522037	1.452472	1.519083 **(43)**	1.520593 **(62)**	1.446833 **(268)**	1.445232	1.514520 **(198)**	1.444818 **(96)**
35	1.491110	1.493078	1.427035	1.490045 **(48)**	1.491546 **(69)**	1.421452 **(275)**	1.419919	1.485623 **(200)**	1.419417 **(101)**
40	1.459410	1.461355	1.400062	1.458311 **(52)**	1.459803 **(73)**	1.394845 **(267)**	1.393416	1.454049 **(201)**	1.392788 **(106)**
45	1.424412	1.426328	1.371219	1.423326 **(54)**	1.424787 **(76)**	1.366819 **(235)**	1.365512	1.419245 **(202)**	1.364712 **(113)**
50	1.385223	1.387140	1.340245	1.384374 **(44)**	1.385816 **(69)**	1.337096 **(176)**	1.335958	1.380513 **(202)**	1.334934 **(121)**

2.2.1.2. Pu^{239} content at 50% burnup for SFA for both HEU and LEU.

Table 2.3 shows the Pu^{239} content for the SFA at 50% burnup for the different participants. Table 2.4 shows the Author's results with a maximum, minimum and average participants' results.

Table 2.3: Participants results of Pu^{239} content at 50% burnup, (g/SFA).

SFA	Ösgae	ANL	Interatom	EIR	JAERI	CNEA	INVAP ESIN2001	INVAP Helios190
HEU	0.42	0.44	0.42	0.45	0.37	0.43	0.42	0.42
LEU	12.30	12.17	11.92	14.80	9.13	12.71	12.93	12.66

Table 2.4: Author results of Pu^{239} content at 50% burnup, (g/SFA), percentage differences between the Author's results and the (max., min., average) participants' results are (*Shown in parentheses, [%]*).

	Author's Results – between parentheses show the percentage difference between Author's result and (Max, Min, Average) value of participants' results						**Participants' Results**		
SFA	**2D model**		**1D-MC model**		**1D-PC Model**		**Max.**	**Min.**	**Average**
HEU	0.43	**(4, 16, 2)**	0.43	**(4, 16, 2)**	0.43	**(4, 16, 2)**	0.45	0.37	0.42
LEU	12.77	**(14, 40, 4)**	13.01	**(12, 42, 6)**	13.30	**(10, 46, 8)**	14.80	9.13	12.33

In table 2.4, it can be seen that the 2D SFA model has the closest results to the average participants' results than the 1D SFA results.

2.2.2. Core Calculation Results.

After generating all macroscopic cross sections for the 1D and 2D models, the HXS program was used to transfer the generated macroscopic cross sections to a library. This library is used to prepare the CITVAP input file.

Recalling that there was two benchmarks (233 & 643), core calculation results would be split into four main results. The first two results correspond to benchmark 233, while the third and the forth are for benchmark 643.

2.2.2.1. K_{eff} calculation for HEU and LEU cores in three states: Fresh (without Xe), BOL and EOL.

The effective multiplication factor (K_{eff}) was obtained for both HEU and LEU cores. Table 2.5 shows the K_{eff} values for three states: Fresh (without Xe), BOL and EOL, as well the reactivity difference ($\Delta\rho$) between the Author and average participants' results are presented between parentheses.

Table 2.5: K_{eff} values for the Author and average participants' results. The reactivity differences between them (*shown in parentheses, [pcm]*) for both 2D and 1D macroscopic cross sections sets.

Core State	Average Participants' Results	Author's 2D Results (*difference in pcm*)		Author's 1D Results (*difference in pcm*)	
	HEU				
Fresh	1.1941	1.1982	**(285)**	1.2032	**(633)**
BOL	1.0353	1.0357	**(40)**	1.0387	**(318)**
EOL	1.0122	1.0126	**(38)**	1.0150	**(277)**
	LEU				
Fresh	1.1755	1.1797	**(303)**	1.1822	**(480)**
BOL	1.0322	1.0317	**(44)**	1.0331	**(83)**
EOL	1.0131	1.0129	**(16)**	1.0141	**(94)**

After that, a comparison was carried out for the reactivity lost from BOL to EOL between the Author and average participants' results, table 2.6.

Table 2.6: Comparison of reactivity lost from BOL to EOL.

Reactivity loss from BOL to EOL ($\Delta\rho$ - %)						
Author result / Difference between Author and (Max., Min., Average) participants' results are (*Shown in parentheses, [%]*)				**Participants' Results**		
Fuel	**Author 2D Result**		**Author 1D Result**		**Max.**	**Min.**	**Average**
HEU	2.20	**(7, 17, 0.5)**	2.24	**(5, 19, 2)**	2.37	1.88	2.19
LEU	1.80	**(7, 19, 1.6)**	1.82	**(6, 20, 0.5)**	1.94	1.51	1.83

A conclusion can be drawn from this step, that the Author result is among other participants' results and the 2D model is close to average participants' results.

2.2.2.2. Thermal and fast flux ratio (LEU/HEU) in BOL state along the X-direction.

The thermal and fast flux ratio was plotted from the center of the core to the end of the reflector along X-axis.

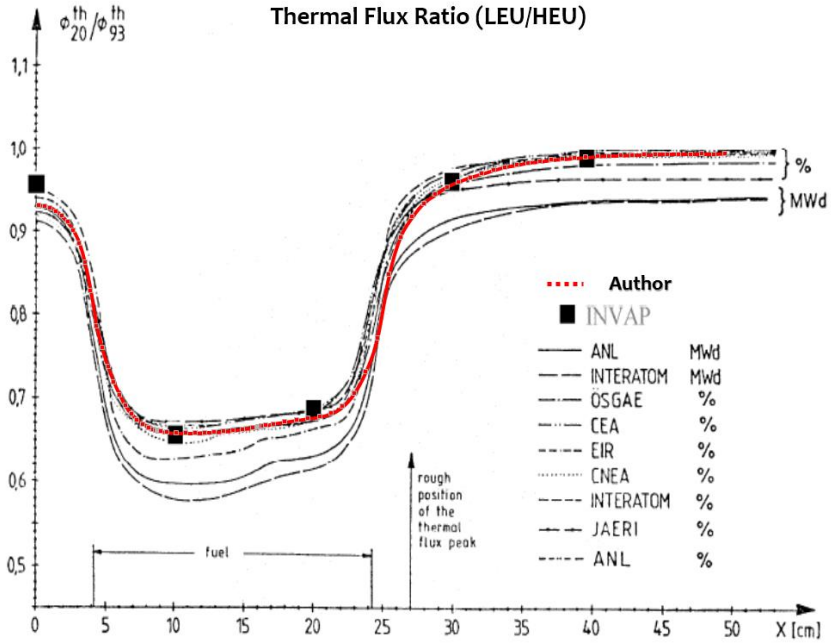

Fig. 2.3: Thermal flux ratio [LEU/HEU] vs. X core distance [cm], [11], the red dotted line is the Author's result.

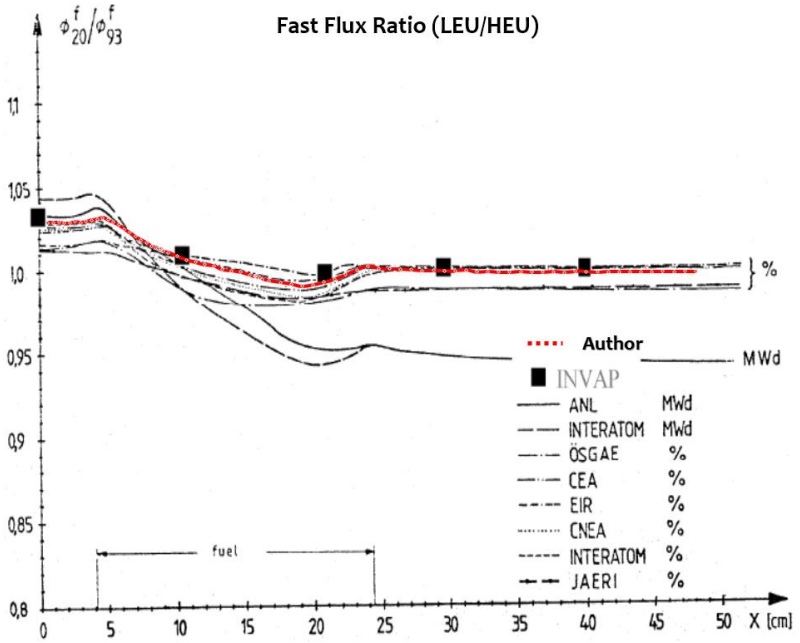

Fig. 2.4: Fast flux ratio [LEU/HEU] vs. X core distance [cm], [11], the red dotted line is the Author's result.

From the previous two figures, it can be observed that the Author's result falls between other participants' results.

2.2.2.3. Control Element Worth (CEW) of four inserted control elements in these core states: HEU (Fresh and BOL) and LEU (Fresh and BOL).

The control element worth calculations were done for a three different control elements: Ag-In-Cd, B_4C and Hf. The Ag-In-Cd plate is 80.5 w/o Ag, 14.6 w/o In and 4.9 w/o Cd. The B_4C plate contains natural boron. The Hf plate contains natural hafnium.

As was mentioned in Appendix-A, there were three different ways of homogenizations for the CFA model. Table 2.7 presents the CEW for the each CFA homogenized model.

Table 2.7: CEW for HEU (Fresh and BOL) and LEU (Fresh and BOL).

Core State	Participant	K_{eff}	Ag-In-Cd [pcm]	B_4C [pcm]	Hf [pcm]
HEU Fresh No Xe	ANL	1.19372	12970	17000	12590
	INTERATOM	-	13300	17200	-
	INVAP (ESIN 2001), [12]	1.19513	13170	17100	15400
	INVAP (Helios 190G), [12]	1.18951	14100	18140	13430
	Author **(**A Model*)	1.20253	13149	15272	16376
	Author **(**B Model*)	-	12384	16177	-
	Author **(**C Model*)	-	12488	16398	-
HEU BOL	ANL	1.03334	17030	21740	16390
	INTERATOM	-	16900	21300	-
	INVAP (ESIN 2001) , [12]	1.03856	16730	21260	19100
	INVAP (Helios 190G) , [12]	1.03706	17710	22350	16760
	Author **(**A Model**)**	1.04040	16834	19073	20271
	Author **(**B Model**)**	-	15859	20321	-
	Author **(**C Model**)**	-	16036	20651	-
LEU Fresh No Xe	ANL	1.16954	11530	15390	11200
	INTERATOM	-	11700	15300	-
	INVAP (ESIN 2001) , [12]	1.17334	11510	15200	13660
	INVAP (Helios 190G) , [12]	1.16973	12350	16190	11810
	Author **(**A Model**)**	1.18183	11428	13559	14505
	Author **(**B Model**)**	-	10757	14316	-
	Author **(**C Model**)**	-	10848	14503	-
LEU BOL	ANL	1.02353	14470	18910	13970
	INTERATOM	-	14200	18300	-
	INVAP (ESIN 2001) , [12]	1.03028	13960	18140	16250
	INVAP (Helios 190G) , [12]	1.02857	14890	19240	14170
	Author **(**A Model**)**	1.03439	14014	16323	17309
	Author **(**B Model**)**	-	13195	17310	-
	Author **(**C Model**)**	-	13328	17562	-

* A, B and C Models are shown in Appendix-A in Fig. A.10

A comparison between the (max., min., average) participants and the Author's results for the CEW in terms of percentage difference is presented in table 2.8.

Table 2.8: Comparison of CEW between the Author and the (max., min., average) participants' results.

Difference between Author and (Max., Min., Average) participants' results, [%]								
Core State	**Author Model**	**Ag-In-Cd, [%]**			**B_4C, [%]**			**Hf, [%]**
		Max.	**Min.**	**Avg.**	**Max.**	**Min.**	**Avg.**	**Avg.**
HEU Fresh No Xe	A Model	7	1	2	16	10	12	26
	B Model	12	5	7	11	5	7	-
	C Model	11	4	7	10	4	6	-
HEU BOL	A Model	5	1	2	15	10	12	22
	B Model	10	5	7	9	4	6	-
	C Model	9	4	6	8	3	5	-
LEU Fresh No Xe	A Model	7	1	3	16	11	13	26
	B Model	13	7	9	12	6	8	-
	C Model	12	6	8	10	5	7	-
LEU BOL	A Model	6	0.4	3	15	10	12	23
	B Model	11	5	8	10	5	7	-
	C Model	10	5	7	9	3	6	-

From table 2.8, it can be concluded that the "*A Model*" for AgInCd CEW, gives a closer result than "*B and C Models*" compared with other participants, while B_4C "C Model" shows the closest result to other participants. The Hf CEW is a way from other participants' results with more than 20% difference. This is because of the self-shielding treatment was not applied to the Hf in the ESIN 2001library. As well, it can be noticed that the values of differences did not change much from fresh calculation to BOL calculation. This is an evidence of a good burnup mathematical model implemented in CONDOR code, in which was verified earlier against WIMS calculations.

2.2.2.4. Feedback reactivity coefficients.

In BOL state, the calculations of reactivity feedback coefficients were taken place for HEU and LEU fuel by changing the following parameters in the SFAs and the CFAs:

I) Water temperature only - 38, 50, 75 and 100 ^{o}C.
II) Water density only - 0.993, 0.988, 0.975 and 0.958 g/cm^3
III) Fuel temperature only - 38, 50, 75, 100 and 200 ^{o}C
IV) Core Void Coefficient - Change Water Density Only - 10%, 20% Void.

I) Change of water temperature only.

By fixing the water density at 0.9984 g/cm^3, which correspond to 20^{o}C, and changing only water temperature by 38, 50, 75 and 100^{o}C. The obtained reactivity difference was compared with a reference water temperature at 20^{o}C.

The split up of the water feedback into density effect and temperature effect means that the physical effect taken into account, under water temperature only, is due to the movement of the hydrogen atoms at different temperatures.

Table 2.9: Reactivity feedback coefficient due to water temperature change only, LEU and BOL core, ($\Delta\rho$ – pcm), percentage difference between Author and average participants' results.

Temperature [^{o}C]	**Author (*difference*)**	**INVAP (ESIN 2001), [12]**	**ANL**	**EIR**	**INTERATOM**
	1.034386	1.03068	1.01823	1.02639	-
20	RP*	RP	RP	RP	-
38	-129	-124	-148	-153	-
50	-214	-204	-245	-251	-
75	-387	-372	-443	-451	-
100	-550	-535	-636	-640	-
Feedback coefficient [pcm/^{o}C]	**-6.90 (*9%*)**	**-6.69**	**-7.95**	**-8.00**	**-7.72**

* RP: Reference Point.

Table 2.10: Reactivity feedback coefficient due to water temperature change only, HEU and BOL core, (Δρ – pcm), percentage difference between Author and average participants' results.

Temperature [ºC]	Author (*difference*)	INVAP (ESIN 2001) , [12]	ANL	EIR	INTERATOM
	1.040399	1.03864	1.02878	1.02692	-
20	RP*	RP	RP	RP	-
38	-180	-168	-215	-216	-
50	-303	-280	-357	-356	-
75	-553	-510	-652	-642	-
100	-789	-731	-939	-918	-
Feedback coefficient [pcm/ºC]	**-9.90 (*8%*)**	**-9.13**	**-11.74**	**-11.48**	**-10.78**

* RP: Reference Point.

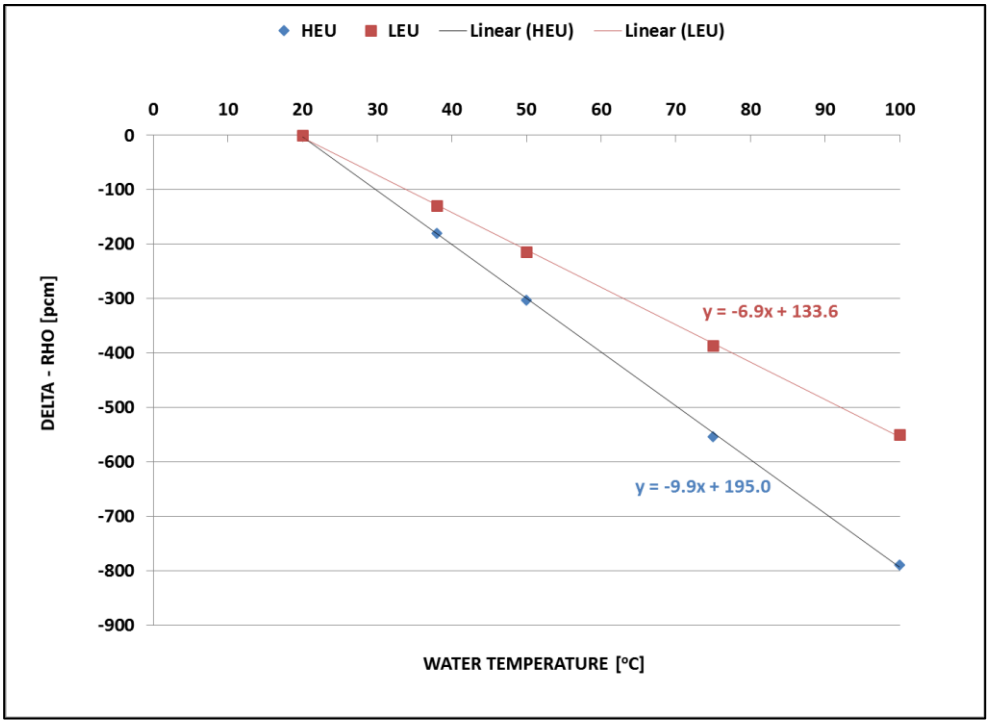

Fig. 2.5: Reactivity change due to increasing water temperature only for HEU and LEU.

From table 2.9 and 2.10, it can be observed that the author result is within other participants' results and close to the average participants' results by less than 10%.

II) Change of water density only.

By fixing the water temperature at 20°C and varying water density only by 0.993, 0.988, 0.975 and 0.958 g/cm^3. The reactivity difference was compared with a fixed reference water density at 0.993 g/cm^3.

Table 2.11: Reactivity feedback coefficient due to water density change only, LEU and BOL core, (Δρ – pcm), percentage difference between Author and average participants' results.

Density [g/cm^3]	**Author (*difference*)**	**INVAP (ESIN 2001) , [12]**	**ANL**	**EIR**	**INTERATOM**
	1.034376	1.029180	1.015850	-	-
0.993	RP*	RP	RP	RP	-
0.988	-137	-133	-148	-140	-
0.975	-505	-488	-543	-526	-
0.958	-999	-964	-1076	-1046	-
Feedback coefficient [pcm/(g/cm^3)]	**28559 (*2%*)**	**27536**	**30743**	**29886**	**27996**

* RP: Reference Point.

Table 2.12: Reactivity feedback coefficient due to water density change only, HEU and BOL core, (Δρ – pcm), percentage difference between Author and average participants' results.

Density [g/cm^3]	**Author (*difference*)**	**INVAP (ESIN 2001) , [12]**	**ANL**	**EIR**	**INTERATOM**
	1.040399	1.037320	1.026590	-	-
0.993	RP*	RP	RP	RP	-
0.988	-118	-116	-125	-125	-
0.975	-430	-425	-457	-462	-
0.958	-855	-842	-910	-918	-
Feedback coefficient [pcm/(g/cm^3)]	**24439 (*3%*)**	**24066**	**26000**	**26229**	**24128**

* RP: Reference Point.

It can be noticed that in LEU fuel case the difference between the Author and average participants' results was 2% while for HEU fuel case the difference obtained was 3%. In addition, the Author results were within other participants' results.

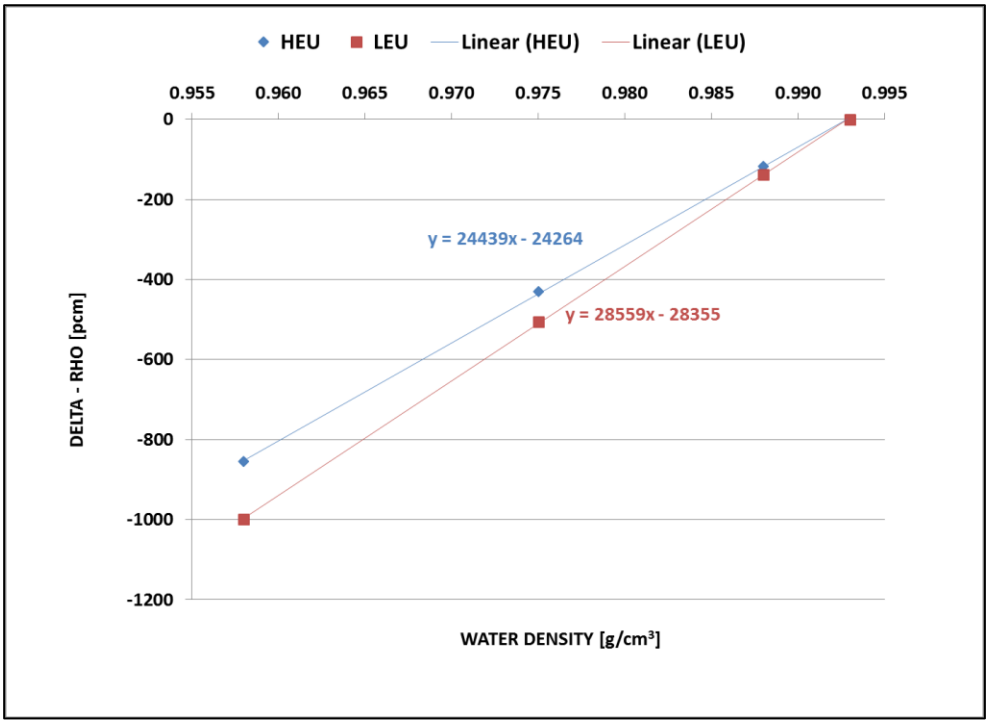

Fig. 2.6: Reactivity change due to increasing water density only for HEU and LEU fuel.

III) Change of fuel temperature only.

These calculations were carried out for a fixed water temperature and density at 20°C and 0.9984 g/cm^3, respectively. The results of reactivity change due to fuel temperature increase only, were calculated with respect to a fixed fuel temperature at 38°C.

Table 2.13: Reactivity feedback coefficient due to fuel temperature change only, LEU and BOL, core (Δρ – pcm), percentage difference between Author and average participants' results.

Temperature [°C]	**Author (*difference*)**	**INVAP (ESIN 2001) , [12]**	**ANL**	**EIR**	**INTERATOM**
	1.034386	1.030238	1.028390	1.026930	-
38	RP*	RP	RP	RP	-
50	-30	-25	-31	-26	-
75	-89	-79	-95	-81	-
100	-146	-131	-157	-135	-
200	-358	-322	-391	-336	
Feedback coefficient [pcm/°C]	**-2.20 (*4%*)**	**-1.99**	**-2.41**	**-2.07**	**-1.98**

* RP: Reference Point.

Table 2.14: Reactivity feedback coefficient due to fuel temperature change only, HEU and BOL core, (Δρ – pcm), difference between Author and average participants' results in terms of fuel feedback coefficient.

Temperature [^{o}C]	**Author (*difference*)**	**INVAP (ESIN 2001) , [12]**	**ANL**	**EIR**	**INTERATOM**
	1.040399	1.038620	1.028390	1.026930	-
38	RP*	RP	RP	RP	-
50	0.09	-0.46	-0.66	-0.20	-
75	-1.11	-1.67	-1.70	-0.70	-
100	-1.75	-2.60	-2.36	-1.30	-
200	-3.60	-6.86	-4.35	-3.50	-
Feedback coefficient [pcm/^{o}C]	**-0.02 (*0.01 pcm/^{o}C*)**	**-0.042**	**-0.027**	**-0.022**	**-0.036**

* RP: Reference Point.

It can be seen here that the fuel feedback coefficient in LEU fuel had a higher value than in HEU fuel. That is because of the higher amount of the resonant isotope (U^{238}) existed in LEU fuel. This high value is a favorable effect because the fuel feedback coefficient is a prompt reactivity feedback. The percentage difference between the Author result and average participants' results were 4% in case of LEU, which is equivalent to 0.09 pcm/^{o}C with respect to participants' average fuel feedback coefficients. On the other hand, the difference in fuel feedback coefficient between the Author and average participants' results in case of HEU fuel was 0.01 pcm/^{o}C. Both Author's results are within the acceptable limit of difference.

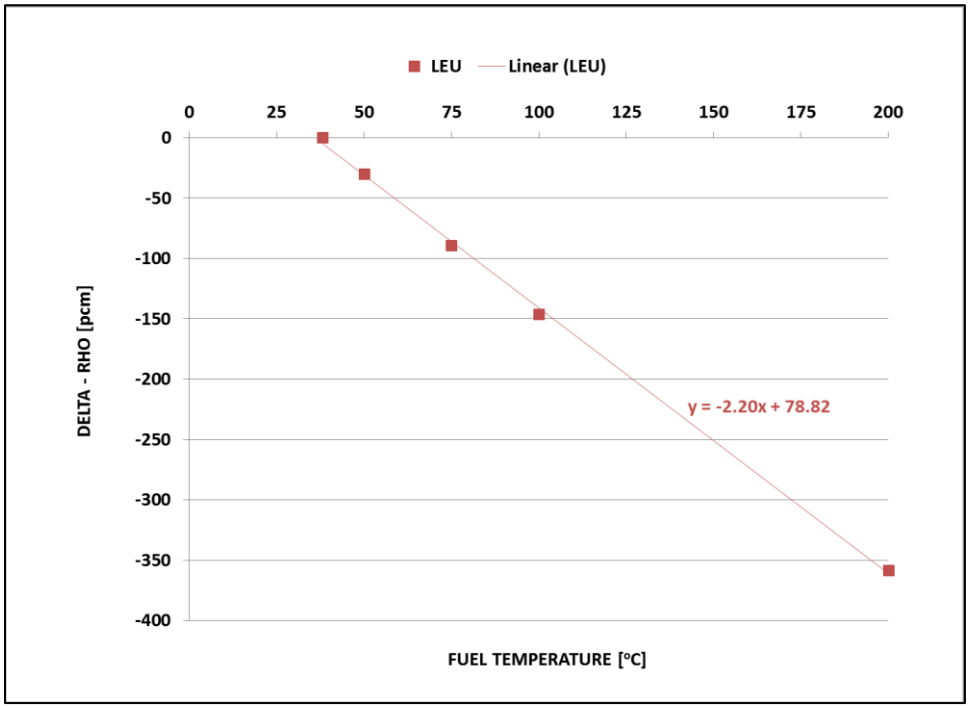

Fig. 2.7: Reactivity change due to increasing fuel temperature only for LEU.

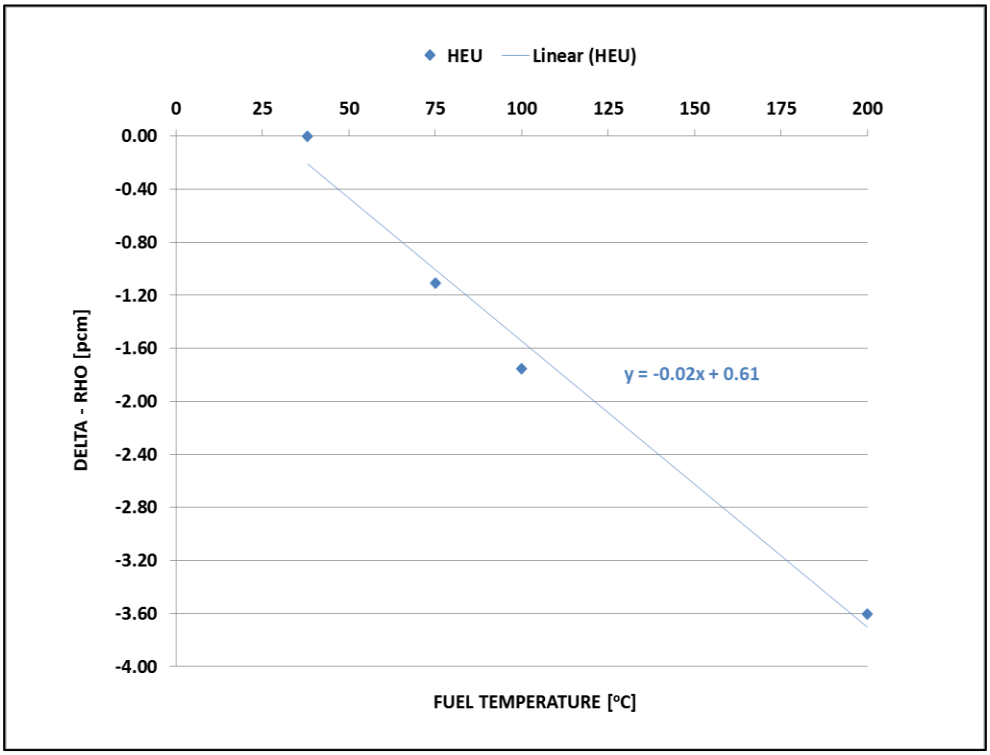

Fig. 2.8: Reactivity change due to increasing fuel temperature only for HEU.

IV) Change of void content in the water only.

These calculations were done with respect to a zero void content that correspond to a water temperature and density at 20°C and 0.9984 g/cm^3, respectively. The void content in water is 10% and 20% which correspond to a water density of 0.8986 and 0.7987 g/cm^3, respectively.

Table 2.15: Reactivity feedback coefficient due to water void change only, LEU and BOL core (Δρ – pcm), percentage difference between Author and average participants' results.

Void content, [%]	**Author (*difference*)**	**ANL**	**EIR**	**INTERATOM**
	1.034376	1.017400	1.015604	-
0	RP*	RP	RP	-
10	-3025	-3272	-3190	-2965
20	-6853	-7471	-7210	-6689
Feedback coefficient† [pcm/ (%)]	**-383 (*3%*)**	**-412**	**-402**	**-372**

* RP: Reference Point.

† This value was obtained by taking the corresponding reactivity difference at 20% void and 10% void over 10% void. This is the method adopted by other participants.

Table 2.16: Reactivity feedback coefficient due to water void change only, HEU and BOL core (Δρ – pcm), percentage difference between Author and average participants' results.

Void content, [%]	**Author (*difference*)**	**ANL**	**EIR**	**INTERATOM**
	1.040399	1.02794	1.026918	-
0	RP*	RP	RP	-
10	-2615	-2796	-2818	-2580
20	-6056	-6516	-6484	-5923
Feedback coefficient† [pcm/ (%)]	**-344 (*4%*)**	**-372**	**-367**	**-334**

* RP: Reference Point.

† This value was obtained by taking the corresponding reactivity difference at 20% void and 10% void over 10% void. This is the method adopted by other participants.

It could be concluded from the previous two tables that void feedback coefficient for the author result is among other participants' results. As well, the difference between the average value of participant's and the Author results was 4% for HEU fuel and 3% for LEU fuel.

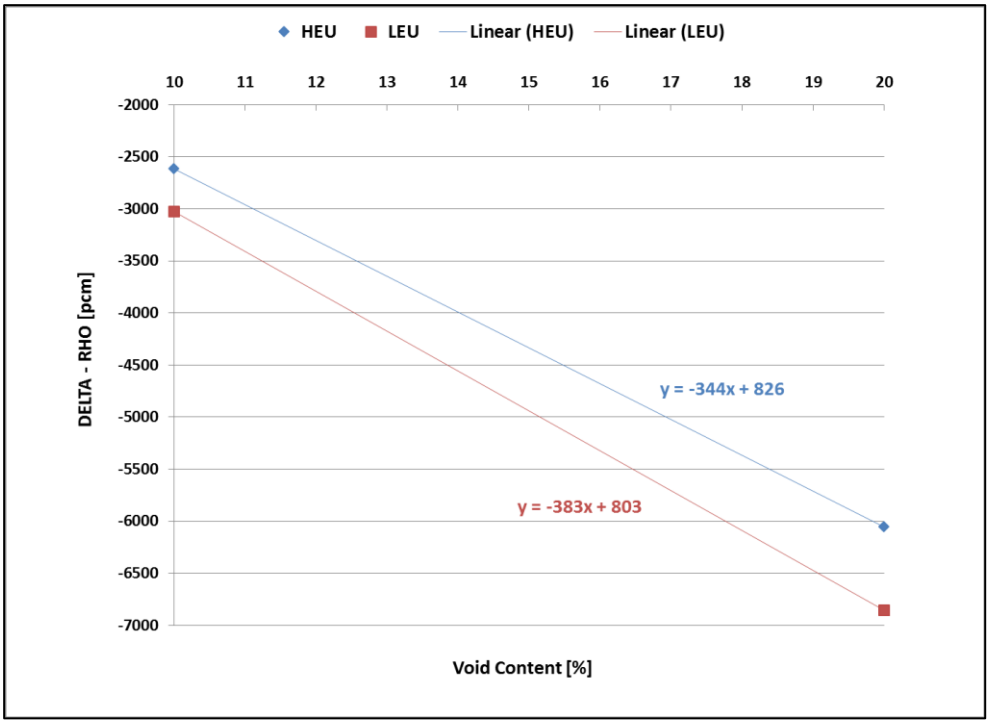

Fig. 2.9: Reactivity change due to only increasing water void content for HEU and LEU.

In this chapter, the calculation line CONDOR-CITVAP was verified against different calculation tools used by 10 different participants. The verification process took place for the following parameters: (a) K_{∞} as a function of burnup, (b) Pu^{239} content at 50% burnup, (c) K_{eff} in three core states: Fresh (without Xe), BOL and EOL, (d) thermal and fast flux ratio in BOL state along the X-axis, (e) CEW, (f) water temperature feedback coefficients, (g) water density feedback coefficient, (h) fuel temperature feedback coefficient, and (i) void feedback coefficient. A good agreement were obtained between the Author and average participants' results.

CHAPTER 3: RA-6 EXPERIMENTAL BENCHMARK

3.1. Introduction.

RA-6 is an open pool type research reactor that utilizes MTR plate type fuel. It is located in Centro Atómico, San Carlos de Bariloche, Río Negro, Argentina. It was commissioned in 1982 by INVAP. The core at that time used a spent High Enrichment Uranium (HEU) fuel that was obtained from RA-3 research reactor that is located in Ezeiza, Argentina. The HEU fuel was of around 90% enrichment of fuel meat UAl_x – Al. The core power was 0.5 MW_{th}.

Due to the call of proliferation concerns, the core was converted in 2008 to a Low Enrichment Uranium (LEU) fuel with less than 20% enrichment. The power of the converted core was upgraded to 3 MW_{th}. The new Fuel Assembly (FA) has a meat of U_3Si_2 – Al with aluminum cladding. Cadmium wires are located along the axial direction of the FA in order to reduce the high reactivity in the initial loading and minimize core perturbations. The Control Element (CE) is of a fork type with blades fitting into guide plates.

One of the commissioning procedures of the converted core was FAs loading. The minimum number of FAs in the core depended on the core critical state. This was achieved by approaching to criticality by the uranium mass. The initial critical core configuration was defined as the first critical core configuration (Core No. 7) while the final critical core configuration was defined as the first operating core configuration (Core No. 11).

The first critical core configuration had 16 Standard Fuel Assemblies (SFAs), 4 Control Fuel Assemblies (CFAs). The core configuration at that stage was reflected by light water. The first operating core, was a core of 15 SFAs, 5 CFAs and reflected by graphite and light water.

The approach to criticality by CEs experiment was recorded for both the first critical and first operating core configurations.

In the first operating core configuration, a series of safety measurements took place. This chapter is focused on the following safety parameters: Control Element Worth (CEW), excess reactivity, total Shutdown Margin (SDM), SDM with a single failure of a control element, isothermal feedback coefficient, void feedback coefficient, power feedback coefficient, and α-kinetic parameter. The CEW was obtained from the calibration of CEs experiment. The outputs of this experiment was the CEW and critical points. Those registered critical points were used later for criticality calculation.

The objective of this chapter is to present a validation of the deterministic calculation line (CONDOR2.62 – CITVAP3.8) for the first critical and the first operating core configurations against the previously mentioned experimental measurements.

3.2. RA-6 Specifications.

In this section, material and geometrical specifications of the RA-6 are provided for the *average measured values*, [13]. When there are an unknown data, a relevant assumption took place.

3.2.1. Material data.

3.2.1.1 Meat composition.

The meat was composed of uranium silicide dispersed in an aluminum matrix. This aluminum was assumed to be a natural aluminum. Table 3.1, 3.2 and 3.3 present the fuel meat composition, the isotopic composition of the uranium and the fuel meat impurity, respectively.

Table 3.1: Fuel meat composition.

Meat	U_3Si_2 – Al
Enrichment	19.77 wt%
U mass per fuel plate	90.36 g
Al mass per fuel plate	25.836 g
U density	4.772 g/cm^3
Si density	0.390 g/cm^3
Al density	1.364 g/cm^3

Table 3.2: Uranium isotopic composition.

Isotope	Composition
U-235	19.77 wt%
U-238	79.974 wt%
U-234	0.144 wt%
U-236	0.112 wt%

Table 3.3: Impurity content in the meat.

EBC* in U_3Si_2	3.09 ppm
EBC in Al	13.7 ppm

*EBC: Equivalent Boron Content.

Table 3.4 shows the homogenized meat composition, which was used in CONDOR's input files, as a single homogeneous material that's include all the sub elements content in weight percent.

Table 3.4: Homogenous meat composition.

Meat density	6.49095 g/cm^3
U-234 content in the meat	0.105866 wt%
U-235 content in the meat	14.5345 wt%
U-236 content in the meat	0.0823399 wt%
U-238 content in the meat	58.7951 wt%
Al content in the meat	20.6923 wt%
Si content in the meat	5.78942 wt%
B content in the meat	5.285508E-04 wt%

3.2.1.2. Cladding composition.

The fuel meat cladding was made of Al-6061. The composition of Al-6061 is presented in table 3.5 and its impurity is provided in table 3.6.

Table 3.5: Al-6061 composition.

Density	2.7 g/cm^3
Al	97.599 wt%
Cu	0.26 wt%
Cr	0.11 wt%
Mg	0.99 wt%
Si	0.67 wt%
Zn	0.001 wt%
Fe	0.27 wt%
Mn	0.09 wt%
Ti	0.01 wt%

Table 3.6: Impurity in the cladding material Al-6061.

Element	Maximum value, [ppm]	Selected value*, [ppm]
Cadmium	30	5
Lithium	40	1
Cobalt	60	60
Boron	10	10

* These values were provided from the fuel fabrication group as a best estimation.

3.2.1.3. Burnable poison.

The burnable poison was made of Cadmium with a purity of 99.9 % and density of 8.65 g/cm^3, the maximum Cadmium impurity content is presented in table 3.7.

Table 3.7: Impurity in the burnable poison (Cadmium).

Element	Maximum value, [ppm]	Selected value*, [ppm]
Boron	10	5
Cobalt	10	5
Silver	100	50

* An assumption was made here that the impurity equal to half the maximum value.

3.2.1.4. Structural materials.

The structural materials were: the side plates, crossbeams, nozzles and control rod guide plates. These structural materials were made of Al 6061-T6 or 6061-T651. Chemical composition and density were not provided. Because of this, Al-6061 was assumed for all the structural materials.

3.2.1.5. Control element absorber composition.

The absorber material of the CE was made of AgInCd. The absorber material composition is provided in table 3.8.

Table 3.8: AgInCd composition.

Density	10.17 g/cm^3
Cd	5.20 wt%
In	14.9 wt%
Ag	79.9 wt%

3.2.1.6. Control element cladding, lower plug and upper support.

The CE cladding, lower plug and upper support were made of stainless steel Type AISI 304L, table 3.9.

Table 3.9: Stainless steel type AISI 304L composition.

	Reference, [13]	**Selected values***
Density	-	7.99 g/cm^3
Fe	Balance	69.5225 wt%
Ni	8 – 12 wt%	10 wt%
Cr	18 – 20 wt%	19 wt%
Si	< 0.75 wt%	0.375 wt%
Mn	< 2 wt%	1 wt%
C	< 0.03 wt%	0.015 wt%
S	< 0.03 wt%	0.015 wt%
P	< 0.045 wt%	0.0225 wt%
N	< 0.1 wt%	0.05 wt%

* These were based on half the reference values.

3.2.1.7. Core support grid.

The core support grid was made of aluminum of purity 99.5 %, composition and density were not specified.

3.2.1.8. Boron Neutron Capture Therapy (BNCT) filter.

The BNCT filter was composed of aluminum and alumina (Al_2O_3) bricks and cadmium sheets, all of them of nuclear purity. Alumina density was measured and found to be 3.96 g/cm^3. Densities of aluminum and cadmium were not specified. It was assumed that the aluminum and cadmium materials were pure of a density of 2.7 g/cm^3 and 8.65 g/cm^3, respectively.

3.2.1.9. Water reactor pool.

The reactor pool is filled with demineralized light water at thermal equilibrium during measurements. According to the specifications, water impurities should not exceed the limits listed in Table 3.10. For the measurements were the water temperature was not reported an assumption took place for the water temperature to be 24ºC, which correspond to a density of 0.9972994 g/cm^3.

Table 3.10: Impurities in water reactor pool.

Element	Maximum value, [ppm]	Selected value*, [ppm]
Iron	0.01	0.005
Copper	0.01	0.005
Chlorine	0.2	0.1

* An assumption was made that the impurity equal to half the maximum value.

3.2.1.10. Graphite blocks.

The graphite was used as a neutron reflector for the first operating core configuration. The density of the graphite was 1.87 g/cm^3. The graphite impurities were not reported. An assumption of 1 ppm of EBC impurity took place.

3.2.2. Geometrical data.

3.2.2.1. Standard Fuel Assembly (SFA).

Table 3.11 shows a summary of the average measured values of the SFA.

Table 3.11: Measured geometrical data for SFA.

Total length, [cm]	91.5	
SFA cross section (WxT), [cm]	7.6 x 8.0	
Fuel Plates Characteristic		
	Internal plates	External plates
Quantity	17	2
Dimensions (HxWxT), [cm]	67.1 x 7.05 x 0.149	73.5 x 7.05 x 0.149
Fuel plate pitch, [cm]	0.42	
Water gap between fuel plates, [cm]	0.271	
Cladding material	Al-6061	
Fuel Meat		
Material	U_3Si_2 - Al	
Dimension (HxWxT), [cm]	62.3 x 6.0 x 0.05066	
Burnable Poisons		
Material	Cadmium wire	
Quantity, (per side plate)	10	
Length, [cm]	50, centered at the height of the meat	
Diameter, [cm]	0.0485	
Location	*Counting from the external fuel plates, these cadmium wires are located at both sides of plate's number 1, 3, 5, 7, 9, 11, 13, 15, 17, and 19.*	
Side Plates		
Material	Al-6061	
Dimensions (HxWxT), [cm]	78 x 8.0 x 0.5	
Fuel Plate Slots		
	Internal	External
Quantity (per side plate)	17	2
Dimensions (HxWxT), [cm]	73.5 x 0.16 x 0.025	78 x 0.16 x 0.025
Note: these fuel plate slots are filled with water and grooved in side plates		

Table 3.11 (cont'd): Measured geometrical data for SFA.

Cadmium Wire Slots		
	Internal	External
Quantity (per side plate)	8	2
Dimensions (HxWxT), [cm]	65.5 x 0.06 x 0.05	70.0 x 0.06 x 0.05
Note: these cadmium wire slots are filled with water and grooved in side plates		
General Information		
Water space between fuel assemblies, [cm]	0.1	

3.2.2.2. Control Fuel Assembly (CFA).

CFA and CE geometrical data are summarized in table 3.12 and table 3.13, respectively.

Table 3.12: Measured geometrical data for CFA.

Total length, [cm]	161.1
CFA cross section (WxT), [cm]	7.6 x 8.0
Fuel Plates Characteristic	
	Only Internal Plates
Quantity	14
Dimensions (HxWxT), [cm]	67.1 x 7.05 x 0.149
Fuel plate pitch, [cm]	0.41
Water gap between fuel plates, [cm]	0.261
Cladding material	Al-6061
Fuel Meat	
Material	U_3Si_2 - Al
Dimension (HxWxT), [cm]	62.3 x 6.0 x 0.05066
Burnable Poison	
Material	Cadmium wire
Quantity (per side plate)	8
Length, [cm]	50, centered at the height of the meat
Diameter, [cm]	0.0485
Location	*Counting from the external fuel plates, these cadmium wires are located at both sides of plates number 1, 3, 5, 7, 8, 10, 12, and 14*
Side Plates	
Material	Al-6061
Dimensions (HxWxT), [cm]	78 x 8.0 x 0.5

Table 3.12 (cont'd): Measured geometrical data for CFA.

Fuel plate slots and cadmium wire slots dimensions are the same for SFA and CFA		
Guide Plates*		
	Internal	External
Quantity	2	2
Dimensions (HxWxT), [cm]	67.1 x 7.05 x 0.13	78 x 7.05 x 0.13
Material	Al-6061	
Guide Plate Slots		
	Internal	External
Quantity (per side plate)	2	2
Dimensions (HxWxT) [cm]	73.5 x 0.025x 0.13	78 x 0.025 x 0.13
Note: these guide plate slots are filled with water and grooved in side plates		
General Information		
Water gap between fuel plate and internal guide plate, [cm]	0.2705	
Water gap between internal and external guide plates, [cm]	0.61	
Water space between fuel assemblies, [cm]	0.1	

***** Guide plates were modeled as a rectangular shape by preserving its volume.

Table 3.13: Measured geometrical data for Control Element.

Control Element Geometry: Fork-Type with blades fitting into guide plates	
Quantity (per CFA)	**2**
Absorber Plate	
Material	AgInCd Alloy
Dimensions (HxWxT), [cm]	63.4 x 6.18 x 0.22
Note: It has a semicircular edges and a 0.1 cm deep circular indentation with a radius of curvature of 0.1625 cm on its positive side	
Control Element Cladding	
Material	Stainless Steel Type AISI 304L
Dimensions (HxWxT), [cm]	86.7 x 6.49 x 0.43
Inner Space in the Cladding	
Dimensions (HxWxT), [cm]	63.4 x 6.35 x 0.29
Note: this internal space is where the AgInCd plate is placed. It can be noticed that there is a small void gap between the inner space and the AgInCd plate.	

Table 3.13 (cont'd): Measured geometrical data for Control Element.

General Information	
Control element stroke, [cm]	63.0
Note: the control element is placed at the center of the water gap between guide plates	

3.2.2.3. Irradiation box.

The irradiation box consists of a block of aluminum with a hole filled with water, table 3.14.

Table 3.14: Measured geometrical data for irradiation box.

Aluminum Block Characteristic		
	Outer Al block	Inner Al block
Dimensions (HxWxT), [cm]	105.7 x 7.81 x 7.63	89.2 x 7.1 x 6.9
Material	Natural aluminum	

3.2.2.4. Graphite block.

The graphite block is composed of a block of aluminum that has a hole where a block of graphite is placed, table 3.15.

Table 3.15: Measured geometrical data for graphite block.

Aluminum Block Characteristic		
	Outer Al block	Inner Al block
Dimensions (HxWxT), [cm]	72.9 x 7.81 x 7.63	67.6 x 7.08 x 6.9
Material	Natural aluminum	
Graphite Block Characteristic		
Dimensions (HxWxT), [cm]	67.5 x 7.0 x 6.8	
Material	Graphite	
Note: the empty space between the inner Al block and graphite block is void		

3.2.2.5. BNCT filter.

The BNCT filter is composed of aluminum bricks, cadmium sheets and alumina bricks, table 3.16.

Table 3.16: Measured geometrical data for BNCT filter.

Aluminum Bricks		
	First	Second
Dimensions (HxWxT) [cm]	82.35 x 77.1 x 17	82.35 x 77.1 x 10
Location	*The first aluminum brick extend from the first row of the core grid to a 17 cm long, then following this is the first cadmium sheet. After that, it comes the second aluminum brick that has a 10 cm thickness.*	
Material	Natural aluminum	
Cadmium Sheets		
Dimensions (HxWxT), [cm]	82.35 x 77.1 x 0.15	
Location	*There is two cadmium sheets. The first is after the first aluminum brick and the second is after the second aluminum brick.*	
Material	Cadmium	
Alumina Bricks		
Dimensions (HxWxT), [cm]	82.35 x 77.1 x 60.3	
Location	*The alumina bricks begins from the second cadmium sheet to the end of the reactor pool.*	
Material	Alumina (Al_2O_3)	

3.2.2.6. Reactor pool and core support grid.

The reactor pool is a cylindrical and made of stainless steel with a 2.4 m diameter and 10.4 m high. The core grid is placed at 8.9 m deep of a rectangular shape of 8x10 positions in which is located over a supporting structure. The thickness of the grid is 20 cm of 99.5% pure aluminum. The core grid's center coincide with the vertical axis of the reactor pool.

3.2.2.7. Core configuration.

The first critical and first operating core configurations are presented in Fig. 3.1 and Fig. 3.2

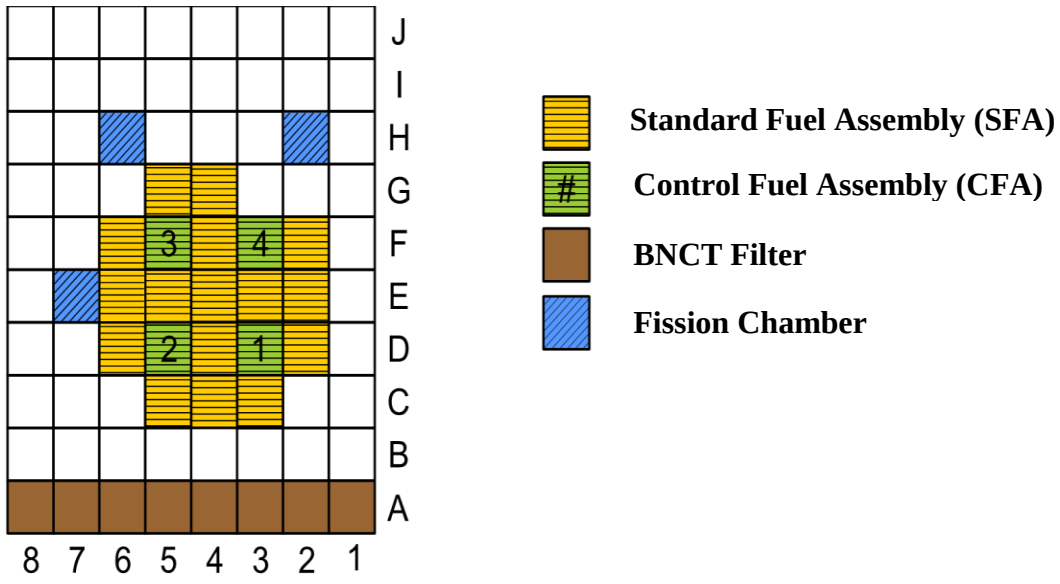

Fig. 3.1: First critical core configuration, (Core No. 7), [16].

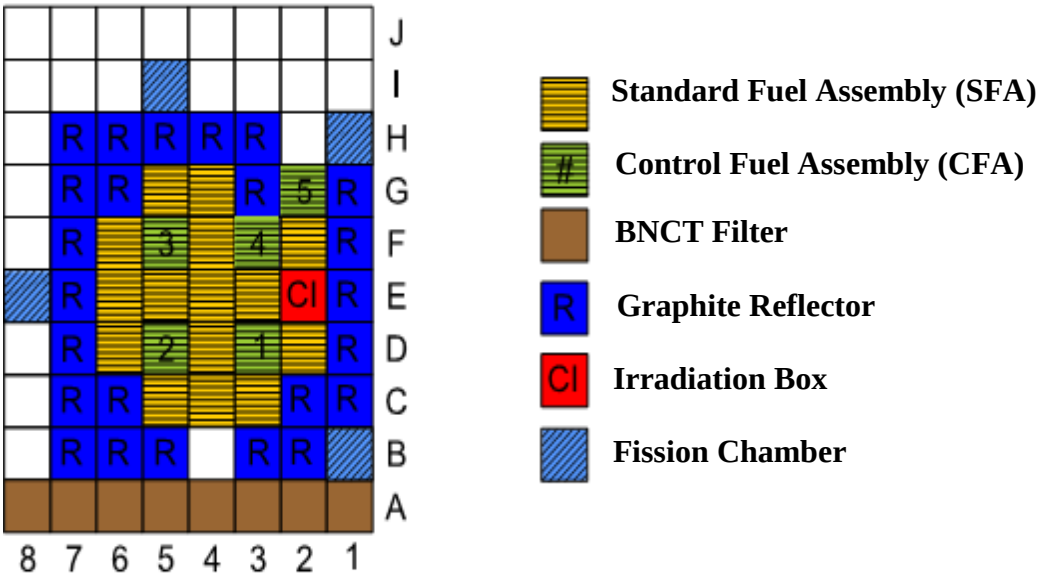

Fig. 3.2: First operating core configuration, (Core No. 11), [16].

3.3. Calculation Models.

The calculation models involve cell calculation models and core calculation models. First, the necessary assumption that was made during modeling is presented under model description subsection. Second, the following cell calculation models are shown: SFA, CFA, graphite reflector, irradiation box, BNCT filter and water reflector. Finally, the core calculation models of both core configurations are demonstrated.

3.3.1. Model description.

The following assumptions were considered in the calculation models:

- The isotopes that did not exist in the ESIN 2001 library, were omitted because of their lower content. Those isotopes belong to the structural material Al-6061. The omitted isotopes and their contents are: Zn (0.001 wt%) and Li (1 ppm).
- Average measured values were used instead of nominal values for the material and the geometrical specifications.
- Half of the maximum impurity content was considered, unless the impurity was specified.
- CE and guide plates were modeled as a rectangle by preserving their volumes.
- The void in the CE between the AgInCd plate and the stainless steel cladding was eliminated by merging the void to the cladding. This process was done under the cladding mass conservation. The result of this process was a reduction in the cladding density.
- The existed void between the graphite block and the aluminum cladding was merged into the cladding. The result of this process was a reduction in the aluminum cladding density.
- A quarter of the 2D cell calculation models for the SFA and CFA was decided because of the symmetry of SFA and CFA.

3.3.2. Cell calculation models.

Cell calculation models include: SFA, CFA, graphite reflector, irradiation box, water reflector and BNCT filter.

3.3.2.1. SFA cell model.

Recalling that, the SFA has cadmium wires along its axial direction. Hence, a two SFA cell models were developed: one with Cd wires and another without. The SFA cell model with Cd wire is the only presented case, Fig. 3.3.

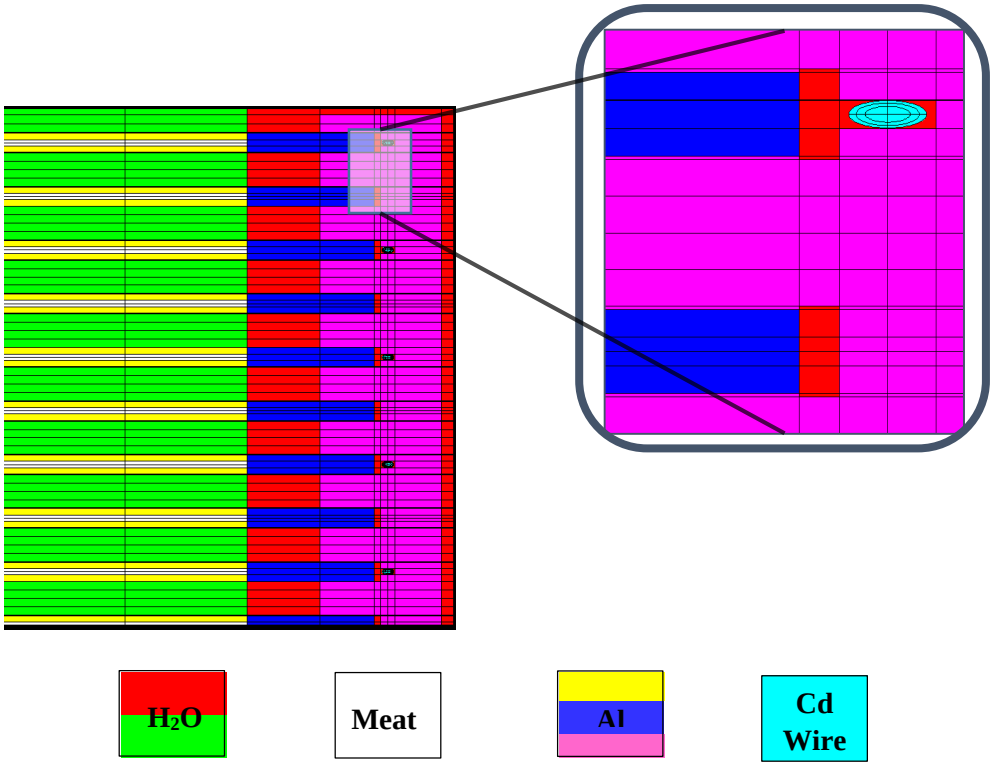

Fig. 3.3: 2D SFA model, on the right it shows a zoom in to the Cd wire.

The reason of having different colors for the same material refer to the homogenization process. The homogenization process took place as a two regions for the quarter model: First region contains aluminum, water and Cd wire whereas the second region has the meat, aluminum and water, Fig. 3.4.

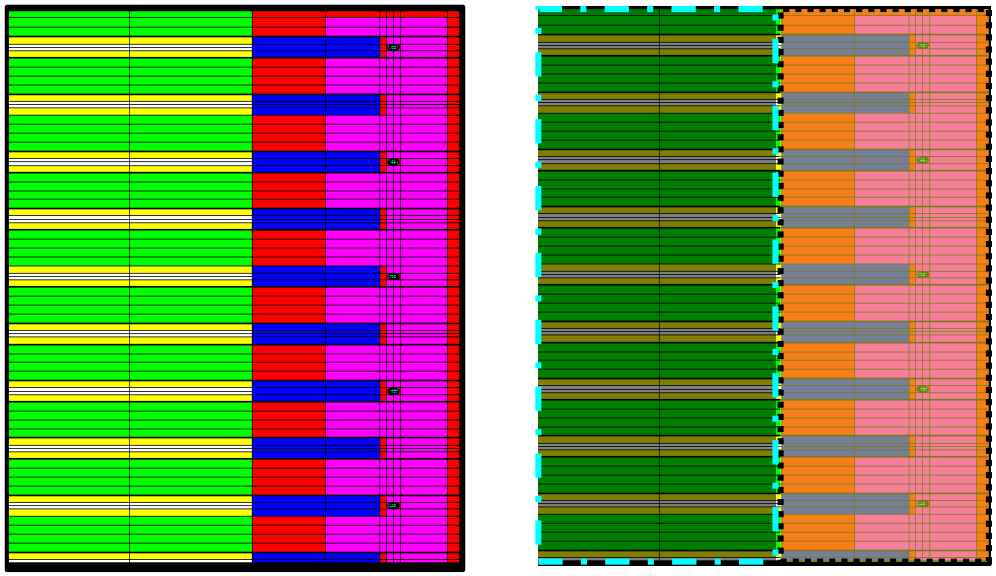

Fig. 3.4: SFA cell model (on the left) and a homogenized model (on the right).

3.3.2.2. CFA cell model.

There were four types of CFA cell models that were modeled. First model had the CFA without Cd wires and the CE was extracted. Second model had the CFA without the Cd wires but with the CE inserted. The third and fourth models were both with Cd wires. The third model had the CE extracted while the forth model had the CE inserted.

In this section, the CFA model with the Cd wire and with the CE inserted is presented with adding a homogenous SFA around the model in order to avoid the reflection of the CE, Fig. 3.5.

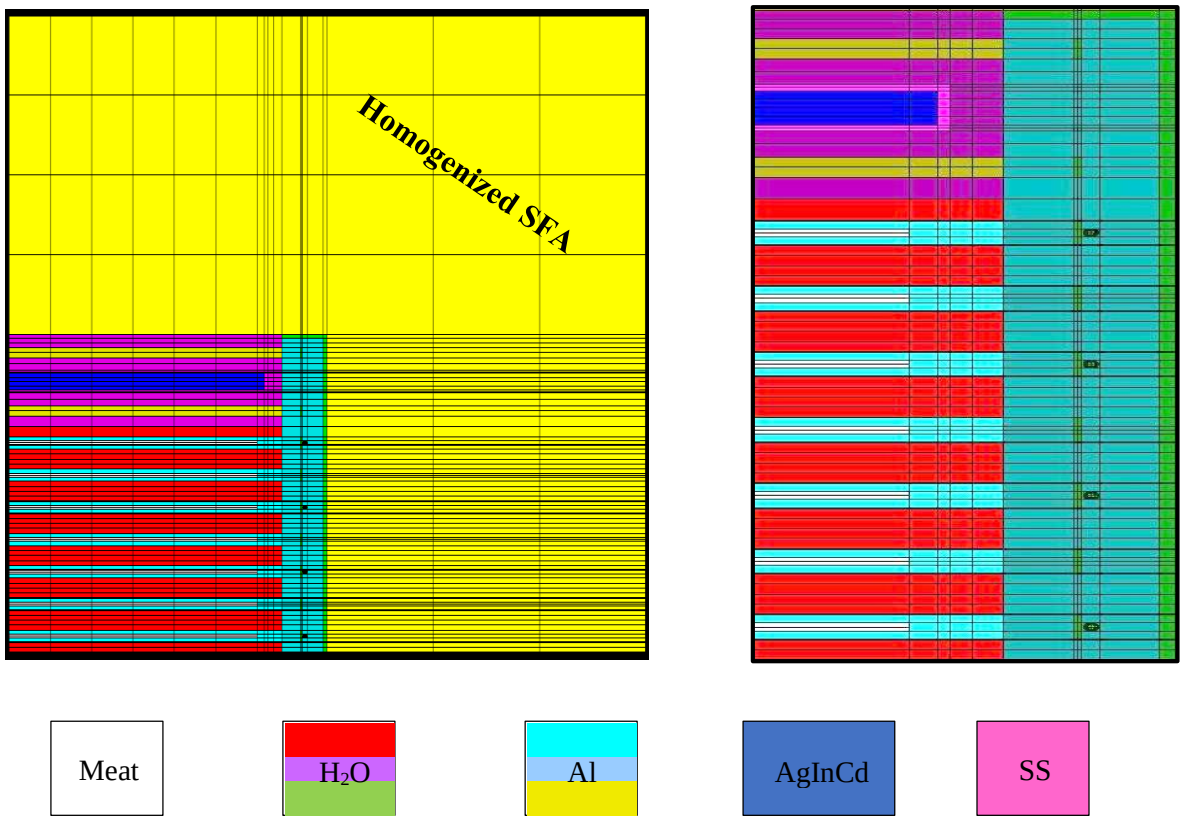

Fig. 3.5: CFA cell model with AgInCd plate inserted and with Cd wire, on the right a zoom in to CFA.

After that, a homogenization process was done as a three regions for the quarter CFA model: the First region includes the aluminum side plate with Cd wires and water frame, whereas the second region had the fuel plates and the water between them. The third region had the aluminum guide plates, the CE and the water in between, Fig. 3.6.

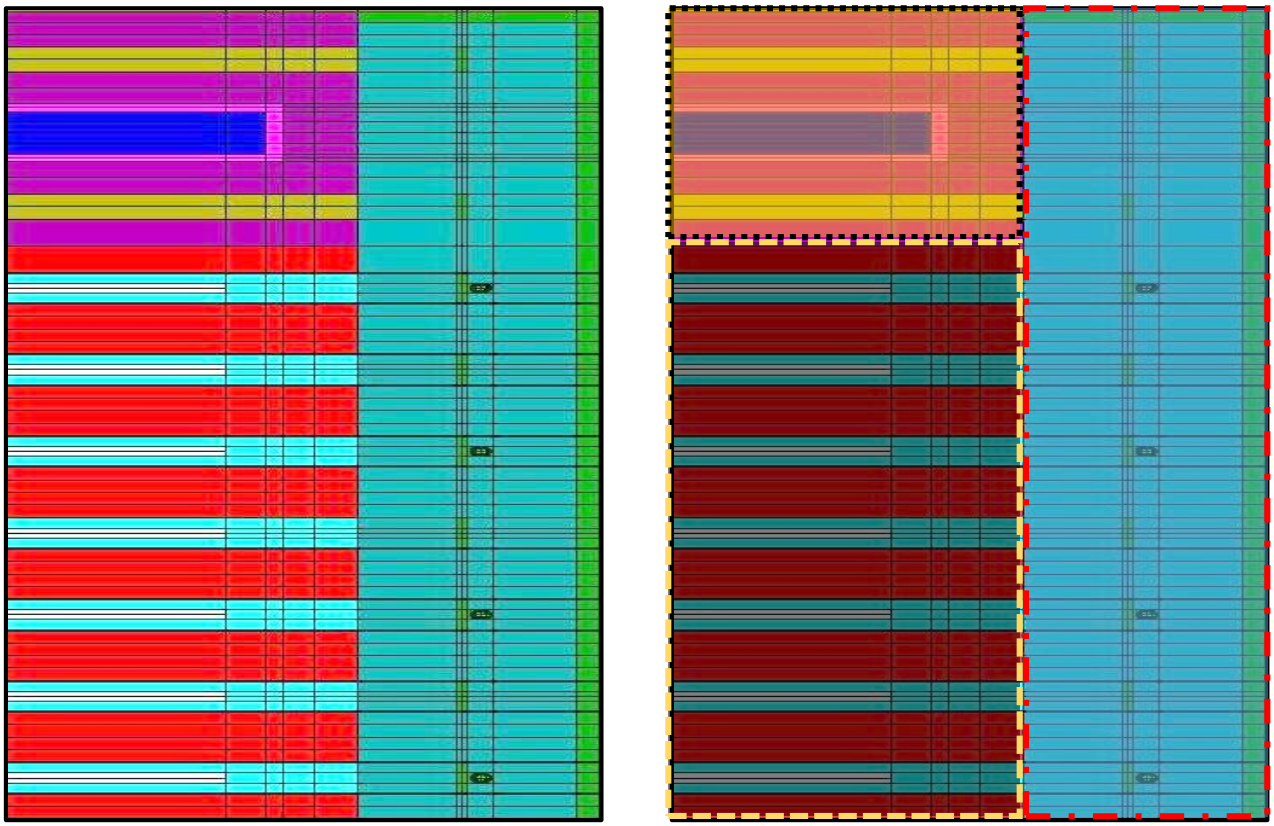

Fig. 3.6: CFA zoom in to the cell model (on the left) and a homogenous model (on the right).

3.3.2.3. Graphite block, water reflector and irradiation box cell models.

As was mentioned before that there was two core configurations for analysis. The graphite blocks and the irradiation box only exist in the first operating core configuration. 2D model was developed for the graphite blocks, irradiation box and water reflector for the first operating core configuration, Fig. 3.7, while for the first critical core configuration, a 1D water reflector model was developed. The water reflector model had 20.0 cm of water reflector: 10 cm water near the core and 10 cm far from the core.

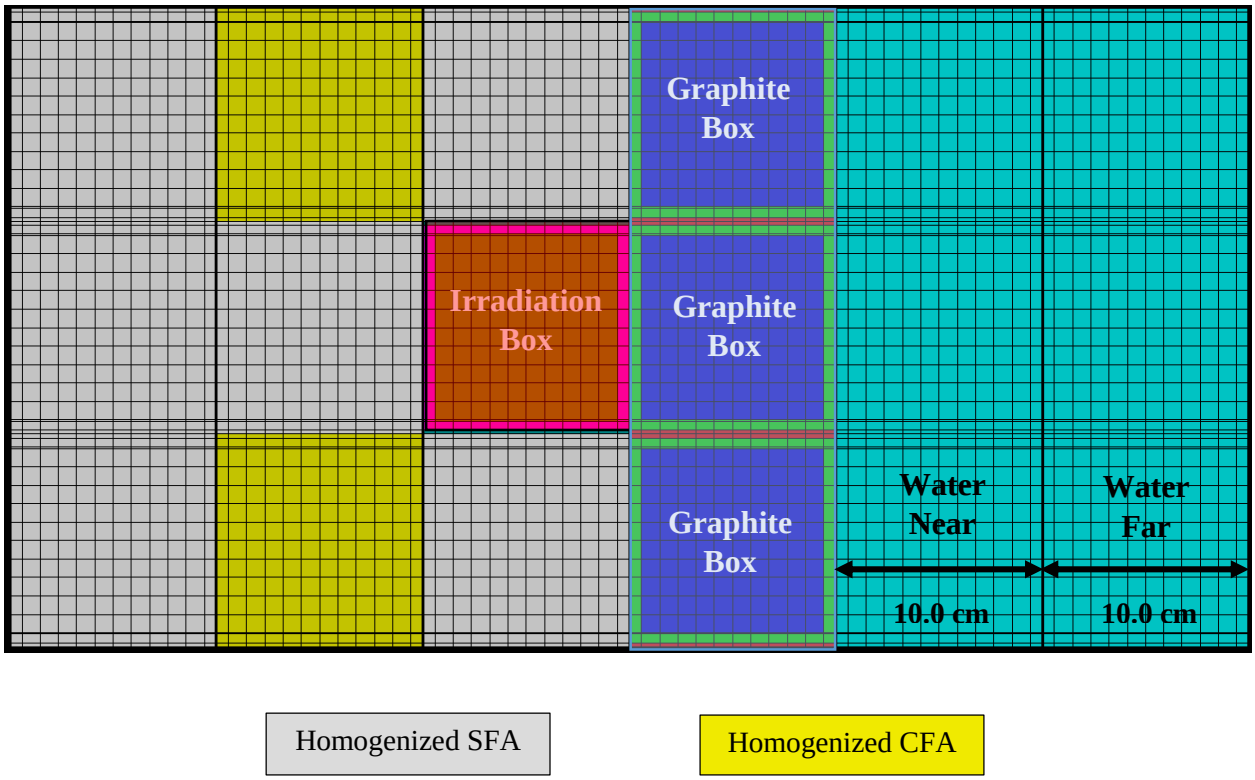

Fig. 3.7: Graphite box, irradiation box and water reflector cell model for core conf. no. 11.

The homogenization process was obtained by homogenizing the graphite block with its aluminum box. The irradiation box homogenization was done by homogenizing the aluminum box with the inner filled water.

3.3.2.4. BNCT filter cell model.

A 1D model was selected along the y-axis of both core configurations to extract the first 8.10 cm of Al filter.

3.3.3. Core calculation models.

A 3D two core models were used for both core configurations. A total of 193 mesh points along x – direction, 159 mesh points along y – direction and 138 mesh points along z – direction were used. The reactor core was reflected by light water. The energy group structure was of 3 groups; the lower limit of each group is: 0.0, 0.625 and 0.821E6 eV. An exception of 10 groups structure was applied in calculating kinetic parameters, which will be explained later in Section 3.4. In z – direction, a channel map of 63.0 cm height and 21 axial layers were used, Fig. 3.8. The 21 axial layers correspond to: 2 layers without Cd, 16 layers with Cd, 2 layers without Cd and the last layer for aluminum. These 21 axial layers were not equidistance.

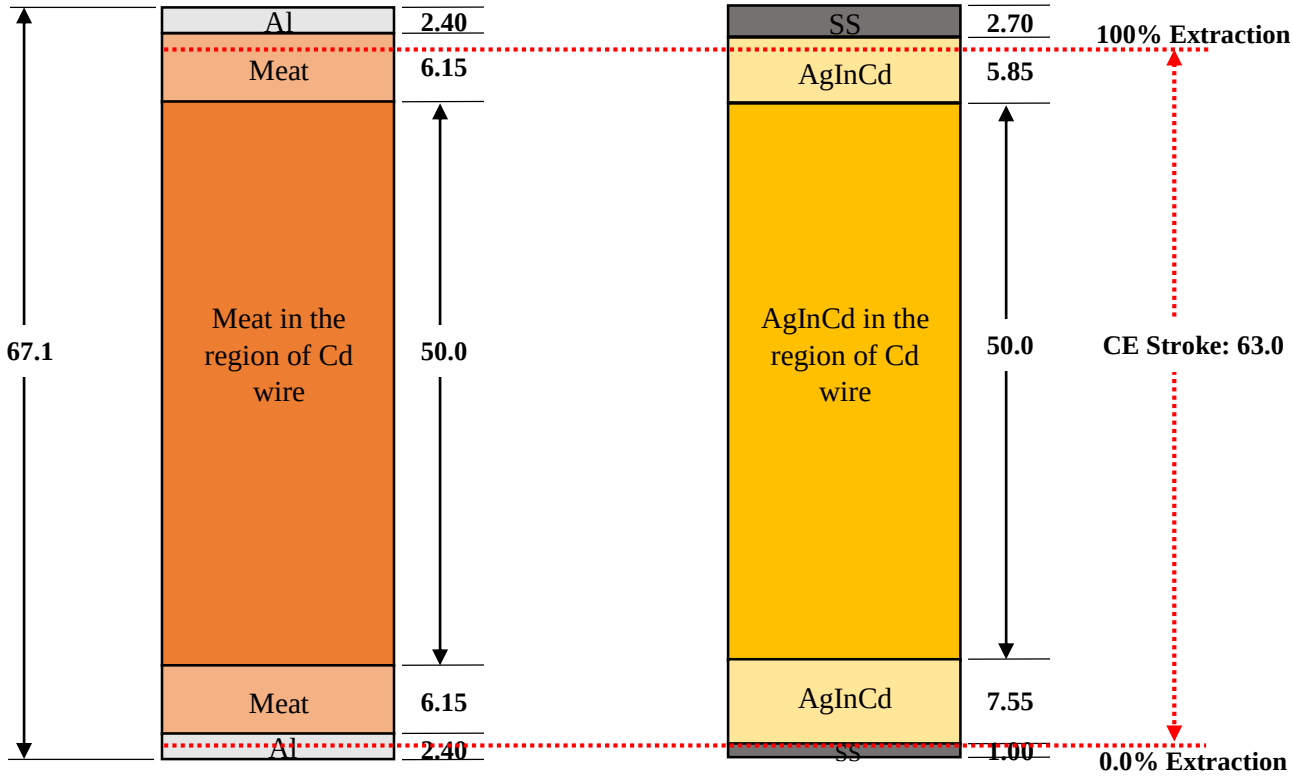

Fig. 3.8: Axial details of core model, FA meat (left) and CE (right). All dimensions are in cm.

Radial details of first critical and operating core models are presented in Fig. 3.9 and Fig. 3.10, respectively.

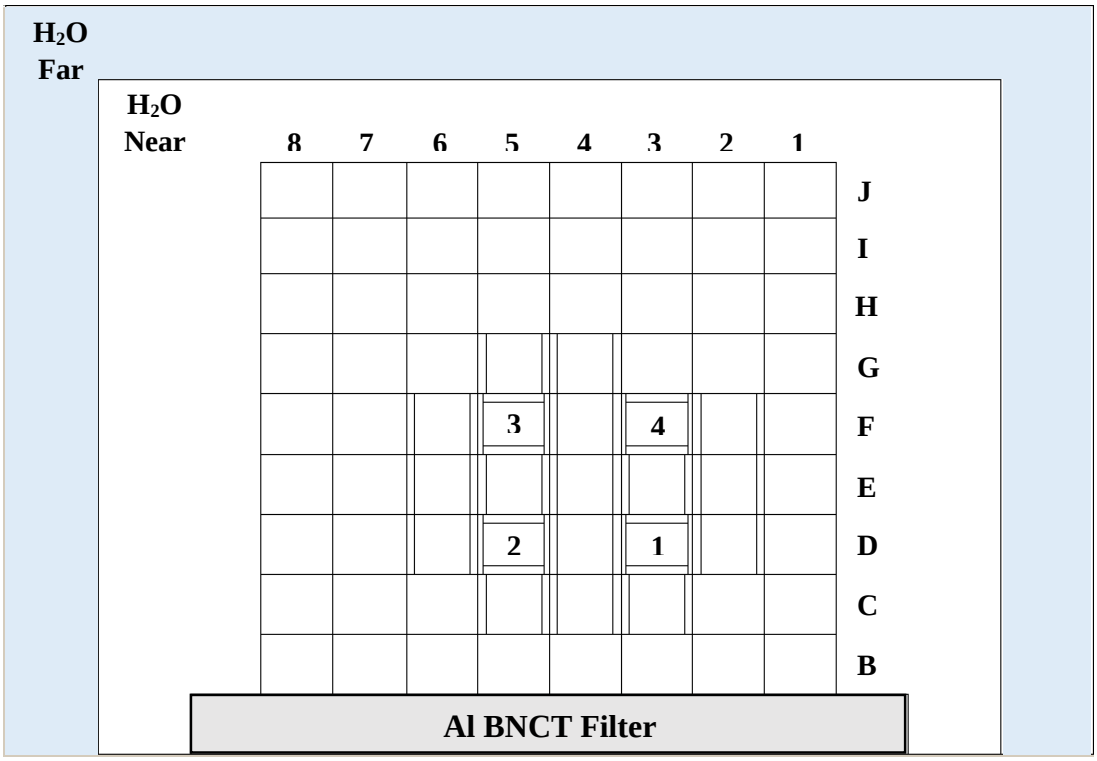

Fig. 3.9: First critical core model, 16 SFAs and 4 CFAs (32.5 Kg of U).

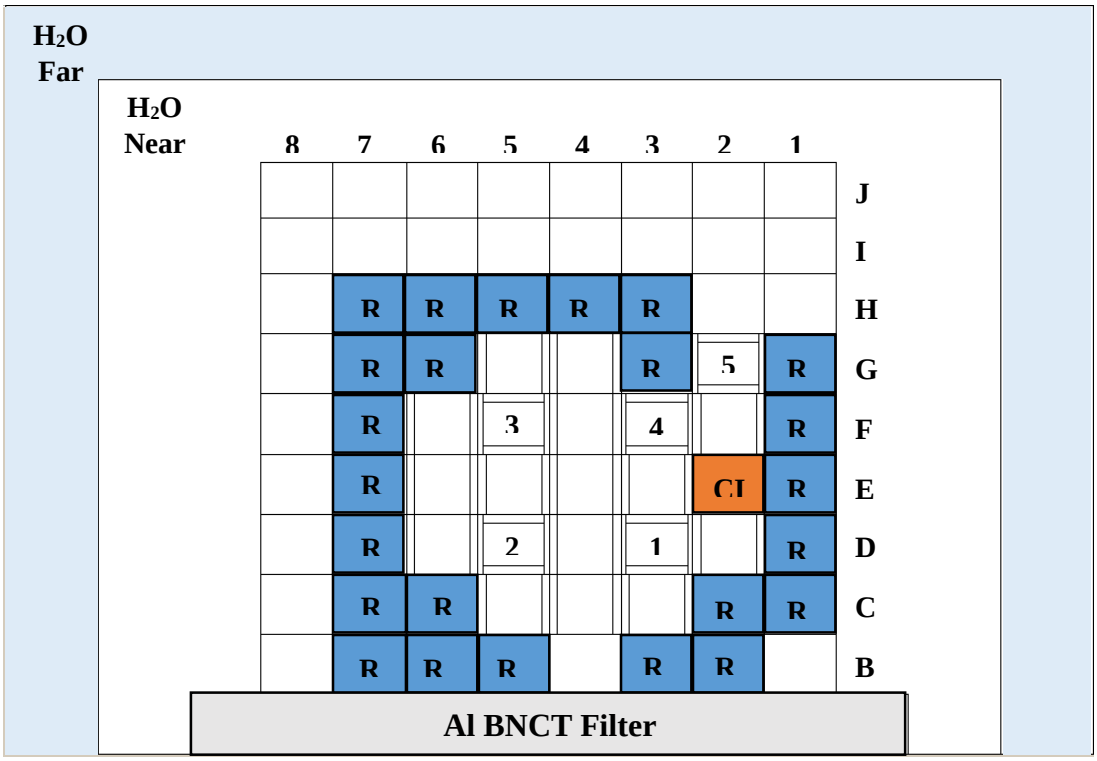

Fig. 3.10: First operating core model, 15 SFAs and 5 CFAs (32.1 Kg of U).

3.4. Results and Analysis.

The following measurements were analyzed in depth using the calculation line CONDOR2.62-CITVAP3.8: Control Elements Calibration, Excess Reactivity, Shutdown Margin, Isothermal Feedback Coefficient, Void Feedback Coefficient, Power Feedback Coefficient and α-Kinetic Parameter.

Regarding the experimental data, the following kinetic constants were used, [14], to obtain the core reactivity, table 3.17.

Table 3.17: Kinetic constants used in processing RA-6 experimental data, [14].

Delayed neutrons groups	Relative yield fraction, β_i/β_{eff}	Decay constant, λ_i, [s^{-1}]
1	0.038	0.0127
2	0.213	0.0317
3	0.188	0.1150
4	0.407	0.3110
5	0.128	1.4000
6	0.026	3.8700
	β_{eff} = 762 pcm	$\sum_{i=1}^{6} \frac{\beta_i}{\lambda_i} = 12.75\ sec$

3.4.1. Control Elements Calibration

3.4.1.1. Experimental procedure

The control elements calibration was experimentally measured as following: First, gradual extraction of a given Control Element (CE) by a step of about 5%, hence, the core state will become supercritical. Due to this supercriticality, the neutron population increased. Second, the evolution of neutron population was recorded to determine the reactor period[2]. From the reactor period, the reactivity of the extracted length is calculated according to the inhour equation using the kinetic constants of table 3.17. Third, to compensate for the inserted reactivity, another CE was inserted, hence, the core state became critical again. Finally, the core critical point was registered, [15]. This process was repeated until achieving a full extraction of the CE. After that process, the calculated reactivity was plotted against the percentage of CE extraction.

[2] Reactor Period: the time needed for the neutron population to be multiplied by e.

The outcomes from the experimental measurement of CEs calibration were: a plot of CE accumulated reactivity vs. percentage of extraction for each CE, the determination of Control Elements Worth (CEWs), a record for the critical and supercritical points.

Critical points for the first operating core configuration were taken from CEs calibration experiment and a single point from approach to criticality by CEs. There was a single critical point registered for first critical core, which was reported from the approach to criticality by CEs. Table 3.18 presents the CEs configuration of the approach to criticality by CEs experiment for the first critical core and the first operating core.

Table 3.18: Approach to criticality by control elements experimental data, [16].

Control Rod No.	**% of Extraction**	
	First Critical Core	**First Operating Core**
1	100.0%	100.0%
2	100.0%	60.2%
3	100.0%	22.0%
4	59.50%	100.0%
5	-	38.9%

3.4.1.2. Calculation procedure

A simulation of the experimental procedure was done by using the recorded critical and supercritical points, [15]. The expected outcomes from this step are as follows:

(a) Criticality calculation simulation using all the registered critical points.

(b) Plot of CEs accumulated reactivity vs. percentage of extraction.

(c) Determination of Control Elements Worth.

3.4.1.3. Results and analysis

Due to its importance, criticality calculation was presented first as a benchmarking for the future calculations.

There was 142 critical points recorded from the CEs calibration of the first operating core configuration and a point for first critical core configuration. The average of the results and 1σ standard deviation of these critical points are summarized in table 3.19.

Table 3.19: Criticality calculation simulation for all the registered critical points [3].

	No. of critical points	Reactivity, [pcm]
First Critical Core	1	556
First Operating Core	142	209 ± 109[4]

The reactivity values of the 142 critical points was plotted against each critical point.

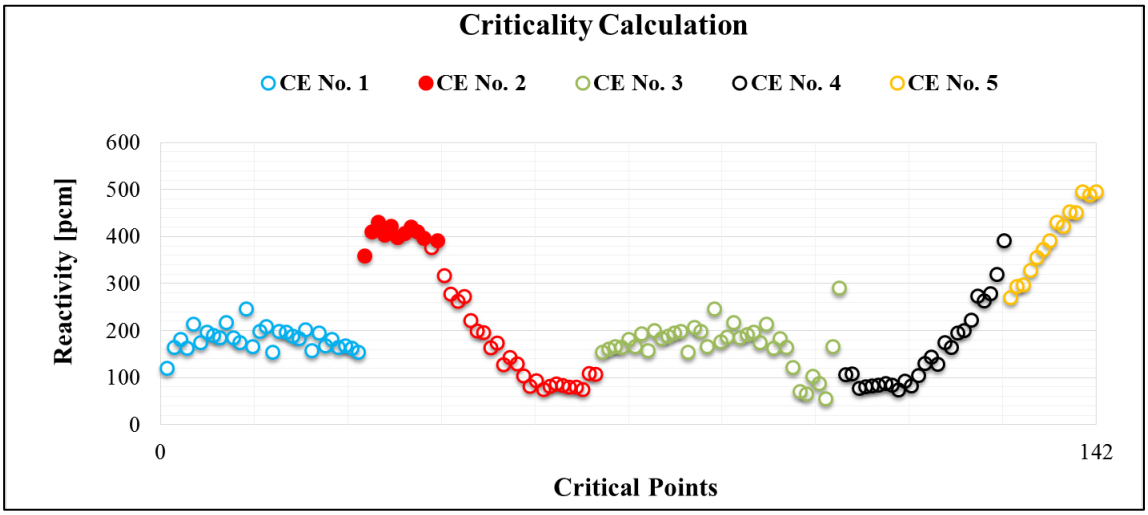

Fig. 3.11: Calculated reactivity for each experimental critical point.

Fig. 3.11 shows the criticality simulation for each registered critical point. It can be noticed an existence of reactivity slope of the calculated reactivity for the critical points of the CE No. 2, in which it begins from the critical point No. 42 to No. 66 (end of critical points of the CE No. 2). From the critical point No. 42 to No. 66, CE No. 2 was calibrated against CE No. 4, which was very close to CE No. 5 (the fine CE), referee to Fig. 3.2. As well, an increase of reactivity was observed for each critical point of CE No. 5, which was at the board of the core where the neutron leakage is significant.

The calculated control elements calibration are presented in Fig.3.12 and 3.13 with the experimental data.

[3] Note: The following results are the final results obtained after the checking process of section 3.5
[4] Correspond to 1σ standard deviation.

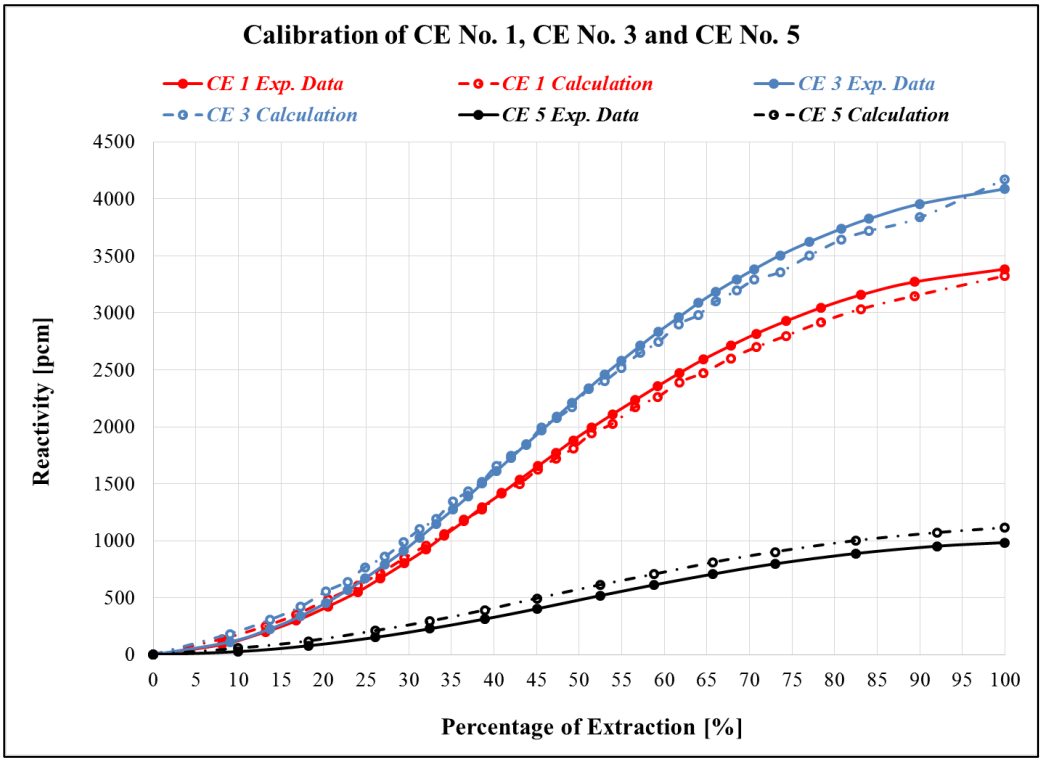

Fig. 3.12: Experimental data and calculated values of the calibration of CE No. 1, CE No. 3 and CE No. 5.

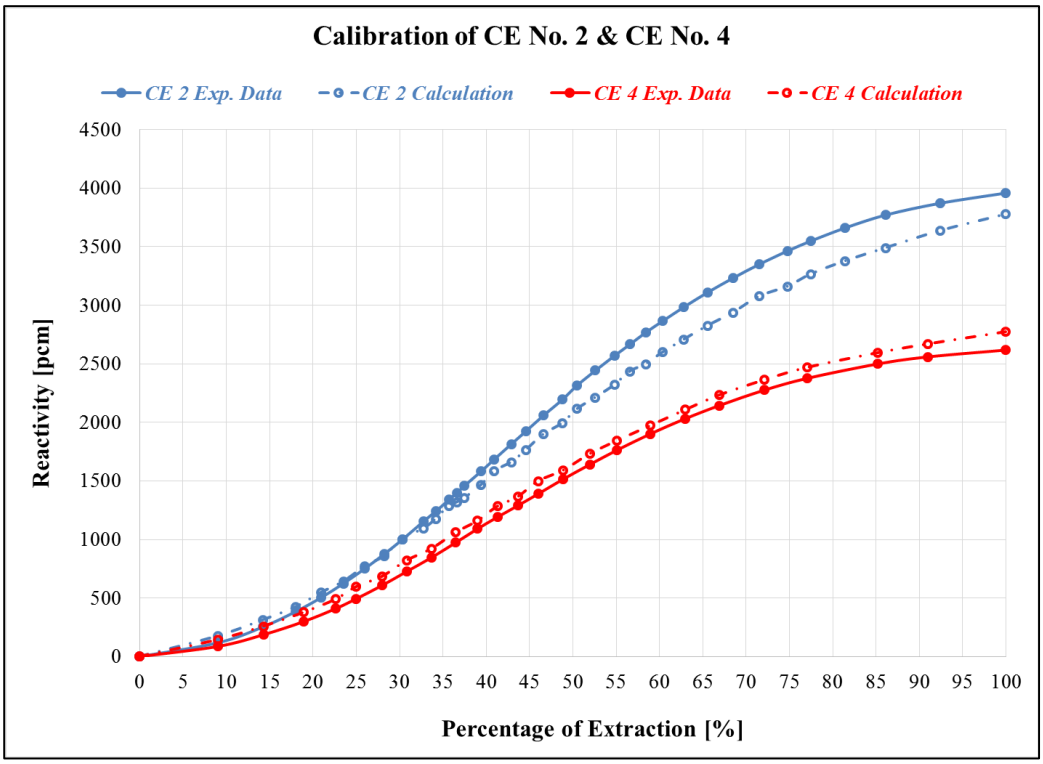

Fig. 3.13: Experimental data and calculated values of the calibration of CE No. 2 and CE No. 4.

The Control Element Worth (CEW) is defined as the total extracted CE reactivity worth. Table 3.20 shows the CEW for each CE and a comparison with the experimental data.

Table 3.20: Calculated and measured control element worth.

	Measured value, [17] [pcm]	**Calculated value, [pcm]**	**Differences with respect to measured value, [%]**
CEW No. 1	3385	3324	2%
CEW No. 2	3958	3775	5%
CEW No. 3	4089	4173	2%
CEW No. 4	2617	2774	6%
CEW No. 5	985	1115	13%

It can be noticed that the highest CEW occurred for CE No.3. All CEW differences were less than 6%, except for CEW No. 5 which gave a higher reactivity worth difference. This difference could be explained due to the fact that CE No. 5 is close to the border of the core, where the neutron leakage is more important. In addition, CE No.5 is so close to CE No. 4, in which a shadowing effect could be affecting the results.

3.4.2. Excess Reactivity and Total Shutdown Margin

3.4.2.1. Definition

The following is the definition of both excess reactivity and total Shutdown Margin (SDM):

- **Excess reactivity:** It is the core reactivity if all CEs were fully extracted.
- **Total SDM:** It is the core reactivity when all CEs are fully inserted.

3.4.2.2. Experimental procedure

The excess reactivity and total SDM were experimentally calculated at the same CEs critical configuration, [15]. Table 3.21 present the CEs critical configuration during the excess reactivity and total SDM measurement.

The excess reactivity was experimentally calculated by summing up only the inserted CEs reactivity worth.

The total SDM was experimentally calculated as the sum of all CEWs minus the excess reactivity, which is equal to the summation of the extracted CEs reactivity worth.

The methodology used to obtain both the excess reactivity and total SDM is called stable period method.

Table 3.21: CEs critical configuration during the measurement of excess reactivity and total SDM measurement, [15].

Control Element No.	% of Extraction
1	32.0%
2	31.2%
3	100%
4	100%
5	100%

3.4.2.3. Calculation procedure

The excess reactivity and total SDM were calculated in a similar fashion of the experimental data; by using the calculated CEs calibration curves, Fig. 3.12 and Fig. 3.13, and the reported CEs critical configuration.

3.4.2.4. Results and Analysis

The calculated and measured excess reactivity and total SDM is presented in table 3.22.

Table 3.22: Calculated value and measured data of excess reactivity and total SDM.

Excess Reactivity and Total SDM					
	Control Element No.	**% of Extraction**	**CEW, [pcm]**	**Extracted CE reactivity worth, [pcm]**	**Inserted CE reactivity worth, [pcm]**
Calculated Values	**1**	32.0%	3324	957	2367
	2	31.2%	3775	1035	2740
	3	100%	4173	4173	0.0
	4	100%	2774	2774	0.0
	5	100%	1115	1115	0.0
Calculated Excess Reactivity, [pcm]					**5107**
Measured Excess Reactivity, [16], [pcm]					**5346**
Differences between calculated and measured excess reactivity, [pcm, %]					**239, 5%**
Calculated total SDM, [pcm]					**-10054**
Measured total SDM[5], [pcm]					**-9687**
Differences between calculated and measured total SDM, [pcm, %]					**367, 4%**

[5] This value was calculated by the Author. During commissioning measurements', this value was obtained by the integral rod drop method because it is more conservative from the safety point of view.

3.4.3. SDM with a Single Failure of a Control Element

3.4.3.1. Definition

- **SDM with a single failure of a CE:** It is the core reactivity when all CEs are fully inserted minus one.

3.4.3.2. Experimental procedure

The SDM with a single failure of a CE was experimentally calculated by summing up all the extracted CEs reactivity worth minus one (to simulate a single failure). This way of calculating the SDM with a single failure of a CE is called the stable period method[6]. The technique used during the commission to measure the SDM with a single failure of a CE was the integral rod drop method[7].

The lowest value of the SDM with a single failure of a CE has an importance in the safety analysis as the worst case scenario. Usually, this value is associated with the failure of the CE that has the highest CEW.

Using the stable period method, the procedure to measure the SDM due to an assumption of a sequential failure scheme in CEs was conducted as follows: First, the core configuration was set to be critical by using all CEs minus at least one. Second, summing up all the extracted portion of CEs reactivity worth minus one, hence, to measure the SDM with a single failure of a CE. Third, this procedure was repeated to simulate the failure of the rest of the CEs. The CE No. 5, which is excluded from the SCRAM signal, was ignored in this sequential failure procedure.

Integral rod drop method, on the other hand, was implemented as follows: First, the core configuration was set to be critical by using all CEs minus at least one. Second, from this CEs critical configuration, all CEs dropped in the core minus one, hence, simulating the SDM with a failure of the non-dropped CE. Third, this procedure was repeated to simulate the failure of the rest of CEs. As was mentioned earlier CE No. 5 was discounted from this sequential failure procedure.

Table 3.23 presents the CEs critical configuration during the measurement of the SDM with a single failure of a CE, [18].

[6] The Author used this method for the analysis.
[7] In order to be a conservative from the safety prospective, the integral rod drop method was used instead of the stable period method.

Table 3.23: CEs critical configuration during the measurement of the SDM with a single failure of a control element, shaded boxes means this CE was excluded from the sequential failure procedure, [18].

	% of Extraction				
	CE No. 1	**CE No. 2**	**CE No. 3**	**CE No. 4**	**CE No. 5[8]**
Simulating Failure of CE No. 1	100%	100%	28.4%	29.0%	100%
Simulating Failure of CE No. 2	100%	100%	28.4%	29.0%	100%
Simulating Failure of CE No. 3	32.0%	31.2%	100%	100%	100%
Simulating Failure of CE No. 4	32.0%	31.2%	100%	100%	100%

3.4.3.3. Calculation procedure

The SDM with a single failure of a CE was simulated using the deterministic calculation line CONDOR-CITVAP. It was obtained as per the experimental procedure by using both the stable period method and the integral rod drop method.

3.4.3.4. Results and Analysis

Experimental analysis is applied first to demonstrate a comparison between the stable period method and the integral rod drop method for the measurement of the SDM with a single failure of a CE.

Table 3.24 and table 3.25 show the experimental data for stable period method and integral rod drop method, respectively. A comparison was carried out between both methods, which are presented in table 3.26.

[8] CE No. 5 is excluded from the SCRAM signal.

Table 3.24: Experimental data of the SDM with a single failure of a CE using the "stable period method".

Experimental data of the SDM with a single failure of a CE "*Stable Period Method*"			
Control Element No.	**% of Extraction**	**CEW, [pcm]**	**Extracted CE reactivity worth, [pcm]**
1	100%	3385	3385
2	100%	3958	3958
3	28.4%	4089	858
4	29.0%	2617	651
5	100%	985	985
SDM with Failure of CE No. 1, [pcm]			**-6451**
SDM with Failure of CE No. 2, [pcm]			**-5878**
Control Element No.	**% of Extraction**	**CEW, [pcm]**	**Extracted CE reactivity worth, [pcm]**
1	32.0%	3385	924
2	31.2%	3958	1056
3	100%	4089	4089
4	100%	2617	2617
5	100%	985	985
SDM with Failure of CE No. 3, [pcm]			**-5582**
SDM with Failure of CE No. 4, [pcm]			**-7053**

Table 3.25: Experimental data of the SDM with a single failure of a CE using the "integral rod drop method".

Experimental data of the SDM with a single failure of a CE "*Integral Rod Drop Method*"		
Control Element No.	**SDM with a Single Failure of a CE From the readings of (CIC[9] -1), [pcm]**	**SDM with a Single Failure of a CE From the readings of (CIC -2), [pcm]**
1	-5959*	-6924[10]
2	-5109[10]	-4737*
3	-5380[10]	-4882*
4	-6836*	-6837[10]

* The only lowered value between the two readings was reported, [17].

[9] CIC: Compensated Ionization Chamber.

[10] These values were obtained by the Author through the application of the equation in Appendix-B.

Table 3.26: Comparison between the stable period method and the integral rod drop method for the experimental measurement of the SDM with a single failure of a CE.

Experimental Data of the SDM with a single failure of a CE			
	Stable Period Method, [pcm]	**Average value of Integral Rod Drop Method, [pcm]**	**Differences, [%]**
SDM with Failure of CE No. 1	-6451	-6442	0.1%
SDM with Failure of CE No. 2	-5878	-4923	16%
SDM with Failure of CE No. 3	-5582	-5131	8%
SDM with Failure of CE No. 4	-7053	-6837	3%

Experimentally speaking, the integral rod drop method has a higher deviation than the stable period method. The main reason of that is the errors induced by harmonics. The harmonics are the deviations of the actual measured spatial flux distribution from the fundamental mode. The prompt harmonics, which are the deviation of the prompt neutron distribution from the prompt persisting mode, are the major contributor to the large systematic errors usually found in the integral rod drop technique. In locations where a CIC is close to a dropped CE (where the harmonics are positive) the measured reactivity is larger than the other measured reactivity from the farthest CIC.

It is worth to mention that the lowest SDM with a single failure of a CE coincide with the failure of CE No. 2 by using the integral rod drop technique, while using the stable period technique the lowest SDM with a single failure of a CE was found with the failure of CE No. 3, which had the highest CEW.

After a deep analyses of the experimental data, a simulation of the SDM with a single failure of a CE was performed as the experimental procedure. Table 3.27 and table 3.28 present the calculated SDM with a single failure of a CE using the two different techniques: stable period method and integral rod drop method.

Table 3.27: Calculated values of the SDM with a single failure of a CE using the "stable period method".

Calculated values of the SDM with a single failure of a CE "*Stable Period Method*"			
Control Element No.	**% of Extraction**	**CEW, [pcm]**	**Extracted CE reactivity worth, [pcm]**
1	100%	3324	3324
2	100%	3775	3775
3	28.4%	4173	929
4	29.0%	2774	733
5	100%	1115	1115
SDM with Failure of CE No. 1, [pcm]			**-6552**
SDM with Failure of CE No. 2, [pcm]			**-6101**
Control Element No.	**% of Extraction**	**CEW, [pcm]**	**Extracted CE reactivity worth, [pcm]**
1	32.0%	3324	957
2	31.2%	3775	1035
3	100%	4173	4173
4	100%	2774	2774
5	100%	1115	1115
SDM with Failure of CE No. 3, [pcm]			**-5881**
SDM with Failure of CE No. 4, [pcm]			**-7280**

Table 3.28: Calculated values of the SDM with a single failure of a CE using the "integral rod drop method".

Calculated values of the SDM with a single failure of a CE "*Integral Rod Drop Method*"	
Control Element No.	**SDM with a Single Failure of a CE, [pcm]**
1	-6026
2	-5161
3	-5250
4	-6550

A comparison between the calculated values and experimentally measured data of the SDM with a single failure of a CE by using both techniques are shown in table 3.29 and table 3.30.

Table 3.29: Comparison between the calculated values and experimentally measured data of the SDM with a single failure of a CE by using the "Stable Period Method".

Comparison of the calculated and measured data – "Stable Period Method"			
	Measured value[11], [pcm]	**Calculated value, [pcm]**	**Differences, [%]**
SDM with Failure of CE No. 1	-6451	-6552	2%
SDM with Failure of CE No. 2	-5878	-6101	4%
SDM with Failure of CE No. 3	-5582	-5881	5%
SDM with Failure of CE No. 4	-7053	-7280	3%

Table 3.30: Comparison between the calculated values and experimentally measured data of the SDM with a single failure of a CE by using the "Integral Rod Drop Method".

Comparison of the calculated and measured data – "Integral Rod Drop Method"			
	Average measured value, [pcm]	**Calculated value, [pcm]**	**Differences, [%]**
SDM with Failure of CE No. 1	-6442	-6026	6%
SDM with Failure of CE No. 2	-4923	-5161	5%
SDM with Failure of CE No. 3	-5131	-5250	2%
SDM with Failure of CE No. 4	-6837	-6550	4%

It can be noticed that the calculation using the stable period method yield a better comparison against experimental data, while higher differences were demonstrated in the case of the integral rod drop method. These higher differences are due to the fact that the spatial temporal flux beyond the integral rod drop method cannot be presented using the calculation line. This is a clear evidence of the previous explanation between the two methods.

[11] These values were obtain by the Author.

3.4.4. Isothermal Feedback Coefficient

3.4.4.1 Definition

- **Isothermal feedback coefficient:** It is the reactivity change per unit temperature change, equation (3.1).

$$\alpha_T = \frac{\rho - \rho_i}{T - T_i} \tag{3.1}$$

Where:
α_T: Isothermal feedback coefficient, [pcm/^{o}C].
ρ_i: Reference core reactivity, [pcm].
T_i: Reference core temperature, [^{o}C].

3.4.4.2 Experimental procedure

The experimental procedure to measure the isothermal feedback coefficient was conducted by heating up the reactor water pool from 24.5^{o}C to 31.5^{o}C by using the primary pump while the reactor power was kept at 100W$_{th}$ throughout the experiment. The heating rate was 1^{o}C/hr. Due to this heating, CE No. 5 was partially extracted in each step to maintain the criticality of the reactor. The percentage of extraction of CE No. 5 was registered, [19], per 0.5^{o}C step increase. There were 15 Critical Positions (CPs) registered in total.

The isothermal feedback coefficient was experimentally obtained by the following procedure[12]:

A) Subtract the reactivity inserted, due to the extraction of CE No. 5, with respect to the previous inserted reactivity. Then, dividing this reactivity difference over 0.5^{o}C gives the isothermal feedback coefficient.
B) Repeating the previous step for every 0.5^{o}C increase. A total of 14 values of the isothermal feedback coefficient were found.
C) An average value and 1σ standard deviation for all the 14 values of the isothermal feedback coefficient were obtained.

3.4.4.3 Calculation procedure

CONDOR-CITVAP calculation line was used to calculate the core reactivity associated with each experimental CP per temperature change. The calculation procedure was conducted as following:

- CONDOR: A library for all the macroscopic cross sections were generated for each temperature change from 24.5^{o}C to 31.5^{o}C in a step of 0.5^{o}C.
- CITVAP: for each temperature associated library, CITVAP was used to calculate core reactivities for all the experimentally registered CPs.

[12] This procedure was applied by the Author in order to obtain the experimental uncertainty associated with the isothermal feedback coefficient measurements. The reported value in Ref [17] was obtained by taking the summation of the ratio of reactivity difference with fixed reference at 24.5^{o}C corresponding reactivity over the temperature increase, then dividing this summation by the number of points.

3.4.4.4 Results and Analysis

An evaluation of the experimental data was carried to determine the experimental uncertainty associated with the measurement of the isothermal feedback coefficient. By applying the experimental procedure mentioned earlier, isothermal feedback coefficient was obtained. Fig 3.14 presents each isothermal feedback coefficients, the average value for all the isothermal feedback coefficients and the associated 1σ standard division.

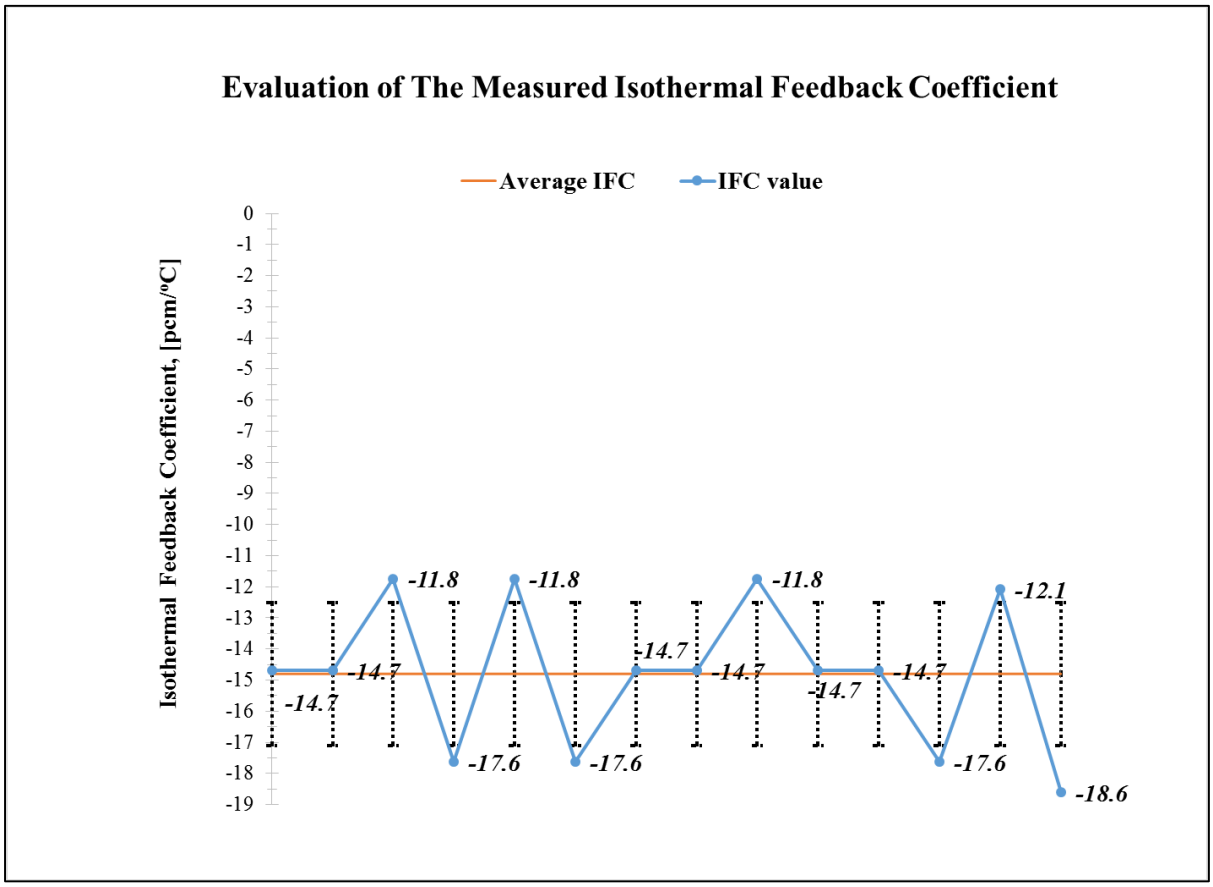

Fig. 3.14: Measurement of the isothermal feedback coefficients.

The calculation procedures were carried out to calculate the isothermal feedback coefficient. A plot of the core reactivity vs. temperature was obtained at the reported CPs and from 24.5°C to 31.5°C, Fig. 3.15.

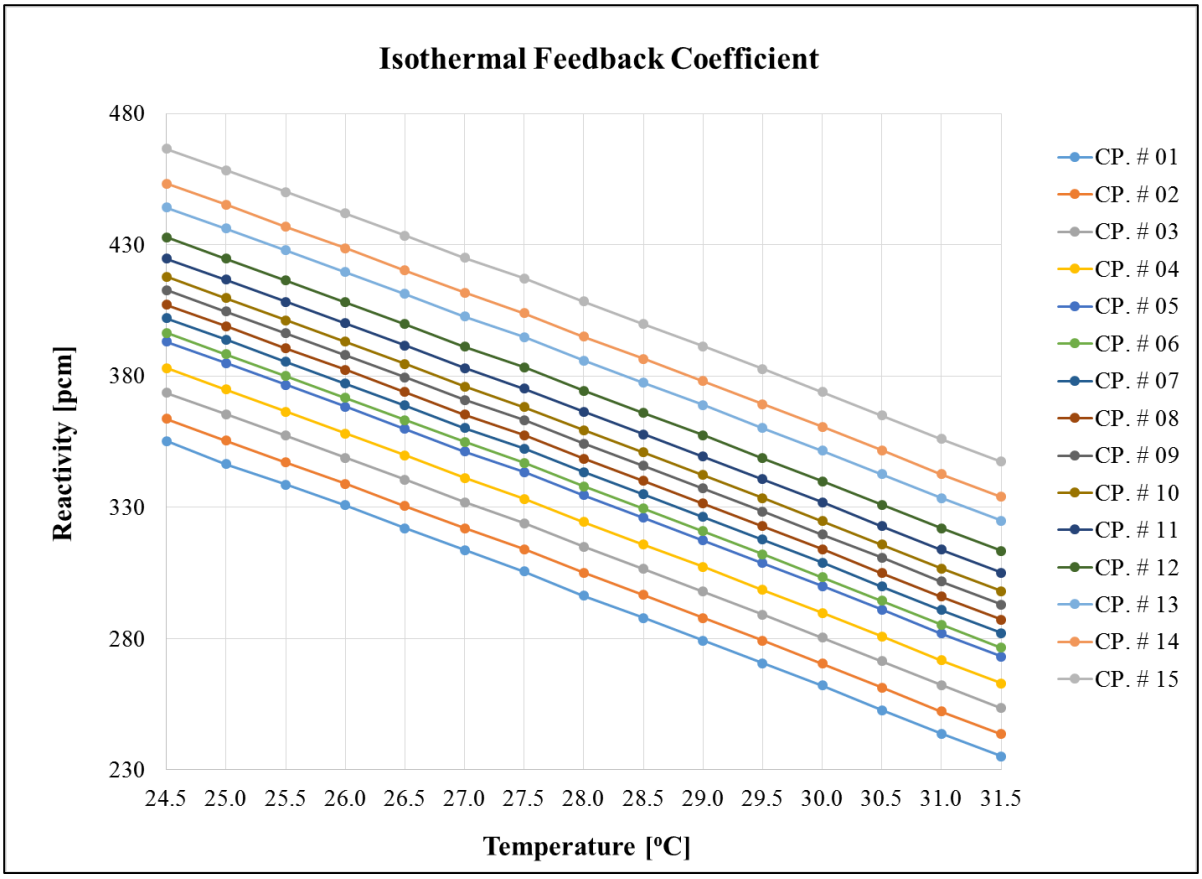

Fig. 3.15: Calculations of the isothermal feedback coefficient.

An average value for all slopes of these lines represent the calculated isothermal feedback coefficient. Table 3.31 presents the experimental data and the calculated value of isothermal feedback coefficient.

Table 3.31: Calculated and measured isothermal feedback coefficient.

	Isothermal Feedback Coefficient, [pcm/ºC]	**Differences with respect to measured value, [%]**
Measured value	-14.80 ± 2.30[13]	16%
Calculated value	-17.10 ± 0.04[14]	

It can be noticed that the calculated value of the isothermal feedback coefficient fall inside the range of the measured data.

[13] Experimental uncertainty at 1σ standard deviation. The average and standard deviation were calculated by the Author.
[14] Statistical uncertainty at 1σ standard deviation.

3.4.5. Void Feedback Coefficient

3.4.5.1 Definition

- **Void feedback coefficient:** It is the reactivity change per percent change of void content, equation (3.2).

$$\alpha_v = \frac{\rho_0 - \rho}{f_v} \tag{3.2}$$

Where:

α_v: Void feedback coefficient, [pcm/% void].
ρ_0: Core reactivity with the presence of void, [pcm].
ρ: Core reactivity without the presence of void, [pcm].
f_v: Percentage of void content, [% void].

3.4.5.2 Experimental procedure

The void feedback coefficient was obtained experimentally by introducing aluminum blades[15] inside the 7th coolant channel, counting from the BNCT filter, for all the SFAs in the core. CE No. 5 was partially extracted, due to the insertion of these aluminum blades, in order to maintain the core criticality state. The CP was recorded twice, table 3.32. The first time was before introducing aluminum blades, the second time was afterward. The increase of water level due to the insertion of these aluminum blades neutronically represent a local loss of the coolant density. The coolant density lost is equivalent to a certain percentage of void content in the core. This percentage was calculated using MCNP5 by changing water density for all SFAs and CFAs. The result of the void content was: (1.5 ± 0.2) % void, [20]. The ratio of the inserted reactivity over the percentage of void content represent the void feedback coefficient.

Table 3.32: Control elements experimental critical configuration during the void feedback coefficient measurement, [21].

Control Rod No.	% of Extraction	
	Before introducing Al blades	After introducing Al blades
1	100%	100%
2	28.7%	28.7%
3	60.5%	60.5%
4	100%	100%
5	0.0%	48.2%

[15] An aluminum blade has a 6.4 cm width, 0.1 cm thickness and a height of the internal plate of a SFA (67.1 cm).

3.4.5.3 Calculation procedure

The void feedback coefficient was simulated using the calculation line CONDOR-CITVAP. Two different approaches were applied:

A) Simulating the exact experimental procedure by inserting an aluminum blade per SFA model in the 7th position of the coolant channel, Fig. 3.16. Macroscopic cross sections were generated using CONDOR for two cases: with and without the Al blade. Then, obtaining the core reactivity difference using CITVAP for: First, by using both macroscopic cross sections libraries (with and without Al blade) for the same CE critical configuration when the Al blades were absent. Second, repeating the pervious step but using the same CE critical configuration after introducing the Al blades. This methodology of calculating the core reactivity difference is independent of CE movement. Another methodology was applied to calculate the core reactivity difference in which it depends on the CE movement. This methodology was done by simulating the two CE critical configurations (before and after the insertion of Al blades) per each macroscopic cross sections library generated. After that, core reactivity differences were obtained for each simulation methodology. The void feedback coefficient for the two methods was found by dividing the reactivity difference over the void percentage content. An average value of the void feedback coefficient for each method is presented in table 3.33.

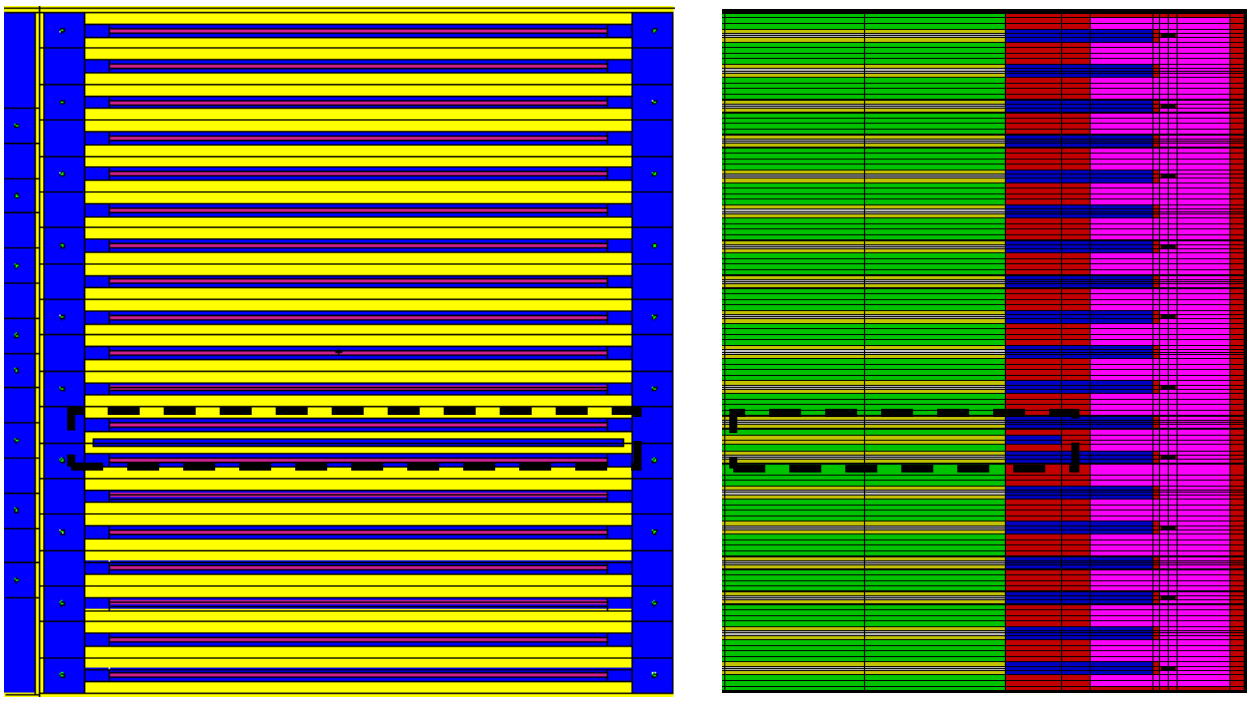

(a) (b)

Fig. 3.16: Location of the Al blade in the SFA model: (a) using MCNP5 code, [20], and (b) using CONDOR code.

B) The second approach was achieved by simulating a reduction in the water density of the SFA and the CFA equal to a presence of 1.5% void. Two set of macroscopic cross sections libraries were generated using CONDOR: one with a reduced water density of 1.5% in the SFA and the CFA, and another with a normal water density. After that, CITVAP was used to calculate the core reactivity difference using both libraries for each CE critical configuration: (a) the one that correspond to the case when the Al blades were not in the core and (b) when Al blades were inserted. A core reactivity difference between the two libraries was obtained for each case. Then, the void feedback coefficient was calculated by taking the ratio of the obtained core reactivity difference for each case over 1.5% of void content. An average value of the void feedback coefficients of this approach is presented in table 3.33.

3.4.5.4 Results and Analysis

The void feedback coefficient was calculated by two approaches and compared with experimental data, table 3.33.

Table 3.33: Calculated and measured void feedback coefficient.

	Void Feedback Coefficient [pcm/% void]	**Differences with respect to measured value [%]**
Measured value, [16]	-302 ± 27	-
First approach calculated value of the independent library method	-359	19%
First approach calculated value of the independent CE movement method	-290	4%
Second approach calculated value	-304	1%

It can be noticed that the calculated void feedback coefficient of the first approach of the method that fixes the CE critical configuration and change the macroscopic cross sections library, and the second approach are within the range of the experimental data. Here, the second approach yield in a more accurate simulation with respect to the experimental data. This is because the second approach simulate voids homogenously distributed in the core. While, the first approach represent voids heterogeneously distributed in the core (local loss of water density). Generally in similar research reactors, the second approach shows a better agreement with experimental data.

3.4.6. Power Feedback Coefficient

3.4.6.1. Definition

- **Power feedback coefficient:** It is the reactivity change per power change, equation (3.3).

$$\alpha_P = \frac{\rho - \rho_i}{P - P_i} \tag{3.3}$$

Where:
α_P: Power feedback coefficient, [pcm/MW_{th}].
ρ_i: Reference core reactivity, [pcm].
P_i: Reference core power, [MW_{th}].

3.4.6.2. Experimental procedure

The power feedback coefficient was indirectly measured by changing the critical position to obtain a power level change. Initially, the reactor power level was at 1KW_{th} critical, cold and without Xenon. Then, the power was raised up to the operating power level that was at 1MW_{th} and the criticality state was maintained. The CE configuration of this criticality state was recorded immediately after the increase of the power level in order to avoid the Xenon buildup. This increase in the reactor power was obtained by extracting CE No. 5. The reactivity difference due to the extraction of CE No. 5 represents the reactivity change due to the power increase. The ratio of the reactivity change per the reactor power increase from 1KW_{th} to 1MW_{th} represents the power feedback coefficient.

3.4.6.3. Calculation procedure

The calculated power feedback coefficient was found by incorporating a thermal-hydraulic model of the RA-6 in CITVAP code. In this framework, forced convection calculation was done to simulate the downstream forced convection flow of the RA-6.

The internally coupling process of TERMIC code into CITVAP code was achieved as following: (a) At the initial power level, axial power density profile was calculated by CITVAP for each SFA and CFA (power generating assemblies). (b) This axial power density profile was transmitted to TERMIC to calculate the axial profiles for fuel temperature, coolant temperature and coolant density. (c) After changing the power level, the axial profiles of the fuel temperature, the coolant temperature and the coolant density are recalculated by TERMIC and then transmitted back to CITVAP. (d) The macroscopic cross sections are adjusted by CITVAP to take into account the changes in the fuel temperature, the coolant temperature and the coolant density. (e) From this adjustment in the macroscopic cross sections, CITVAP calculates the new axial power density profile.

An earlier step was performed to generate a set of macroscopic cross sections that depends on fuel and coolant temperature using CONDOR. The coolant density variable was changed according to the variation in the coolant temperature using an internally embedded function in CONDOR. Namely, when the coolant temperature changes, the coolant density will automatically change.

The adjustment of the macroscopic cross sections is achieved using CITVAP through a liner interpolation. CITVAP can handle at one time an interpolation between macroscopic cross sections per a variable (i.e. fuel temperature, coolant temperature and coolant density). Namely, CITVAP cannot interpolate between macroscopic cross sections that's depend on both coolant temperature and coolant density. Hence, HXS program was used to fix manually the coolant density for all the macroscopic cross sections in order to overcome this interpolation methodology barrier. So, the interpolation that is done here is only for the fuel and the coolant temperature.

The set of macroscopic cross sections that was generated by CONDOR depends on the following fuel temperature: 20°C, 40°C, 60°C and the following coolant temperature: 20°C, 25°C, 30°C.

The internally built-in interpolation mathematical model in CITVAP was implemented as follows, [22]:

- For a given fixed reference fuel temperature ($T_{fuel,\,ref}$) and coolant temperature ($T_{cool,\,ref}$), the interpolation equation for a required macroscopic cross section based on a change in fuel temperature to $T_{fuel,\,1}$ and a change in coolant temperature to $T_{cool,\,1}$ is calculated using equation (3.4).

$$\Sigma_x(T_{fuel,1}, T_{cool,1}) = \Sigma_x(T_{fuel,ref}, T_{cool,ref}) + \Delta\Sigma_x(T_{fuel,1}, T_{cool,ref}) + \Delta\Sigma_x(T_{fuel,ref}, T_{cool,1}) \quad (3.4)$$

Where:

$\sum_x(T_{fuel,1}, T_{cool,1})$: Macroscopic cross section of any reaction type based on an increase in fuel temperature ($T_{fuel,1}$) and coolant temperature ($T_{cool,1}$), [cm^{-1}]. This is calculated by CITVAP.

$\sum_x(T_{fuel,ref}, T_{cool,ref})$: Macroscopic cross section of any reaction type at the fixed reference fuel and coolant temperature, [cm^{-1}]. This is provided from CONDOR.

$\Delta\Sigma_x(T_{fuel,1}, T_{cool,ref})$: Change in macroscopic cross section of any reaction type between the macroscopic cross section at ($T_{fuel,1}, T_{cool,ref}$) and ($T_{fuel,ref}, T_{cool,ref}$), [$cm^{-1}$]. This is provided from CONDOR.

$\Delta\Sigma_x(T_{fuel,ref}, T_{cool,1})$: Change in macroscopic cross section of any reaction type between the macroscopic cross section at ($T_{fuel,ref}, T_{cool,1}$) and ($T_{fuel,ref}, T_{cool,ref}$), [$cm^{-1}$]. This is provided from CONDOR.

Fig. 3.17 explains how the macroscopic cross sections interpolation occurs internally in CITVAP code.

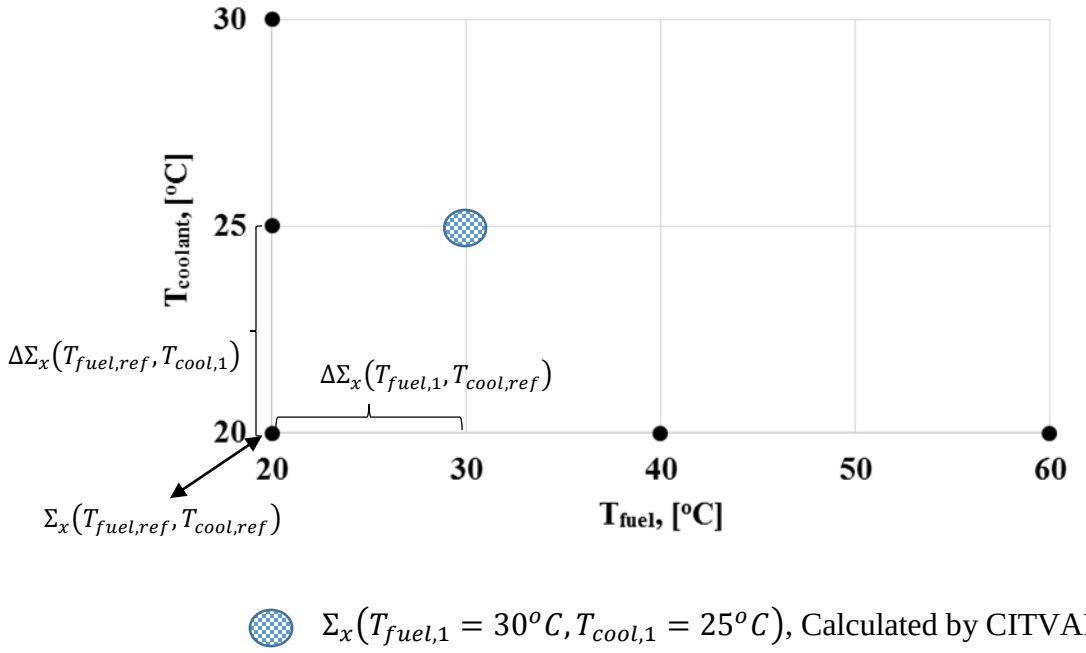

Fig. 3.17: Schematic illustration of CITVAP's macroscopic cross sections interpolation method.

3.4.6.4. Results and Analysis

The thermal-hydraulic external informations that correspond to the calculation of the power feedback coefficient are summarized in table 3.34.

Table 3.34: Thermal-hydraulic information of power feedback coefficient calculation.

For SFAs	
Meat width, [cm]	6.0
Channel width, [cm]	6.6
Channel height, [cm]	0.271
Active length, [cm]	62.3
Plate length, [cm]	67.1
Number of fuel plates	19
Meat half thickness, [cm]	0.02533
Cladding thickness, [cm]	0.04917
Oxide thickness, [cm]	0.0
For CFAs, same as the SFAs except for	
Channel height, [cm]	0.261
Number of fuel plates	14

Table 3.34 (Cont'd): Thermal-hydraulic information of power feedback coefficient calculation.

Thermal Conductivity Data	
Fuel meat, [kW/m.K]	0.048
Gap, [kW/m.K]	0.0023
Cladding, [kW/m.K]	0.165
Other Information	
Water column, [cm]	660
Inlet temperature[16], (ºC)	24.0
Coolant channel flow velocity[17], (cm/s)	91.0
Flow type	Forced – Downward

The power feedback coefficient was calculated using a fixed reference of 20ºC for both the fuel and the coolant temperatures. At those two temperatures, a set of all macroscopic cross sections was generated by CONDOR. Later, additional macroscopic cross sections for the only power generating assemblies were generated one by one for the following fuel and coolant temperatures: T_{fuel}: 40ºC and 60ºC, T_{cool}: 25ºC and 30ºC. When a macroscopic cross section was generated at a fuel temperature (for instant at T_{fuel}= 40ºC), the coolant temperature was kept constant at the reference temperature, and vice versa. Using these macroscopic cross sections and the thermal-hydraulic informations, which were presented in table 3.34, the reactivity difference between the cold condition ($1KW_{th}$) and the hot condition ($1MW_{th}$) is obtained by CITVAP. Then, this reactivity difference is divided by the change in the power level to get the power feedback coefficient. Table 3.35 presents the measured and the calculated values of the power feedback coefficient.

Table 3.35: Calculated and measured power feedback coefficient.

	Power Feedback Coefficient [pcm/ MW_{th}]	**Differences with respect to measured value [%]**
Measured value, [24]	-52	35%
Calculated value	-70	

An improvement was carried out to include the combination effects on the calculated power feedback coefficient:

[16] Inlet temperature was assumed to be 24ºC since it was not reported in Ref [24].
[17] In Ref [24] the pressure drop in the core was assumed to be uniform, which means that the velocity is independent of the FA location in the core.

1) Changing the reference fuel and coolant temperature to match the average value on each core state (cold and hot).

2) Change the temperature of all structural materials, absorber plates and every water to be equal to the average coolant temperature for any corresponded state (cold or hot).

From the previous calculation ($T_{fuel,\ ref}$ = $T_{cool,\ ref}$ = 20^{o}C) the average fuel and coolant temperature was found in the cold and hot conditions. In the cold condition, the average fuel and coolant temperature was at 24^{o}C, which was expected since the inlet temperature was 24^{o}C. In the hot condition, the average fuel and coolant temperature was 32^{o}C and 26^{o}C, respectively.

By applying the two stated above effects, the reference fuel and coolant temperature for each core state was:

(a) At cold condition ($T_{fuel,\ ref}$ = $T_{cool,\ ref}$ = 24^{o}C).

(b) At hot condition ($T_{fuel,\ ref}$ = 32^{o}C, $T_{cool,\ ref}$ = 26^{o}C).

The idea behind changing the reference point in each core state was to improve the way of interpolation in macroscopic cross sections. The other non-generating power assemblies' macroscopic cross sections were set at the average coolant temperature. The power feedback coefficient after these updates is shown in table 3.36.

Table 3.36: An update of the calculated power feedback coefficient value.

	Power Feedback Coefficient [pcm/ MW_{th}]	**Differences with respect to measured value [%]**
Measured value, [23]	-52	15%
Updated value	-60	

More than 50% reduction was gained between the difference in measured and calculated power feedback coefficient due to the two considered effects.

A further sensitivity analysis was introduced to determine how important to consider the average coolant temperature for the structural materials, absorber plates and every water in the core. At power level 1MW_{th} (hot condition), the temperature of these materials were at 26^{o}C (the average coolant temperature in the hot state). In this study, the effect of changing these materials' temperature from 26^{o}C to 24^{o}C (the average coolant temperature in the cold state) was analyzed on the power feedback coefficient. The result of this study, shows a decrease in the power feedback coefficient to a value of -65 pcm/MW_{th}, whereas before was at -60 pcm/MW_{th}. This change in power feedback coefficient is an evidence of how important to include the changing of these materials' temperature in the thermal-hydraulic calculations. The reactivity difference in the hot condition due to the changes of these materials' temperature measures the amount of this sensitivity study. This amount was equal to -2.55 pcm/^{o}C.

3.4.7. α-Kinetic Parameter

3.4.7.1. Definition

- **α-kinetic parameter:** It is defined as the ratio of the delayed neutron fraction over the mean generation time, equations (3.6 and 3.7).

$$\alpha = \frac{\beta_{eff}}{\Lambda} \tag{3.6}$$

$$\Lambda = \frac{l}{k} \tag{3.7}$$

Where:
α: Kinetic parameter, [s^{-1}].
β_{eff}: Delayed neutron fraction, [pcm].
Λ: Mean generation time, [s].
l: Prompt neutron lifetime [s].
k: Effective multiplication factor.

3.4.7.2. Experimental procedure

The α-kinetic parameter was experimentally measured by the noise analysis technique for different subcritical conditions at approximately zero reactor power ($10W_{th}$), [25]. The α values were plotted versus the core reactivity and adjusted by a linear fitting in order to get the value of α when the reactor is critical. This value represent the measured value of α-kinetic parameter.

3.4.7.3. Calculation procedure

The calculation procedure to calculate the delayed neutron fraction and prompt neutron life time was conducted as follows: First, using CONDOR to obtain all microscopic and macroscopic cross sections at 10 energy groups. The microscopic cross sections were generated in CITATION format. Second, using HXS program, the generated macroscopic cross sections were imported to a library to be used later in CITVAP's input file. Third, CITVAP was used to generate a database output file. Forth, this database output file with the early generated microscopic cross sections were used to prepare the input file of POS_LIB program. Fifth, using POS_LIB program, section 000, section 012 and section 020 were generated to be used in another CITVAP's input file. Finally, CITVAP was used to generate the delayed neutron fraction and the prompt neutron life time using the previous 3 generated sections and section 040, which has the information of the delayed neutron spectrum, table 3.37. Hence, α-kinetic parameter is calculated. 10 energy groups were utilized in this regard to distinguish between instantaneous and delay neutron spectrum. The equations of delayed neutron fraction and prompt neutron life time, which were implemented in CITATION II, are described in equation (3.8 and 3.9), [6]. The 10 energy groups are summarized in table 3.38.

$$\beta_{eff} = \sum_{j=1}^{6} \beta_{eff}^{j} = \frac{\sum_i V_i \ \sum_g \chi^+(j,g) \phi_{i,g}^* \sum_b \beta_{b,j} \ N_{b,i} \ \sum_n \sigma_{f,n,b,i} \ \phi_{i,n}}{\sum_i V_i \ \sum_g \chi(g) \ \phi_{i,g}^* \ \sum_n \nu \ \Sigma_{f,n} \ \phi_{i,n}} \quad (3.8)$$

$$l = k \frac{\sum_i \frac{V_i}{\mathrm{v}(n)} \phi_{i,n}^* \phi_{i.n}}{\sum_i V_i \ \sum_g \chi(g) \ \phi_{i,g}^* \ \sum_n \nu \ \Sigma_{f,n} \ \phi_{i,n}} \quad (3.9)$$

Where:

β_{eff}^{j}: Delayed neutron fraction for a given precursor family j, [pcm].

V_i: Volume associated to mesh i, [cm^3].

$\chi^+(j,g)$: Delayed neutron spectrum for a precursor family j and an energy group g.

$\phi_{i,g}^*$: Adjoint flux in mesh i associated to energy group g.

$\beta_{b,j}$: Delayed neutron fraction for b nuclide and a precursor family j, [pcm].

$N_{b,i}$: Atomic density for b nuclide in mesh i, [$at.cm^{-3}$].

$\sigma_{f,n,b,i}$: Fission microscopic cross section associated to energy n, b nuclide and mesh i, [cm^2].

$\phi_{i,n}$: Flux in mesh i for energy n, [$n.cm^{-2}.s^{-1}$]

$\chi(g)$: Total delayed neutron spectrum associated to energy group g.

ν: Number of neutrons produced by fission.

$\Sigma_{f,n}$: Fission macroscopic cross section for energy n, [cm^{-1}].

l: Prompt neutron lifetime, [s].

k: Effective multiplication factor.

$\mathrm{v}(n)$: Neutron velocity as a function of energy n, [$cm.s^{-1}$].

Table 3.37: Delayed neutron spectrum, [26].

Energy groups	Delayed neutrons groups						Instantaneous neutrons
	Group 1	Group 2	Group 3	Group 4	Group 5	Group 6	
1	5.309E-03	1.220E-01	7.060E-02	1.240E-01	1.018E-01	8.897E-02	0.7452790
2	6.727E-02	2.523E-01	2.612E-01	2.348E-01	2.200E-01	2.650E-01	0.1160090
3	1.594E-01	3.208E-01	2.746E-01	2.607E-01	2.515E-01	2.606E-01	0.0676054
4	2.729E-01	1.605E-01	1.969E-01	1.855E-01	1.951E-01	1.944E-01	0.0358692
5	2.913E-01	1.145E-01	1.424E-01	1.390E-01	1.783E-01	1.236E-01	0.0180814
6	2.038E-01	2.986E-02	5.478E-02	5.606E-02	5.345E-02	6.768E-02	0.0170127
7	0.000E+00	0.000E+00	0.000E+00	0.000E+00	0.000E+00	0.000E+00	0.0001489
8	0.000E+00	0.000E+00	0.000E+00	0.000E+00	0.000E+00	0.000E+00	0.0000000
9	0.000E+00	0.000E+00	0.000E+00	0.000E+00	0.000E+00	0.000E+00	0.0000000
10	0.000E+00	0.000E+00	0.000E+00	0.000E+00	0.000E+00	0.000E+00	0.0000000

Table 3.38: Energy group structure used for kinetic parameter calculation.

Energy groups	Upper energy limit of each group, [eV]
1	1.00000E+07
2	0.82085E+06
3	0.50000E+06
4	0.30200E+06
5	0.18300E+06
6	0.11100E+06
7	5.53080E+03
8	2.10000E+00
9	6.25060E-01
10	8.19680E-02

3.4.7.4. Results and Analysis

The delayed neutron fraction and the prompt neutron life time were found using the previous mentioned calculation procedures. The calculations of kinetic parameters were performed at a cold condition in a critical situation. A sensitivity analysis was carried out to check the influence of the following two situations on α-kinetic parameter: (a) all CEs are out of the core, (b) all CEs are in the core. Table 3.39 presents the calculated kinetic parameters along with the two studied cases.

Table 3.39: Calculation values of the delayed neutron fraction, the prompt neutron life time, neutron lifetime and α-kinetic parameter.

	Original Study	**Sensitivity Analysis**	
	Critical state	**All CEs out**	**All CEs in**
β_{eff}, [pcm]	767.3	763.2	765.3
***l*, [μs]**	42.5	44.7	41.6
Λ, [μs]	42.8	42.7	46.8
α, [s^{-1}]	179.3	178.7	163.4

A comparison between measured data and calculated value is shown in table 3.40.

Table 3.40: Calculated and measured α-kinetic parameter.

	α-kinetic parameter, [s^{-1}]	**Differences with respect to measured value, [%]**
Measured value, [17]	180.8 ± 0.9	0.8%
Calculated value	179.3	

Another sensitivity analysis was performed to check the effect of changing the core state from cold to hot state. The effect on the α-kinetic parameter was negligible.

3.5. Comparison Against MCNP5.

In this section, the following calculations' results is demonstrated:

- A verification of CONDOR2.62 cell calculations against MCNP5.1.6 calculations. The cell models of SFA and CFA, section 3.3, in both codes were identical as well as the material specifications.
- An evaluation of the CE absorber material microscopic cross section at the ESIN 2001 library was carried out.
- Criticality calculations were performed using MCNP5.1.6 in order to check for the existence of a reactivity slope, as mentioned earlier.

3.5.1. SFA and CFA Cell Calculations Verification.

A verification calculations was carried out to verify the deterministic cell calculation CONDOR2.62 with the stochastic MCNP5.1.6 code. Table 3.41 shows a comparison between CONDOR2.62 and MCNP5.1.6 calculation for the SFA and the CFA cell models' infinite multiplication factor.

Table 3.41: CONDOR2.62 comparison against MCNP5.1.6 for K_∞.

	Verification Process	CONDOR 2.62	MCNP5.1.6	Reactivity Difference, [pcm]
1	SFA cell model without Cd wires	1.616747	1.63001	500
2	SFA cell model with Cd wires	1.489125	1.49648	305
3	CFA cell model without Cd wires and without the CE	1.529065	1.54278	593
4	CFA cell model with Cd wires and without the CE	1.400634	1.40895	420
5	CFA cell model without Cd wires and with the CE	1.356369	1.34423	666
6	CFA cell model with Cd wires and with the CE	0.923173	0.91848	554

After that, macroscopic absorption cross section of the absorber material of the CE (AgInCd) was calculated using MCNP5.1.6 and compared with CONDOR2.62 calculation. The CONDOR2.62's microscopic cross sections library was the ESIN 2001, whereas MCNP5.1.6 was

ENDF/B-VI. The comparison was performed at 3 energy groups for the CFA cell model without Cd wires and with the CE. Table 3.42 presents this comparison.

Table 3.42: Comparison in the absorption macroscopic cross section of AgInCd.

	Absorption Macroscopic Cross Section of AgInCd		
Energy group	**CONDOR2.62 (ESIN 2001), [cm^{-1}]**	**MCNP5.1.6 (ENDF/B-VI), [cm^{-1}]**	**Difference, [%]**
1 (10 MeV – 0.821 MeV)	3.9283E-03	4.5206E-03	13%
2 (0.821 MeV – 0.625 eV)	2.1805E-01	2.7160E-01	20%
3 (0.625 eV – 0.0 eV)	7.5583E+00	7.7908E+00	3%

Due to the existence of 20% difference in the epithermal region, a deeper analysis was carried out. This analysis was done to compare the absorption microscopic cross sections between ESIN 2001 library and MCNP's output file for a 69 energy groups for the following elements: 47107 (Ag-107), 47109 (Ag-109), 48113 (Cd-113) and 49000 (Natural-In). Fig. 3.17, 3.18 and 3.19 shows the absorption microscopic cross sections for the previous elements.

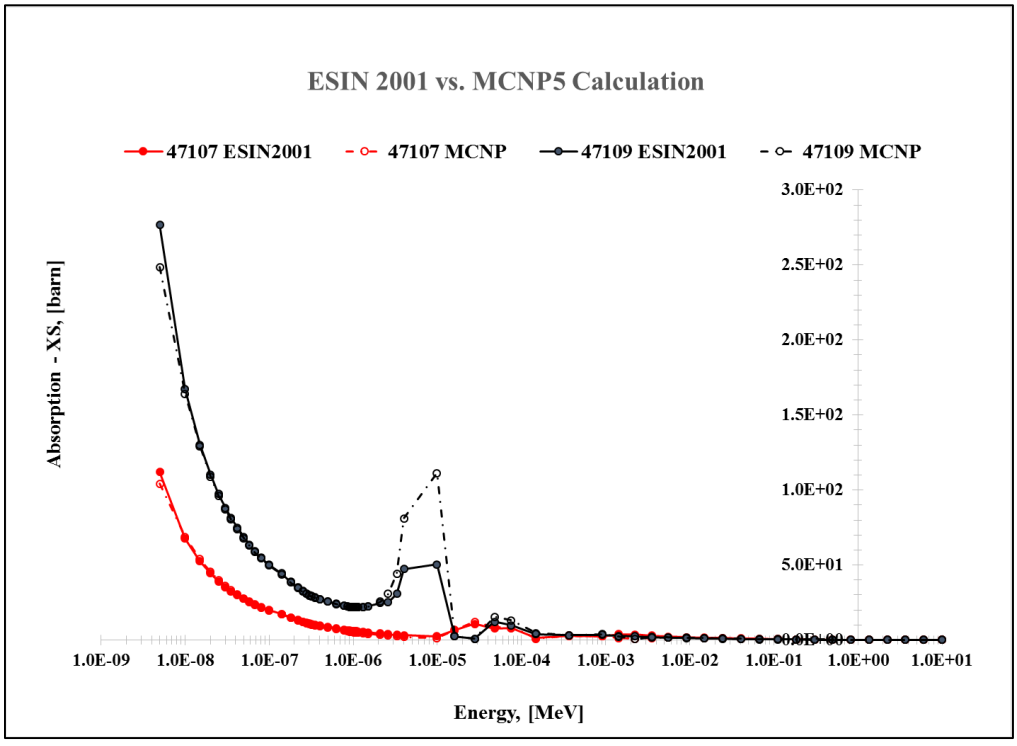

Fig. 3.18: Absorption microscopic cross sections for Ag-107 and Ag-109 using ESIN 2001 and MCNP5.1.6 calculations.

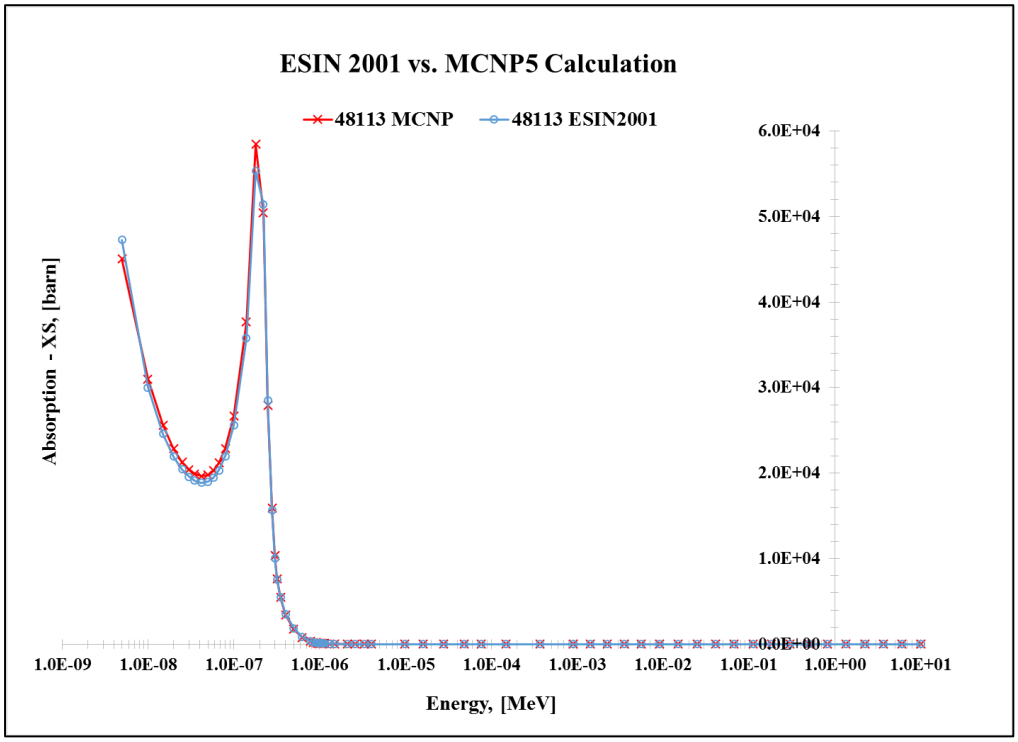

Fig. 3.19: Absorption microscopic cross sections for Cd-113 using ESIN 2001 and MCNP5.1.6 calculations.

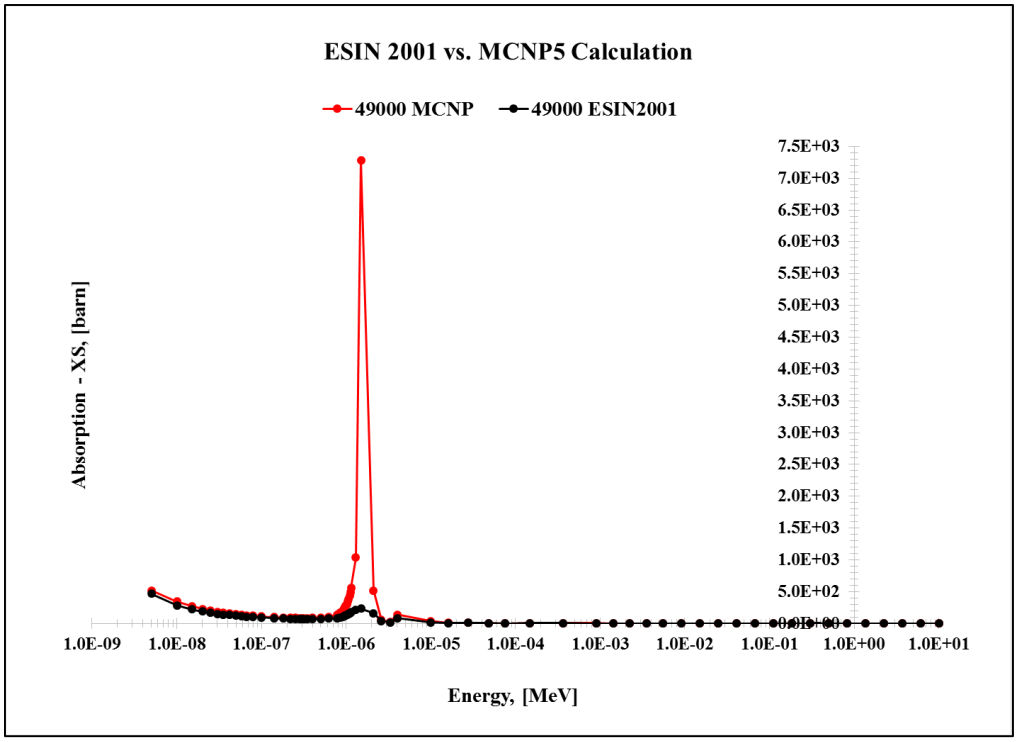

Fig. 3.20: Absorption microscopic cross sections for Natural Indium using ESIN 2001 and MCNP5.1.6 calculations.

There was a significant difference for Ag-109 and natural Indium in the epithermal region. This difference is due to the spatial self-shielding treatment. The spatial self-shielding treatment of ESIN 2001 was not applied for the RA-6 CE. In order to take account for the self-shielding treatment, MCNP's microscopic cross sections in the epithermal region were used in CONDOR's input file via "RESONANCE XS_EFFECTIVE" card. After that, CONDOR's infinite multiplication factor was reevaluated and compared again against MCNP5.1.6 for both CFA cell models with the CE and (without/with Cd wires). This comparison is presented in table 3.43.

Table 3.43: K_∞ comparison between MCNP5.1.6 and CONDOR2.62 for both CFA cell models (without/with Cd wires) and with the CE inserted.

	Verification Process	CONDOR 2.62	MCNP5.1.6	Reactivity Difference, [pcm]
5	CFA cell model without Cd wires and with the CE	1.351861	1.34423	-420
6	CFA cell model with Cd wires and with the CE	0.919874	0.91848	-165

All these changes of microscopic cross sections were applied previously on Section 3.4.

3.5.2. Criticality Calculation using MCNP5.1.6.

The objective of this study is to check the existence of the reactivity slope of CE No. 2 critical points (Refer to Fig. 3.11) with MCNP5.1.6. A simplified core model was developed for this comparison. Fig. 3.20 shows the reactivity obtained using MCNP and the calculation line CONDOR-CITVAP for the registered critical points of CE No. 2.

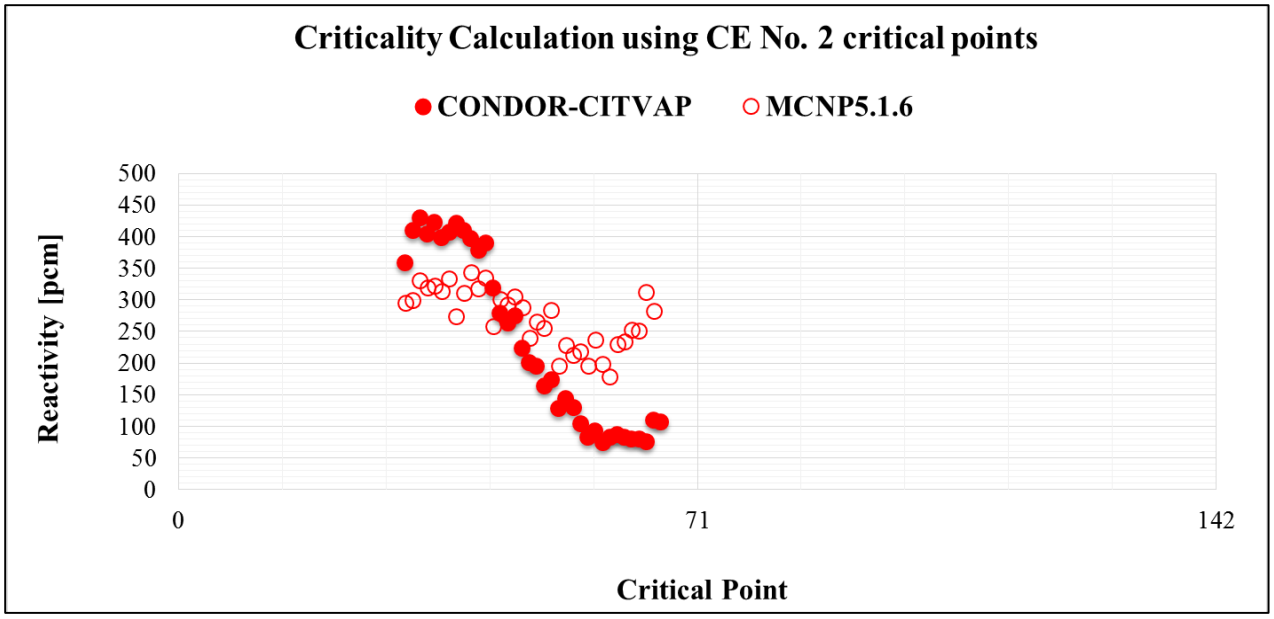

Fig. 3.21: Criticality calculation for the registered critical points of CE No. 2 using MCNP5.1.6 and CONDOR-CITVAP.

It can be observed that the small reactivity slope appeared with MCNP calculations. There should be a further analysis in this regard. Recalling that, CE No. 2 was mostly calibrated against CE No. 4. CE No. 4 was very close to CE No. 5, which was located at the core border. The interaction between CE No. 4 and CE No. 5 should be studied carefully.

CHAPTER 4: CONCLUSION

The deterministic calculation line CONDOR-CITVAP was validated against the IAEA numerical benchmark and the RA-6 experimental benchmark. This research was done to fulfill the following objectives:

- Learn the calculation line through the use of a well-defined benchmark (IAEA numerical benchmark).
- Expand the experimental base line validation of the calculation line through the use of RA-6 experimental benchmark.
- Develop a predictable model for the RA-6 reactor using the calculation line. Then, validating this model against the measured data during the RA-6 commissioning.
- Seeking to improve the calculation – experiment comparison in order to examine the experimental details that is not measured so far.
- Using Monte Carlo calculation tool, if possible, in case of a discrepancy between the calculation line and the experimental data.

4.1. Summary.

The results obtained from the IAEA numerical benchmark were satisfying and within other participants' results. The following cell and core parameters were compared against participants' results: K_∞ as a function of burnup, Pu^{239} content at 50% burnup, K_{eff} in three core states: Fresh (without Xe), BOL and EOL, thermal and fast flux ratio in BOL state along the X-axis, CEW, and feedback coefficients. The previous cell and core parameters were applied for HEU and LEU fuel. A summarized results of the core parameters for LEU fuel is shown in table 4.1.

In the RA-6 experimental benchmark, the following experiments were analyzed: approach to criticality by control elements, control elements calibration, measurement of excess reactivity, total Shutdown Margin (SDM), SDM with a single failure of a control element, isothermal feedback coefficient, void feedback coefficient, power feedback coefficient and α-kinetic parameter. These experiments were utilized to expand the validation of the calculation line CONDOR-CITVAP. A summary of the obtained differences between the measured data and the calculated values is presented in table 4.2.

Table 4.1: Summary of the obtained differences between the average participants and the Author's results of the IAEA numerical benchmark in the case of LEU fuel using CONDOR2.62-CITVAP3.8.

Core State	Compared variable	Differences with respect to average participants' results
Fresh	**Excess Reactivity**	303 pcm (2%)
	Total CEW (AgInCd – "B Model")	9%
BOL	**Excess Reactivity**	44 pcm (2%)
	Total CEW (AgInCd – "B Model")	8%
	Water temperature feedback coefficient	9%
	Water density feedback coefficient	2%
	Fuel temperature feedback coefficient	4%
	Void feedback coefficient	3%

Table 4.2: Summary of the obtained differences between the measured data and the calculated values of the RA-6 experimental benchmark using CONDOR2.62-CITVAP3.8.

Compared variable	Differences with respect to measured data
Criticality Calculation	(209 ± 109) pcm
CEW No. 1	2%
CEW No. 2	5%
CEW No. 3	2%
CEW No. 4	6%
CEW No. 5	13%
Excess Reactivity	239 pcm (5%)
Total SDM	367 pcm (4%)
SDM with Failure of CE No. 1	2%
SDM with Failure of CE No. 2	4%
SDM with Failure of CE No. 3	5%
SDM with Failure of CE No. 4	3%
Isothermal Feedback Coefficient	16%
Void Feedback Coefficient	0.7%
Power Feedback Coefficient	15%
α-Kinetic Parameter	0.8%

The following comments are applied to table 4.1 and table 4.2:

- Author's results of the IAEA numerical benchmark were within other participants and close to the average participants' results.
- The difference in the excess reactivity was similar in magnitude for the IAEA numerical benchmark and RA-6 experimental benchmark.
- Total CEW was calculated for the RA-6 benchmark; the difference between the measured data and calculated value was equal to 0.8% even though the difference for CEW No. 5 was 13%. On the other hand, the difference in the total CEW of the IAEA benchmark was 9% and there was no information regarding each CEW percentage difference.
- Void feedback coefficient gave a good agreement with both benchmarks: IAEA benchmark (3%) and RA-6 benchmark (0.7%).

4.2. Recommendation.

Based on the obtained differences between the measured data and calculated values, these recommendations are outlined:

- An investigation should be applied to understand the existence of 13% difference between the measured data and the calculated value of CEW No. 5.
- Experimental reevaluation should be applied to the measurement of the isothermal feedback coefficient in order to understand the existence of the high standard deviation of the experimental data.
- In order to reduce the obtained difference in the power feedback coefficient, the thermal-hydraulic code in CITVAP should be improved to take into account the macroscopic cross sections changes of the non-generating power elements. E.g. Irradiation box.

The author would like to emphasize on the development of an experimental measurement and/or estimation of the non-measured and/or non-estimated safety parameters. E.g. fuel temperature feedback coefficient, moderator temperature feedback coefficient, etc. Those experimental data would extend the experimental base line validation. As well as, knowing these experimental data would make us sure that they are within the acceptable limit of the Nuclear Regulatory Authority.

References

[1] I. Mochi, “INVAP's Nuclear Calculation System”, Science and Technology of Nuclear Installations, Vol. 2011, Article ID 215363, November 23, 2010.

[2] E. Villarino, “CONDOR Calculation Package”, International Conference on the New Frontiers of Nuclear Technology: Reactor Physics, Safety and High-Performance Computing. Physor 2002, Seoul, Korea, October 7-10, 2002.

[3] E. Villarino, R. Stamm'ler, A.Ferri and J.Casal, “HELIOS: Angularly-dependent Collision Probabilities”, Nuclear Science and Engineering: 112, 16-31 (1992).

[4] E. Villarino, “POS_LIB v2.0 User Manual”. May 2012.

[5] E. Villarino, C. Lecot and I. Mochi, “CITVAP v3.8 improved version of CITATION II MTR_PC v3.0 system: User Manual”. March, 2012.

[6] T. B. Fowler, D. R. Vondy and G. W. Cunningham, “Nuclear Reactor Core Analysis Code: CITATION”, ORNL-TM-2496, Revision 2, July 1971.

[7] E. Villarino and I. Mochi, “FLUX v2.0 User Manual”.

[8] Y. AlZaben, “Safety Parameters Validation After the Commissioning of RA6 Core Conversion To LEU Fuel”, 6th International Symposium on Material Testing Reactors, Bariloche, Argentina, October 28-31, 2013.

[9] IAEA, “Research Reactor Core Conversion from the Use of Highly Enriched Uranium to the Use of Low Enriched Uranium Fuels Guidebook”, TECDOC-233, IAEA, Vienna, 1980.

[10] IAEA, “Research Reactor Core Conversion Guidebook”, TECDOC-643V3, IAEA, Vienna, 1992.

[11] S. Matzkin, “Benchmark of IAEA”, INVAP, September, 1998.

[12] M. Brizuela, “Benchmark of IAEA: Safety-Related Problem”, INVAP, October, 2005.

[13] S. P. Bazzana and J. I. Márquez Damián, IEU-COMP-THERM-014, “RA-6 Reactor: Water Reflected, Water Moderated U (19.77)3Si2-Al Fuel Plates”. International Handbook of Evaluated Criticality Safety Benchmark Experiments, 2010.

[14] R.J. Tuttle, “Delayed Neutron Yields in Nuclear Fission”, Proc. Consultants’ Meeting on Delayed Neutron Properties, INDC (NDS) – 107/G, P. 29, IAEA, Vienna, 26-30 March 1979.

[15] J. M. Longhino, Registro Puesta en Marcha RA-6, REG-06NBX-PM-B2-06 Rev. 1, “Calibración en Reactividad de Barras de Control y Determinación del Exceso de Reactividad del Núcleo de Operación”.

[16] Santiago Bazzana, “Desarrollo, Análisis Y Evaluación De Experimentos Neutrónicos En El RA-6”, Master Thesis, Balseiro Institute, March 2012.

[17] H. Blaumann, ITA-06NBX-433 Rev. 0, “Evaluación de Ensayos de la Etapa B2”.

[18] J. M. Longhino, Registro Puesta en Marcha RA-6, REG-06NBX-PM-B2-07 Rev. 1, “Medición de Margen de Antirreactividad con falla de la Barra de mayor peso”.

[19] J. M. Longhino, Registro Puesta en Marcha RA-6, REG-06NBX-PM-B2-15 Rev. 1, “Medición del Coeficiente de Reactividad por Temperatura”.

[20] A. Weir, ITA-06NBX-412 Rev.1, “Cálculos de Cambio de Reactividad por Fracción de Vacío con el Código MCNP5”.

[21] J. M. Longhino, Registro Puesta en Marcha RA-6, REG-06NBX-PM-B2-12 Rev. 0, “Medición del Coeficiente de Reactividad por Vacío”.
[22] Darío Pieck, “Desarrollo Y Validación Experimental De Un Algoritmo De Acople Neutronico-Termohidraulico Para Reactores De Investigación”, Master Thesis, Balseiro Institute, June 2010.
[23] G. Ortiz Uriburu, IS-06NBX-405 Rev. 1, “Informe Final de Seguridad”.
[24] J. M. Longhino, Registro Puesta en Marcha RA-6, REG-06NBX-PM-C2-04 Rev. 0, “Medición del Coeficiente de Reactividad por Potencia”.
[25] A. Gómez, Registro Puesta en Marcha RA-6, REG-06NBX-PM-B2-08 Rev. 0, “Estimación del Parámetro Alfa y de la Potencia Mediante la Técnica de Ruido Neutrónico – Primera Etapa”.
[26] Y. Ronen and Ed., “CRC Handbook of Nuclear Reactor Calculations”, CRC Press, Boca Raton, Florida, 1986.
[27] J. M. Longhino, Procedimiento Puesta en Marcha RA-6, PRO-06NBX-PM-B1-08 Rev. 1, “Medición de Margen de Antirreactividad”.

Appendix-A: IAEA Numerical Benchmarks; Specifications, Requirement and Calculation Models.

This appendix contains the following informations: IAEA numerical benchmark specifications, required cell & core calculations, and cell & core calculations models.

A.1. Benchmark Specifications.

Table A.1: Geometrical specifications, [8].

Geometrical specifications	
Active core height	60 cm
Extrapolation height	8 cm (8 cm distance from the core, the cosine – shaped flux goes to zero).
2D Calculation Only (X,Y)	
Space at the grid plate per fuel assembly	7.7 cm x 8.1 cm
Fuel assembly cross section	7.6 cm x 8.05 cm including support plate 7.6 cm x 8.00 cm without support plate
Meat dimension (UAl_x – Al)	6.3 cm x 0.051 cm
Cladding (Aluminum)	6.3 cm x 0.038 cm
Support plate (Aluminum)	0.475 cm x 8.05 cm
Number of fuel plates per Standard Fuel Assembly (SFA)	23 identical plates, each 0.127 cm thick

Table A.1 (Cont'd): Geometrical specifications, [8].

Number of fuel plates per Control Fuel Assembly (CFA)	17 identical plates, each 0.127 cm thick
Identification of the six remaining plates position of the CFA	Four guide plates of pure Aluminum each 0.127 cm thick occupying the first, the third, the twenty-first and the twenty-third position. Between each set of guide plates there is a water gap. The remaining two plates correspond to the two control elements in which are inserted in the water gap.

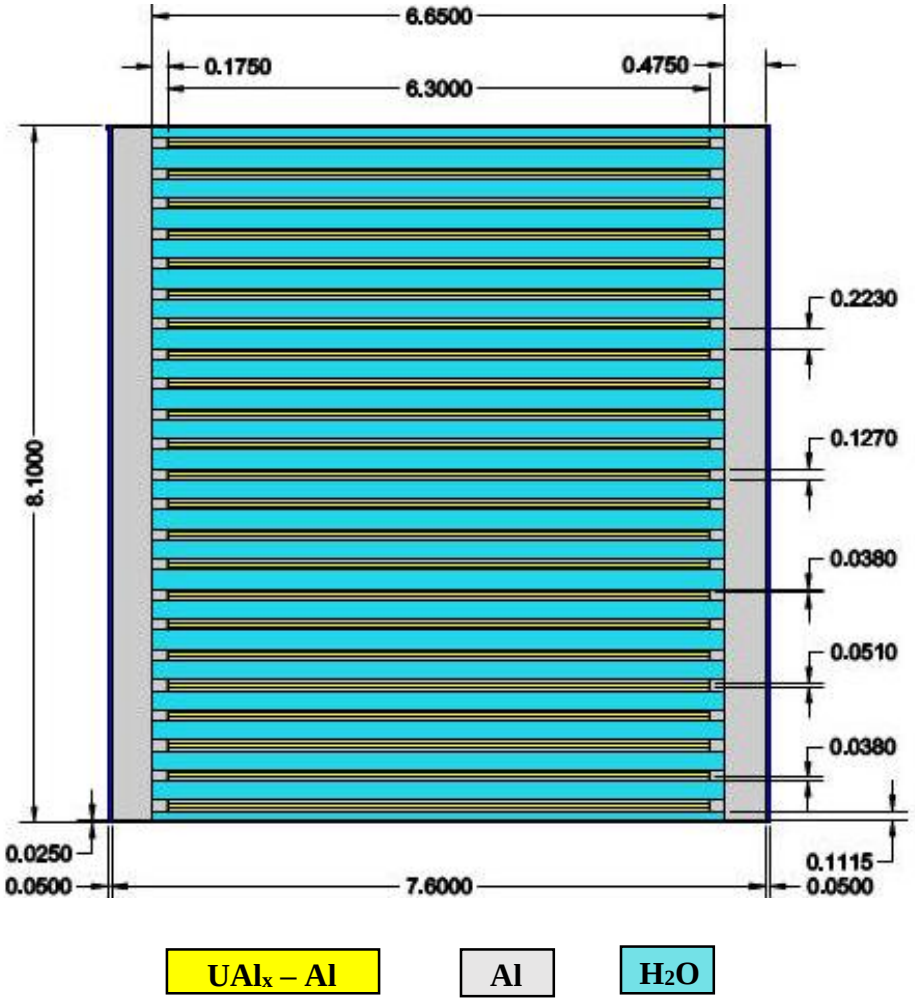

Fig. A.1: Standard Fuel Assembly (SFA), (All dimensions in cm).

Table A.2: Material specifications, [8].

Material specifications		
Fuel (UAl_x – Al) (Meat) **Only U^{235} and U^{238} in the fresh fuel**	**HEU**	Enrichment: 93 w/o (weight %) U^{235} 280 g U^{235} per SFA, which corresponds to 12.174 g U^{235} per each fuel plate. 21 w/o of Uranium in the UAl_x – Al.
	MEU	Enrichment: 45 w/o U^{235} 320 g U^{235} per SFA, (23 plates). 40 w/o of Uranium in the UAl_x – Al.
	LEU	Enrichment: 20 w/o U^{235} 390 g U^{235} per SFA, (23 plates). 72 w/o of Uranium in the UAl_x – Al.
Aluminum		Pure Aluminum (Density = 2.7 g/cm^3)
Graphite (Reflector)		Pure Graphite (Density = 1.7 g/cm^3)

Table A.3: Reactor condition, [8].

Reactor condition	
Total Power	10 MW_{th} (Power buildup by 3.1 x 10^{10} fission/Joule)
Thermal hydraulic data	Water temperature : 20^{o}C Fuel temperature: 20^{o}C Pressure at core height: 1.7 bar
Xenon – State	Homogeneous Xenon content corresponding to average power density.

A.1.1. Energy Group Structure for Core Calculation.

- Thermal group with 0 eV < E_n < 0.625 eV
- Epithermal group with 0.625 eV < E_n < 5.531 KeV
- Fast group with E_n > 5.531 KeV

A.1.2. Core Geometry.

The core is made of 21 SFA and 4 CFA; it has a central irradiation box just filled with water. As well, it is reflected in two sides by a row of graphite and then surrounded by water reflector as it is shown in Fig. A.2.

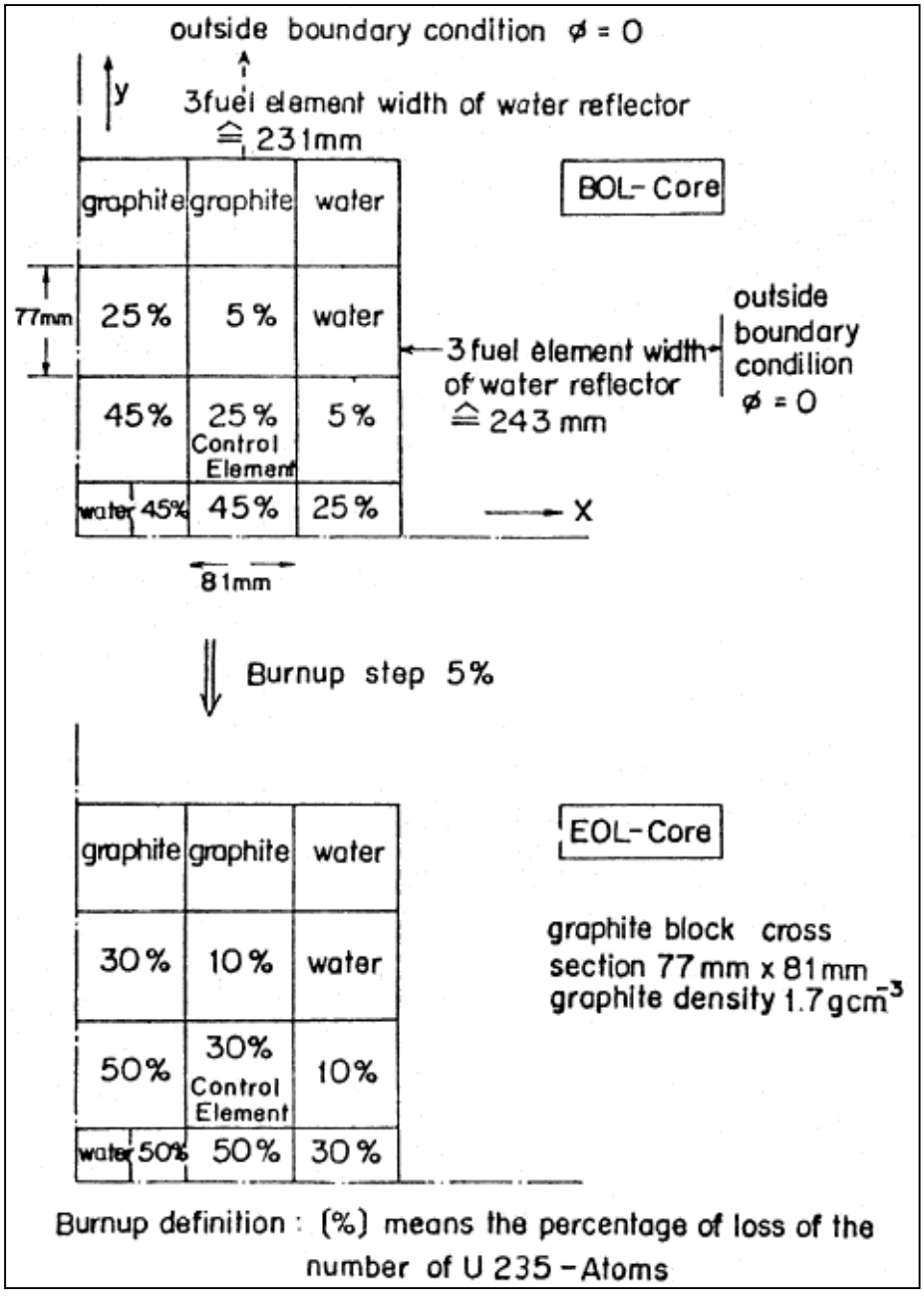

Fig. A.2: Quarter of core configuration in BOL and EOL states, [8].

A.1.3. Benchmark–643 Specification.

This benchmark is a continuation of (IAEA – benchmark – 233), but with changing the central irradiation box as follows: replacing the water in the central flux trap with a 7.7 cm x 8.1 cm block of aluminum containing a square hole of 5 cm on each side filled with water.

Table A.4: Control element specifications, [9].

Control element geometry: Fork-type with blades fitting into guide plates	
Length	60 cm
Thickness	0.318 cm; 0.31 cm thick absorber with a 0.004 cm layer of nickel on each surface of Ag-In-Cd and B_4C blades. 0.31 cm thick absorber for Hf blades (No Nickel Layer).
Width	6.6 cm
Absorber materials	
Ag-In-Cd	80.5 w/o Ag, 14.6 w/o In, 4.9 w/o Cd Density of Ag-In-Cd: 9.32 g/cm^3 Density of Ag = 7.50 g/cm^3 In = 1.36 g/cm^3 Cd = 0.46 g/cm^3 Ni = 8.90 g/cm^3
B_4C	Density of B_4C = 2.52 g/cm^3
Hf	Density of Hf = 13.3 g/cm^3

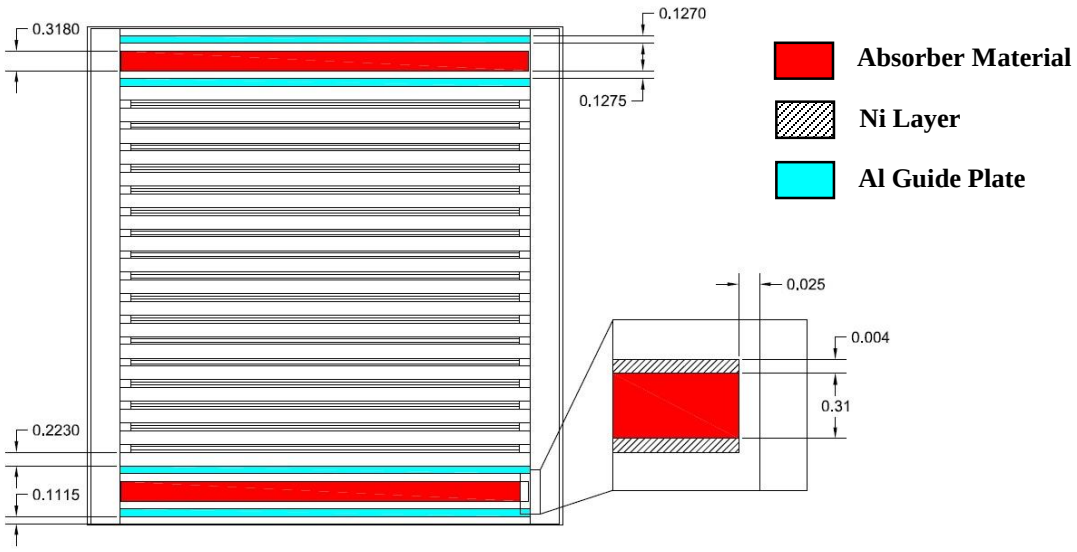

Fig. A.3: Control Fuel Assembly with control element inserted, other dimensions are exactly the same as in SFA, (All dimensions in cm).

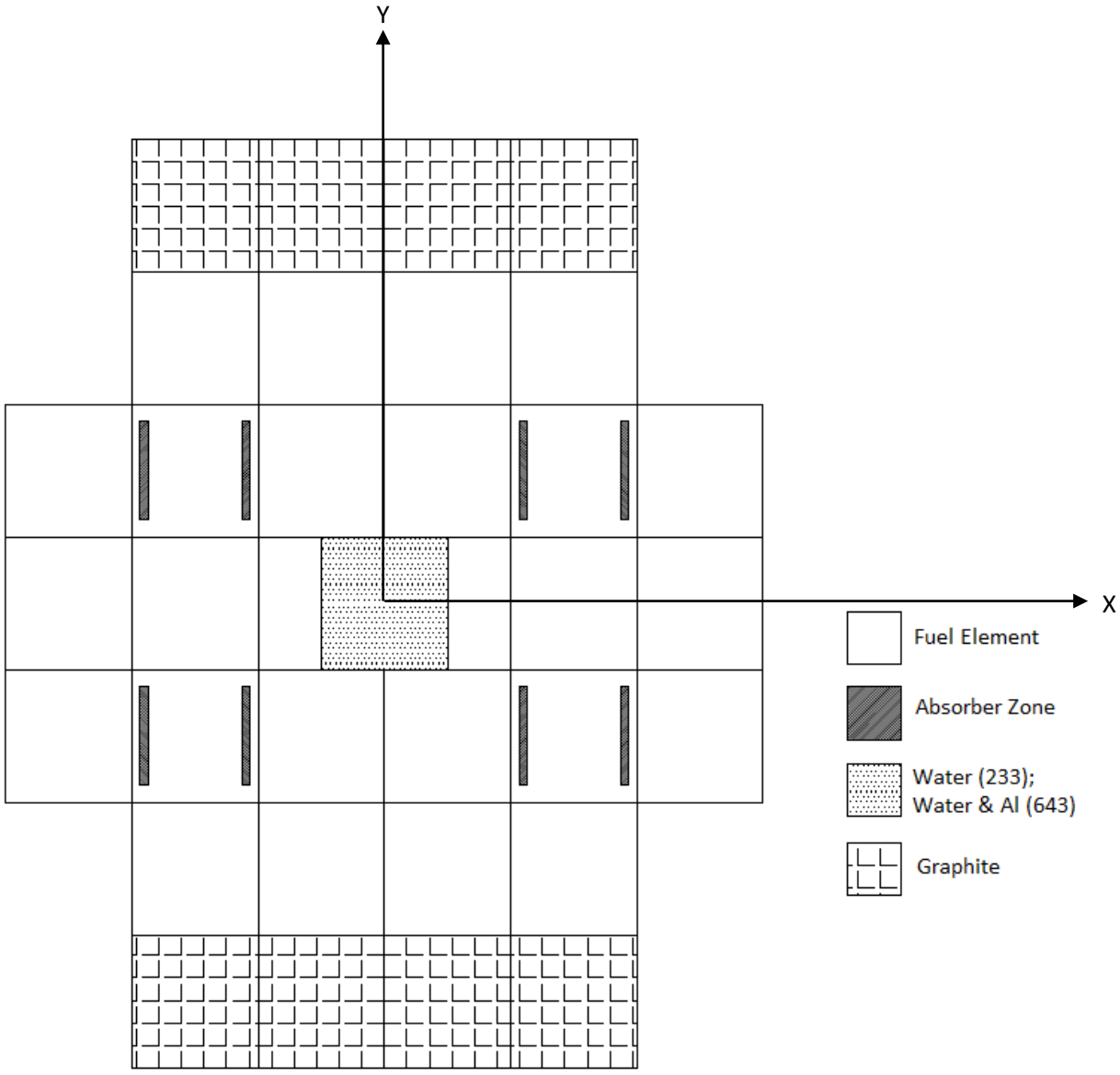

Fig. A.4: Core configuration for Benchmark-233 and 643, [11].

A.2. Bechmark Requirements.

There was a set of requirements agreed to be done among all participants. In this work, the following requirements were selected:

A.2.1. Cell Calculation Verification.

- Checking K_{∞} as a function of burnup (Lost of U^{235} %) for both HEU and LEU.
- Checking Pu^{239} content at 50% burnup for SFA for both HEU and LEU.

A.2.2. Core Calculation Verification.

- Checking K_{eff} of the core for HEU and LEU in three states:
  Fresh (without Xe), BOL and EOL.

- Checking thermal and fast flux ratio (LEU/HEU) in BOL state along the X-direction.

- Control Element Worth (CEW) of four inserted control elements in these states:
  HEU (Fresh No Xe and BOL) and LEU (Fresh No Xe and BOL).

- Reactivity feedback coefficients (BOL core, HEU and LEU) is calculated changing the following conditions in all the SFAs and CFAs only:

  1) Water temperature only: 38, 50, 75 and 100 ºC
  2) Water density only: 0.993, 0.988, 0.975 and 0.958 g/cm^3
  3) Fuel temperature only: 38, 50, 75, 100 and 200 ºC
  4) Core void coefficient - changing water density only by: 10%, 20% Void.

A.3. Calculation Models.

In this section, it will be demonstrated two calculation models: cell and core models. For the cell models, there are five different models: Standard Fuel Assembly (SFA), Control Fuel Assembly (CFA), water reflector, graphite reflector, and central irradiation box model.

A.3.1. Cell Calculation Models.

A.3.1.1. SFA model.

SFA model was obtained by 1D and 2D models. For the 1D model, there were two ways utilized to do the modeling using the volume ratio conservation. First, conserving the meat thickness. Second, conserving the pitch distance. The 1D model consisted of three slabs: the meat, the aluminum and the water slab, while the 2D model was a quarter of the SFA, Fig. A.1, because the SFA was symmetrical.

First: 1D Meat Conservation (MC) model.

The idea beyond this way of modeling is to keep the physics of the problem. The most critical part here is the meat thickness. So, to implement this method half of meat thickness was preserved and other slabs thicknesses' was calculated based on keeping the same volume ratio. The aluminum slab thickness was found by:

$$Thickness_{AL} = \left(\frac{V_{AL}}{V_{Meat}}\right) * {}^{1}/_{2} * Thickness_{Meat} \quad \text{(A.1)}$$

The water slab thickness was calculated by:

$$Thickness_{Water} = \left(\frac{V_{Water}}{V_{Meat}}\right) * {}^{1}/_{2} * Thickness_{Meat} \quad \text{(A.2)}$$

Where:

Meat thickness = 0.051 cm

V_{AL}: Aluminum volume = 1180.9 cm^3

V_{Meat}: Meat volume = 443.4 cm^3

V_{Water}: Water volume = 2117.9 cm^3

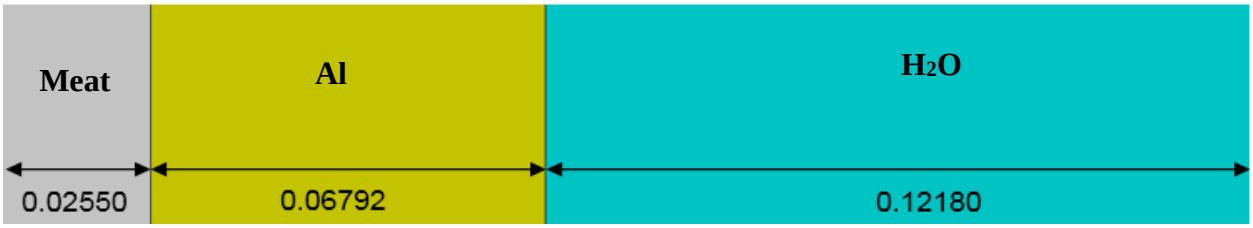

Fig. A.5: 1D Meat conservation model of SFA, (All dimensions are in cm).

Second: 1D Pitch Conservation (PC) model.

The idea of this model is to preserve the pitch distance, which is the distance between center to center of two neighboring fuel elements. The meat thickness was calculated by:

$$Thickness_{Meat} = P * \frac{V_{Meat}}{V_T} * {}^{1}/_{23} * {}^{1}/_{2} \quad \text{(A.3)}$$

Where:

P: pitch distance = 8.1 cm

V_T: total volume (Meat + Al + Water) = 3742.2 cm^3

Aluminum thickness and water thickness were calculated as in equation (A.1) and (A.2), respectively, but *without* dividing by 2 since it was included in equation (A.3).

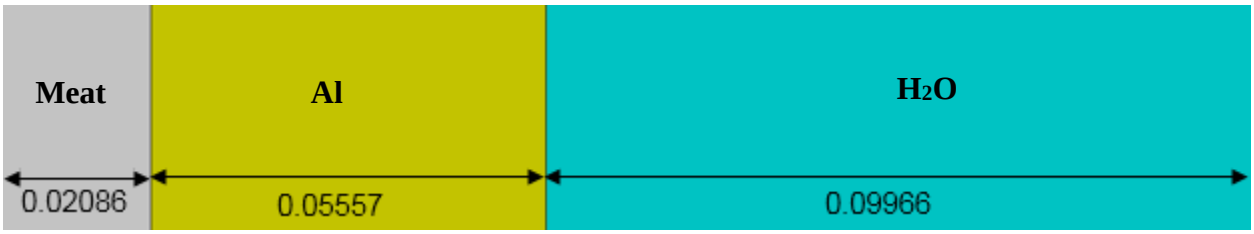

Fig. A.6: 1D Pitch conservation model of SFA, (All dimensions are in cm).

In the previous two models, MC and PC, all the three slabs were homogenized to get the macroscopic cross sections for the 1D SFA model.

Third: 2D SFA model.

The 2D dimensions were taken from Fig. A.1. The way that the cell code (CONDOR) treat this problem is by HRM. In which, the separation of each box was chosen to be at the middle of each water channel in order to make the white boundary assumption valid.

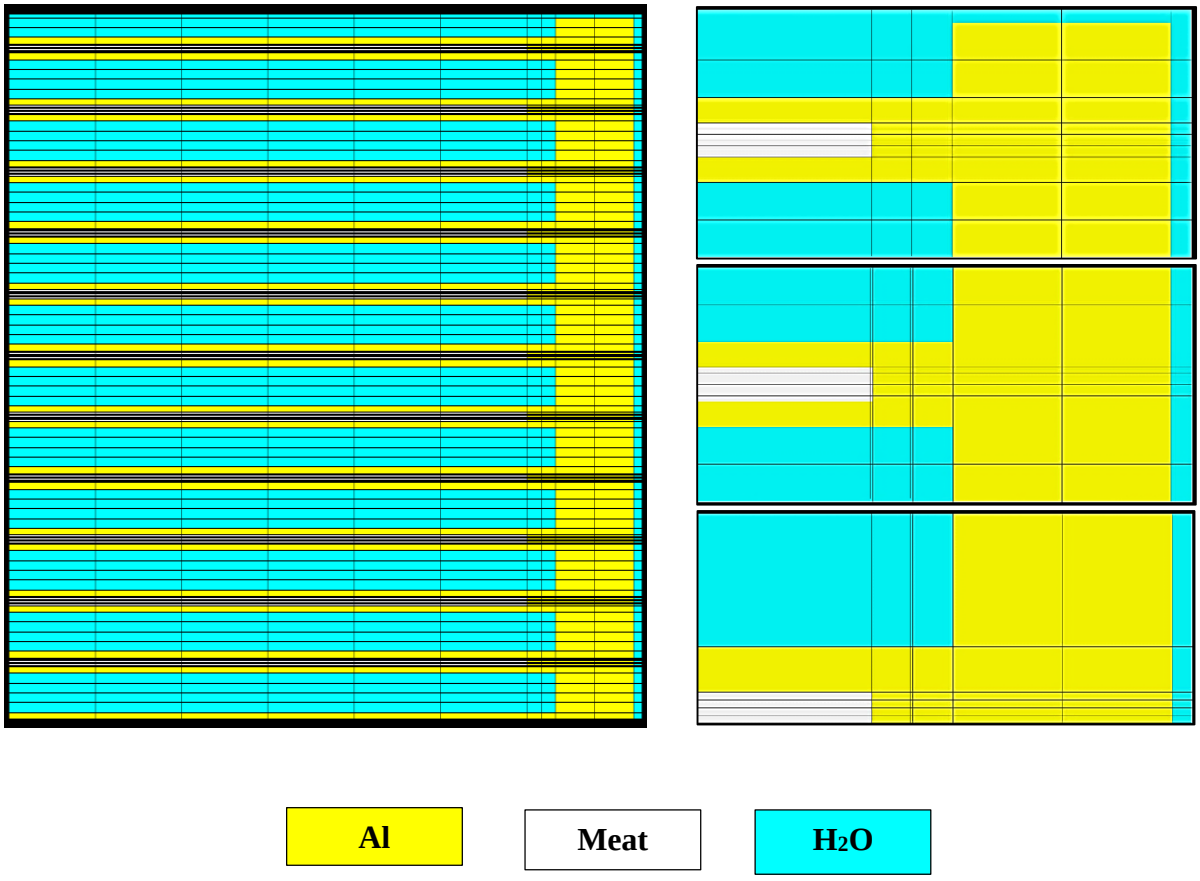

Fig. A.7: SFA 2D Model, on the right it shows a zoom in to each cell-box that was built in CONDOR input file.

The way of homogenization that was done here is to homogenize everything together and get the macroscopic cross sections for the 2D SFA model.

A.3.1.2. CFA model.

The CFA was modeled by 1D and 2D, for each one of them there are two models: one with absorber plate inserted and another without it. The 1D CFA was modeled along the Y-axis direction of Fig. A.3 by taking its half and adding a homogenized SFA on its left side, to avoid the repetition of the absorber plate on the left side. The 2D model, on the other hand, was taken as a quarter of Fig. A.3. Here it will be shown only the models with the absorber plate inserted.

First: 1D CFA model.

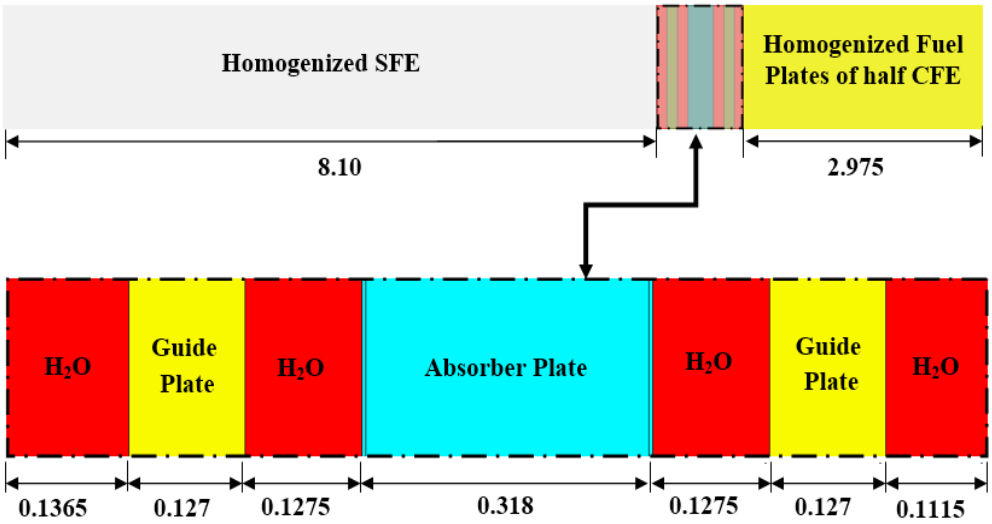

Fig. A.8: 1D CFA model, (All dimensions are in cm).

Second: 2D CFA model.

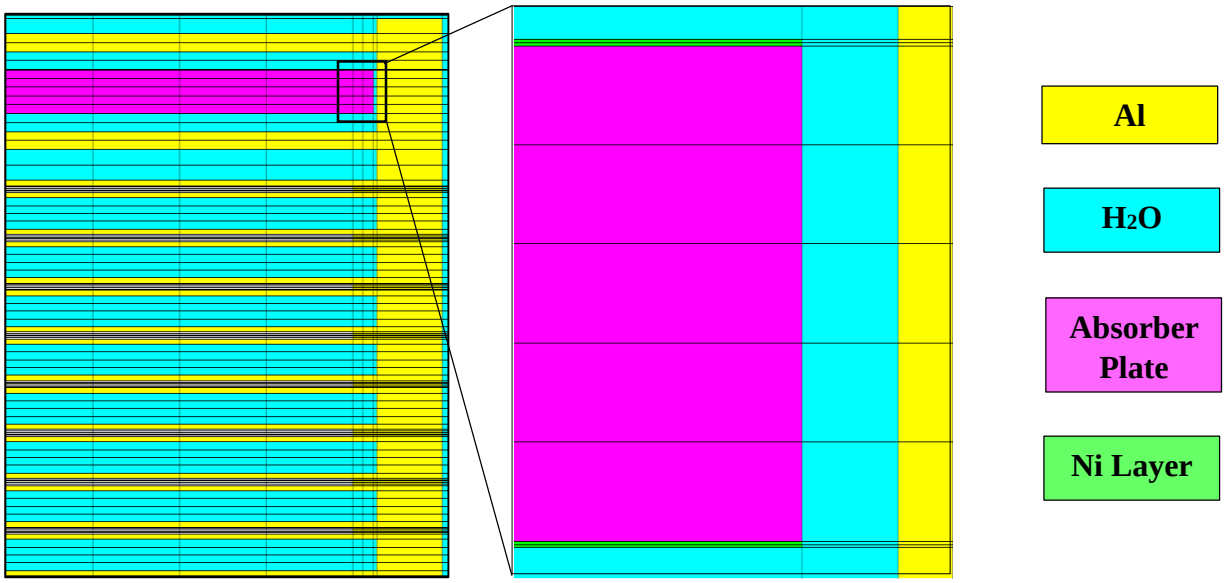

Fig. A.9: A quarter of 2D CFA model with control plate inserted.

Due to the criticality of the CFA model, a detailed homogenization process was carried on. The homogenization of the 1D CFA model was as follows: First, to homogenize the central part of Fig A.8 that contain the control plate and its guide plate, then extract one set of macroscopic cross sections for this part. Second, extracting a set of macroscopic cross sections for the homogenized fuel plate of the half CFA. These two sets of cross sections would be transferred into a 2D CFA model as in (Fig. A.10.A) to be used later in core model.

While, the homogenization process for 2D CFA took place as follows:

First, three regions model with two different sets of cross sections in which all CFA model was homogenized except for the absorber plate and its Ni cladding, (Fig. A.10.A).

Second, five regions with three different sets of cross sections that correspond to the following, (Fig. A.10.B):

A) Al frame with water frame.
B) Two guide plates (Al) with absorber region in between.
C) Fuel plates with its water moderator.

Third, three regions with two different sets of cross sections, see (Fig. A.10.C).

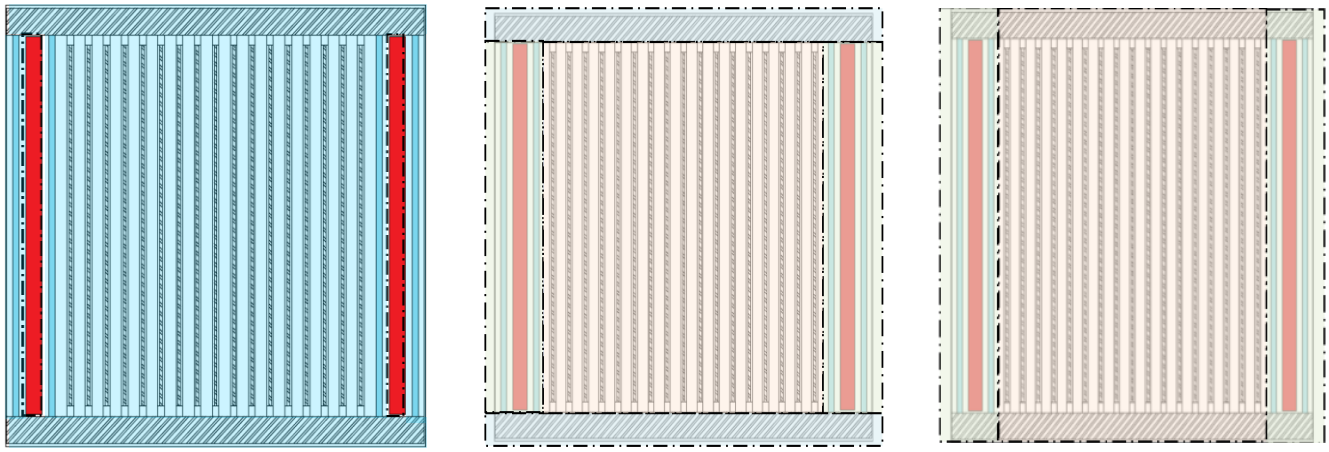

(A) (B) (C)

Fig. A.10: 2D CFA homogenization process, (A): first homogenization, (B): second homogenization and (C): third homogenization.

A.3.1.3. Reflector model.

Here we have two type of reflector: water and graphite. In order to generate a model for them, a 1D model was generated along X-axis of Fig. A.4 for the water reflector while the graphite reflector was generated along Y-axis.

First: water reflector model along X-axis.

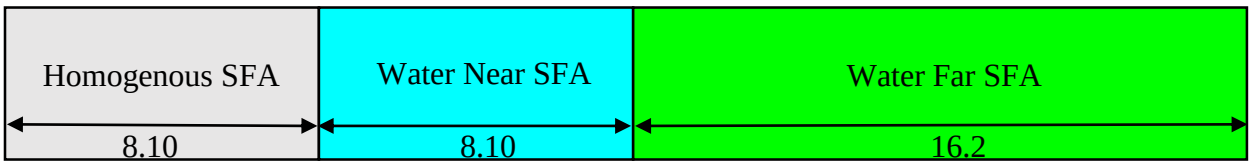

Fig. A.11: Water reflector model (Near and Far) along X-axis, (All dimensions are in cm).

Second: graphite reflector model along Y-axis.

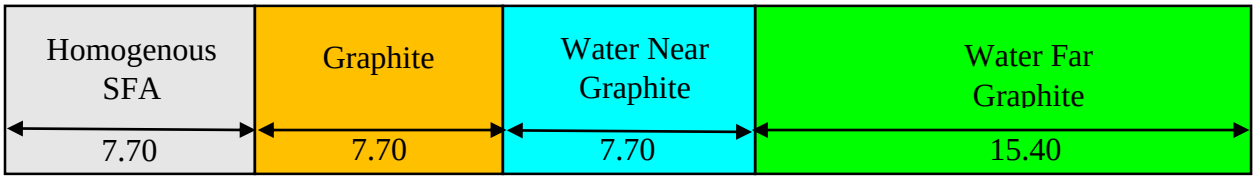

Fig. A.12: Graphite reflector model along Y-axis, (All dimensions are in cm).

A.3.1.4. Central irradiation box model.

The main difference between 233 and 643 benchmark was the central irradiation box. In benchmark 233, the central region was filled just with water while in benchmark 643 the central region was a box of aluminum with a hole filled with water, as mentioned earlier. A 1D model was generated along X-axis to get the macroscopic cross sections for the central irradiation box.

First: Central region model for benchmark-233.

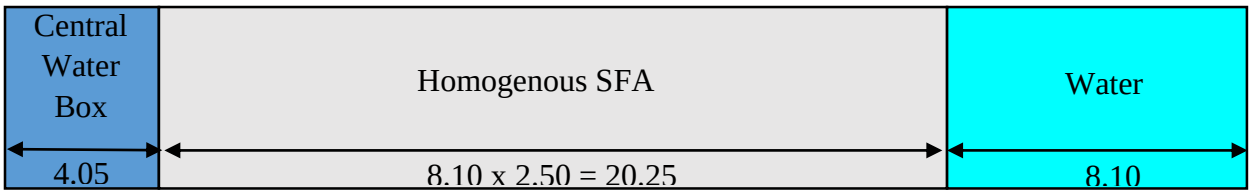

Fig. A.13: Central irradiation water model (benchmark-233), (All dimensions are in cm).

Second: Central region model for benchmark-643.

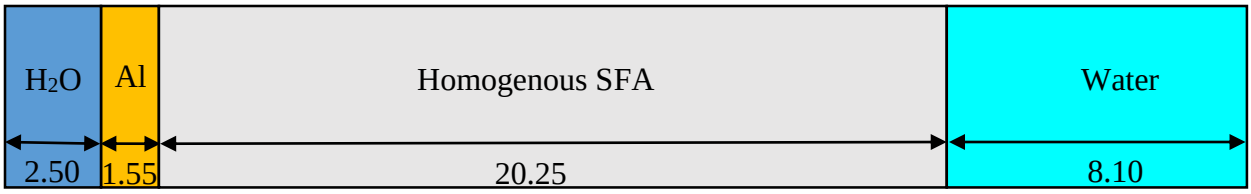

Fig. A.14: Central irradiation (H_2O and Al) model (benchmark-643), (All dimensions are in cm).

A.3.2. Core Model.

A 2D quarter, due to core symmetry, was modeled by CITVAP code for both benchmarks. A total of 84 mesh intervals in the X-direction and 74 in the Y-direction were used. The reactor core, including graphite rows, is reflected on all sides by water with a thickness corresponding to three elements each. A reflector saving of 8 cm was used in order to calculate the axial buckling, which simulates the axial leakage. The axial buckling (B_z^2) was found equal to 1.70873E-03 cm^{-2}.

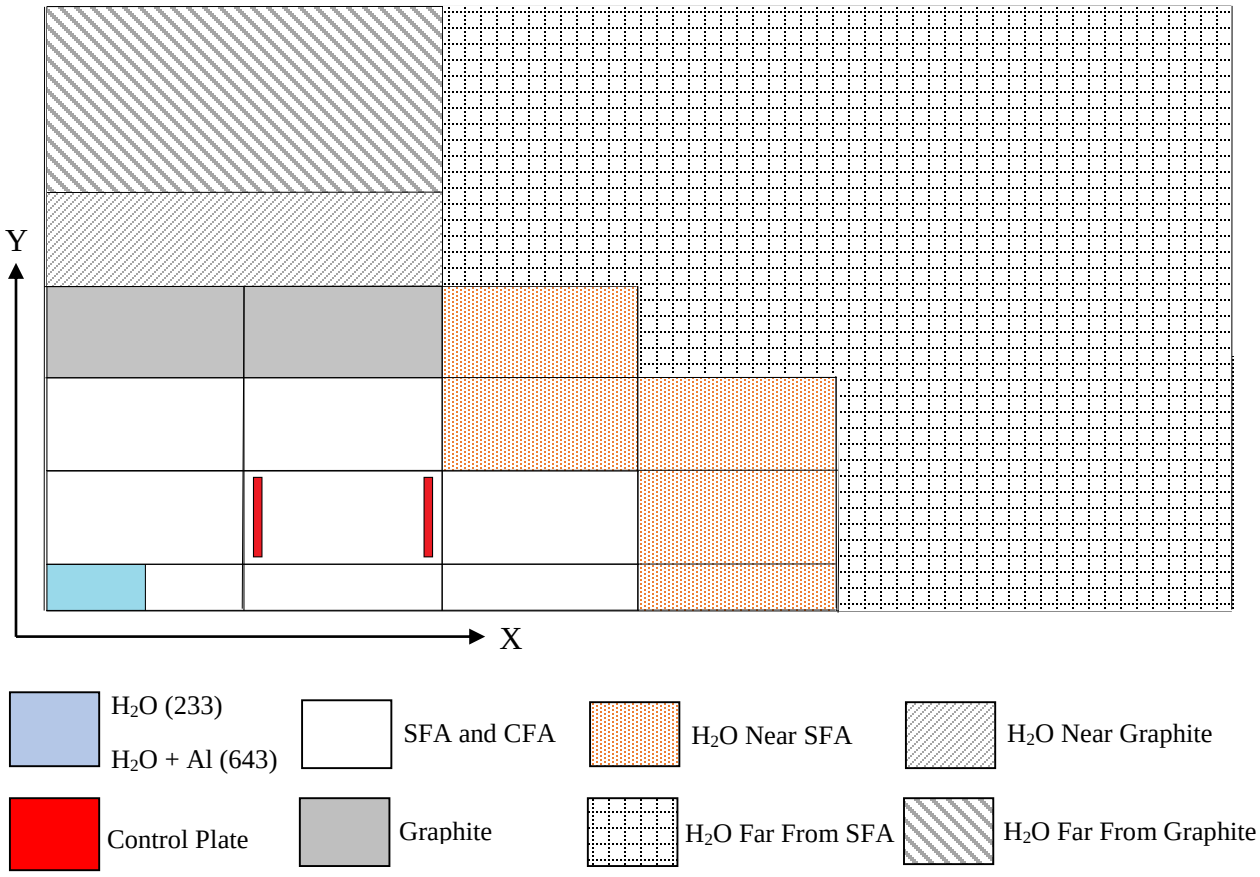

Fig. A.15: CITVAP model for a quarter core.

Appendix-B: Experimental Calculation of the SDM with a Single Failure of a Control Element Using the Integral Rod Drop Method.

In section 3.4.3.4, the experimental calculation of the negative reactivity insertion in the SDM with a single failure of a control element using the integral rod drop method was done by using equation (B.1), [26].

$$\rho_{SCRAM} = -\left[\frac{N(0) - N_f}{\int_0^{\infty}\left(N(t) - N_f\right)dt - \int_0^{\Delta T}\left(1 - r(t)\right)\left[N(t) - N_f\right]dt}\right]\sum_{i=1}^{6}{\beta_i}/{\lambda_i} \qquad \text{(B.1)}$$

Where:

N(t): Proportional signal of neutronic flux, [Ampere or Volt].

N(0): Initial stable value of neutronic flux proportional signal, [Ampere or Volt].

N_b: Final stable value of neutronic flux proportional signal, [Ampere or Volt].

r(t): Normalized function that describe the negative reactivity insertion.

ΔT: Time duration of the insertion, [sec].

β_i: Delayed neutron fraction in group i, [pcm].

λ_i: Decay constant of precursors in group i, [pcm].

Using the old data of the SDM with single failure of a control element [17], which were obtained by using the kinetic constants of ENDF/B-VI.8, and the updated data in ref. [16] made the calculation of the SDM with single failure of a control element for the two Compensated Ionization Chambers (CIC) possible. The updated data, which correspond to the use of the kinetic constants of Tuttle, in ref [16] contains only the data of the lowest value of SDM of the two reading of the CICs. For the sake of comparison, both reading of the CIC was necessary. A sample calculation of SDM with single failure of a control element No. 3 is presented below.

$$\left(\frac{\rho_{CIC-1}}{\rho_{CIC-2}}\right)_{old} = \left(\frac{\rho_{CIC-1}}{\rho_{CIC-2}}\right)_{updated} \quad \text{(B.2)}$$

Where:

$\rho_{CIC\text{-}1,\ old}$: Negative reactivity calculated from CIC -1 using the kinetic constants of ENDF/B-VI.8 $\rho_{CIC\text{-}1,\ old}$ = -4666 pcm (reported from ref [17]).

$\rho_{CIC\text{-}2,\ old}$: Negative reactivity calculated from CIC -2 using the kinetic constants of ENDF/B-VI.8 $\rho_{CIC\text{-}2,\ old}$ = -4234 pcm (reported from ref [17]).

$\rho_{CIC\text{-}1,\ updated}$: Negative reactivity calculated from CIC -1 using the kinetic constants of Tuttle $\rho_{CIC\text{-}1,\ updated}$ was initially unknown.

$\rho_{CIC\text{-}2,\ updated}$: Negative reactivity calculated from CIC -2 using the kinetic constants of Tuttle $\rho_{CIC\text{-}2,\ updated}$ = -4882 pcm (reported from ref [16]).

Using equation (B.2) made the calculation of both values of negative reactivity insertion possible, which correspond to CIC-1 and CIC-2. All values of the SDM with single failure of a control element of both readings (CIC-1 and CIC-2) was previously presented in table 3.25.